Conceptual design of a thermoplastic composite cross-car beam

Master's Thesis

August 16, 2023

A.C.C. Kajim

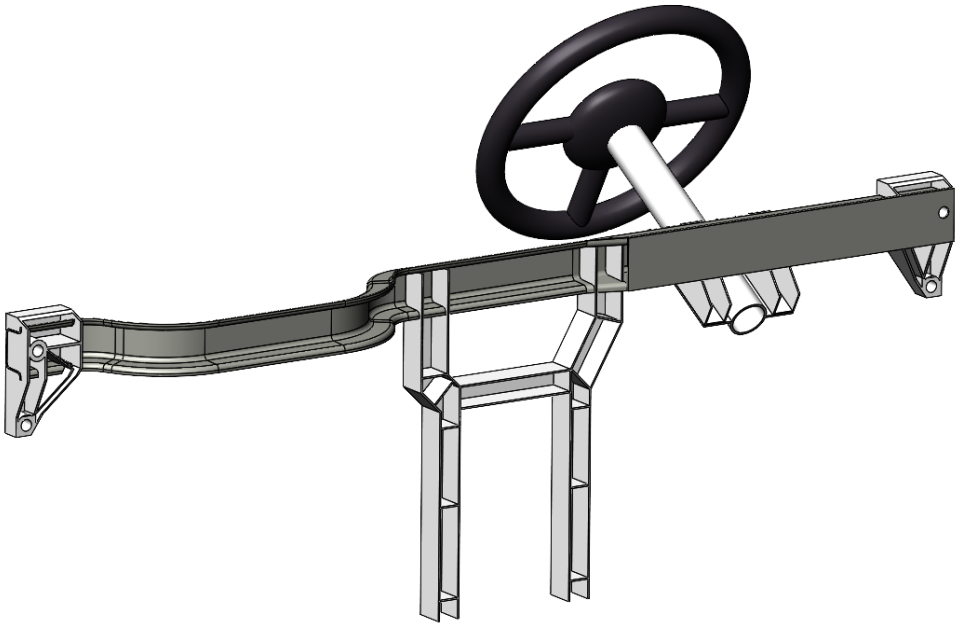

Supervisors:
Dr. ir. M. Baltussen, Lightyear
Dr. ir. W.J.B. Grouve, University of Twente

Lightyear
Automotive Campus 70
5708 JZ Helmond
The Netherlands

Production Technology group
Department of Engineering Technology
Mechanical Engineering
University of Twente
Enschede
The Netherlands

Abstract

Thermoplastic composites have garnered interest in the automotive world due to their potential to lightweight parts. However, several challenges hold back widespread adoption. This thesis aims to design a thermoplastic continuous fiber composite high-volume ready structural cross-car beam and to provide an overview of the challenges in the analysis and implementation of a thermoplastic composite structural part. This is done both by giving an overview of the available literature and by simulating a composite part to compare different material options.

Thermoplastic composite parts can be manufactured at the required cycle time for high-volume production using pick and place for blank forming and press forming followed by overmolding. The research highlights the complexity of composite part design and simulation, particularly in optimizing variables such as fiber angles and local reinforcements, and addressing anisotropic behavior and production-related issues affecting strength significantly. This report focuses only on stiffness simulations, as especially strength and crash simulations require advanced validated material models, which were not available at the start of this thesis. Weight reduction compared to an aluminum CCB was found to be challenging using glass fiber. This was only possible by lowering the eigenfrequency requirement, possible due to the superior damping properties of composites. Despite this, the cost of the weight saving exceeds what is acceptable in automotive.

Contents

Acronyms

ATP Automated Tape Placement. 25

BEV Battery Electric Vehicle. 6

CCB Cross-Car Beam. 1
CF Carbon Fiber. 12

DMA Dynamic Mechanical Analysis. 37

EV Electric Vehicle. 1

FVF Fiber Volume Fraction. 7

GF Glass Fiber. 7

ICE Internal Combustion Engine. 6

LFT Long Fiber Thermoplastic. 11

N Newton. 6
NVH Noise, Vibration, and Harshness. 2

PA Polyamide. 10
PA6 Polyamide-6. 7
PP Polypropylene. 7
pre-preg pre-impregnated ply. 10

RH Relative Humidity. 6

SFT Short Fiber Thermoplastic. 9

Tg glass transition temperature. 12
TPC Thermoplastic composite. 2

UD Unidirectional. 10

List of Figures

List of Tables

Chapter 1

Introduction

1.1 Goals

The aim of this thesis is to design a thermoplastic continuous fiber composite high-volume ready structural Cross-Car Beam (CCB) and show the challenges in the analysis and implementation of the CCB.

The requirement for continuous fibers specifically is set as it has better properties compared to discontinuous fibers, especially regarding strength and impact, see fig. 3.2.1b. However, continuous fiber composites are more challenging in production. Parts are considered structural if they support the vehicle weight and road shock, or absorb and manage the collision energy [24]. The CCB will also be designed specifically for Electric Vehicles (EVs).

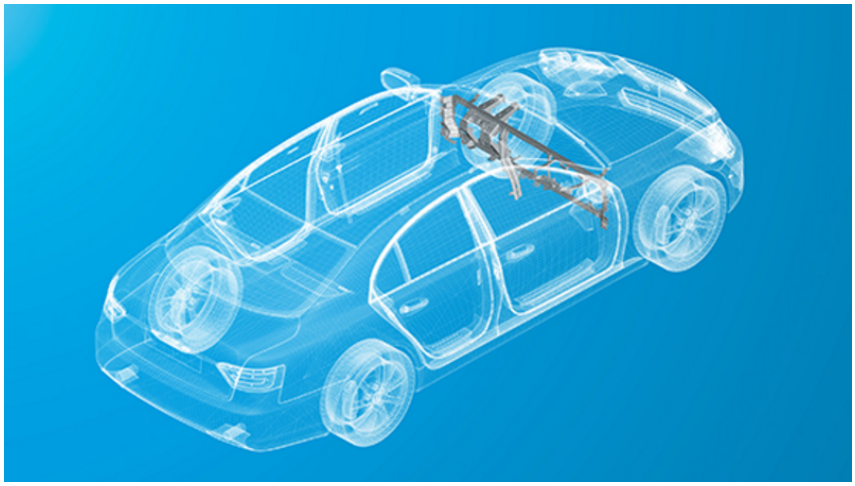

Figure 1.1.1: The CCB and its location in the car [1]

1.2 Why use thermoplastic composites in automotive

The automotive industry is looking at lightweighting options for multiple reasons. The biggest reason is to reduce the environmental impact of cars, as required by regulations [25]. Lighter cars have a higher energy efficiency. Lightweighting also reduces material usage in production. It also can have a snowball effect with secondary weight-saving benefits as a lighter frame means a lighter motor will suffice and so on. A lighter car could also have the added benefit of a lower total cost of ownership due to lower energy consumption [26]. In the case of EVs, the higher energy efficiency means a higher range per kWh, potentially reducing the required battery size, which is a large part of the cost and weight of an EV [27]. In higher-segment cars, the lightweighting is done primarily to improve the handling and performance of the car.

Composites open up opportunities for lightweighting in automotive due to their high strength-to-weight and stiffness-to-weight ratio. Composites increase design flexibility as they introduce additional design freedom through fiber orientation. It can also improve the comfort of the car by reducing the Noise, Vibration, and Harshness levels, generally referred to as NVH, due to its high damping compared to aluminum and steel. This is especially important in EVs where the lack of a distinct engine sound makes the sound from other parts more noticeable. Composite generally also have a high fatigue resistance [28, 29]. On top of this corrosion is no concern for composites, reducing secondary finishing operations [30]. In the event of a crash, composites can also have a higher energy absorption capability [31, 32], although this strongly depends on the loading scenario.

Fiber-reinforced polymers, composites from here on, are composite materials that consist of fibers and a matrix, which is the glue holding the fibers together. The type of matrix can either be a thermoset or a thermoplastic. A thermoset matrix undergoes an irreversible chemical crosslinking process as it goes from a liquid to a hardened matrix during curing. A thermoplastic matrix on the other hand can be molten and reshaped multiple times by heating it. This opens up other manufacturing and recycling options. Currently, continuous fiber composites are mostly made using thermoset matrices as they usually have higher temperature resistance and superior mechanical properties. Next to this, the production process of thermoset matrices is easier due to their lower viscosity compared to thermoplastics, which significantly improves fiber impregnation. It also has good formability and tack before curing, allowing easy hand layup. However, the production process of thermoset composites is very slow and expensive for high-volume production compared to Thermoplastic composite (TPC) and metal production processes [19]. Due to the high cost, and slow production process, but high mechanical properties (thermoset) composites are used mostly in aerospace and racing industries where saving weight is of paramount importance. The fastest cycle time for thermoset products is minutes [19], but most processes take much longer. Especially for automotive these process times should be compared with the speed of stamping and welding steel sheets taking seconds and the cycle time of a part is about a part per minute [7].

The production process of TPCs can be very similar to what is currently the standard in automotive mass manufacturing such as stamp forming and injection molding, making it easy to integrate in existing processing chains. Next to the lower cycle time compared to thermosets, TPC production can be automated to a much higher degree. With the use of injection molding a large number of parts can be integrated, reducing part count. Since thermoplastics can be remelted welding and recycling of thermoplastics composites is possible too. As an added benefit over thermoset composites, TPCs have an infinite shelf life, not requiring cold storage, and have much easier and safer pre-processing handling [33]. TPCs have a high potential for mass manufacturing, but some challenge still exists as will be discussed in chapter 4.

Part I

Materials, Production, and Design

The first part of this report contains an overview of the general design of the CCB. First, the current CCBs in the market are given together with the requirements for a typical CCB. Followed by suitable TPC materials and production methods. This includes the comparison of different composite materials and layups with metals using material indices and a simplified initial design approximation of the CCB with analytical calculations. Based on this two concept designs are given, of which one concept is chosen and worked out further. Then in the second part of this report, the chosen design will be modeled and simulated. Tests have also been done to determine some required material parameters.

Chapter 2

Background Cross-Car Beam

2.1 Function of the cross-car beam

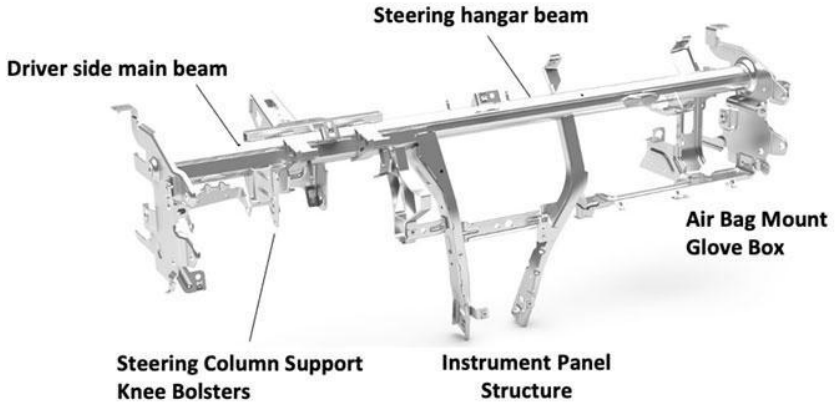

Figure 2.1.1: The CCB and its functions [2]

The CCB is located behind the instrument panel and runs horizontally from side to side in the car, as is shown in fig. 1.1.1. It is the main structural carrier for the steering wheel column and the instrument panel. It also protects the occupants in case of a side crash, as is illustrated in fig. 2.1.1 [34]. In a frontal crash, the beam can also absorb energy from an intruding firewall from the front, a moving steering column, or support the instrument panel which can absorb energy from the impact of the knees [34]. Next to the instrument panel, smaller parts can be attached to the beam too, such as the glove box, the airbags, and the infotainment screen.

The CCB directly influences how the car is perceived by the occupants. As it supports the steering column, any flex or vibration in the steering wheel or center console screen can be perceived as an issue with the car or a low-quality vehicle [34]. The vibrations can also cause structural problems such as fatigue. The eigenfrequency of the CCB and steering wheel should be above the eigenfrequencies of the body of the car as well as the parts next to it to prevent resonance. Around the resonance frequency, a little force can cause very high vibrations. The eigenfrequency requirement is often one of the most challenging requirements for the CCB to fulfill [35].

2.2 Requirements

The requirements for the CCB are a combination of general requirements for automotive parts and requirements specifically for the CCB. The requirements are both safety and comfort related. Next to that,

the composite beam should be an improvement over the current CCB options, hence some requirements are set for that too. The requirements set for the CCB that will be designed are as follows:

- Temperature range: -40 to 115 degrees $°C$ [36].
- Relative Humidity (RH) range: 0 - 100 % [36].
- The eigenfrequency has to exceed 35 (33+2) Hz [34].
  - A lower eigenfrequency requirement might suffice for composites due to their high damping, more on this in section 8.7.
- A downward force of 150 Newton (N) in the middle of the beam shall lead to a displacement of less than 1 millimeter and cause no permanent deformation.
- A load at the center of the steering wheel of 250 N sideways or 600 N downwards shall lead to less than 3 and 4 millimeter deflection respectively and cause no permanent deformation.
- The energy absorption of the composite CCB must be equal to or higher than an equivalent aluminum CCB in a side impact test.
- The CCB has to meet the requirements for at least 15 years.
- An increase in cost should be no more than 17 EU/kg saved weight, more on this in section 3.5.
- The composite CCB should have a production cycle time of minutes maximum to be suitable for high-volume production [7, 37].
- The weight of the composite CCB should be similar to or lower than that of a comparable aluminum CCB.

2.3 Benchmarking cross-car beams

In order to set a benchmark for the composite CCB to be compared to it is important to know the different designs of the CCBs currently used in vehicles. In the vehicle database of A2MAC1 [3] the CCBs of 51 Battery Electric Vehicles (BEVs) have been compared. It was decided to only look at BEVs and not at Internal Combustion Engine (ICE) cars to minimize the difference. The engine in an ICE car could influence the energy the CCB needs to absorb. BEVs also lack a gearbox or axle under the center console, which is often used to attach the CCB to thus giving better support to the CCB. Additionally, ICE cars are being replaced by BEVs at an increasing rate [38].

First, the shape, weight, and materials of current CCBs are looked at after which an overview of composite CCBs is given. Finally, the shape of the CCB that is to be designed is chosen.

2.3.1 Current cross-car beams in the market

The CCBs that are in the database can be put into four main categories shape-wise, as shown in fig. 2.3.1. The straight extruded beam, shown in fig. 2.3.1a, seems to generally be used in smaller cheaper vehicles and is usually the heaviest of the four types. The intricate injection molded or die-cast beams such as in fig. 2.3.1d are usually made of magnesium, or even glass fiber polypropylene TPC, which is found in higher segment cars only. Both use lightweight materials and the high level of function integration it enables, resulting in injection molded and die-cast beams being the lightest option of the four. Although the design between the magnesium and TPC CCBs can differ substantially. The other two options are less clearly divided. It could be a choice based on the packaging of the components or carry-over experience from other cars in the same manufacturer. The double-size beams are usually two extrusions that are connected together. Whereas the curved beam is usually produced by hydroforming an extruded beam, although welded connections are also seen. It is also common to have a thicker beam at the driver's side for extra stiffness for the steering wheel, as is clearly visible in fig. 2.3.1b.

The material generally used for the CCB is steel or aluminum for the beam itself. Extruded magnesium and die-cast magnesium are used too. As is shown in table 2.1 the majority of CCBs are made of steel. Some cars also have a magnesium part holding the steering wheel and an injection molded composite for the rest of the beam.

The branches of the beam which hold other parts can be plate work of metal or an over-injection molded, TPC which gives the ability to integrate functions and stiffeners more easily, as is shown in fig. 3.1.1. The high level of function integration saves assembly time and part count, thus reducing costs. This composite is usually Polyamide-6 (PA6) or Polypropylene (PP), reinforced with Glass Fiber (GF). The Fiber Volume Fraction (FVF) in automotive injection molded parts was found to usually be between 30-60% of GF [3].

The weight of the CCB including branches ranged between 4 and 12 kg, with most between 5 and 9 kg. The trend is for heavier and more expensive cars to have lighter CCBs. As they often use more expensive lightweight materials and the frame of the car is stronger so the CCB has to absorb less energy.

Currently, the more expensive cars tend to have a CCB made out of either die-cast magnesium, a hydro-formed aluminum tube with overmolded fiber-reinforced reinforcements and branches, or an overmolded stamped steel beam [3].

Table 2.1: Materials of CCBs of EVs in the A2MAC1 database [3]

Material	Number	Percentage of total
Steel	33	64%
Aluminum	11	21%
Magnesium	8	15%

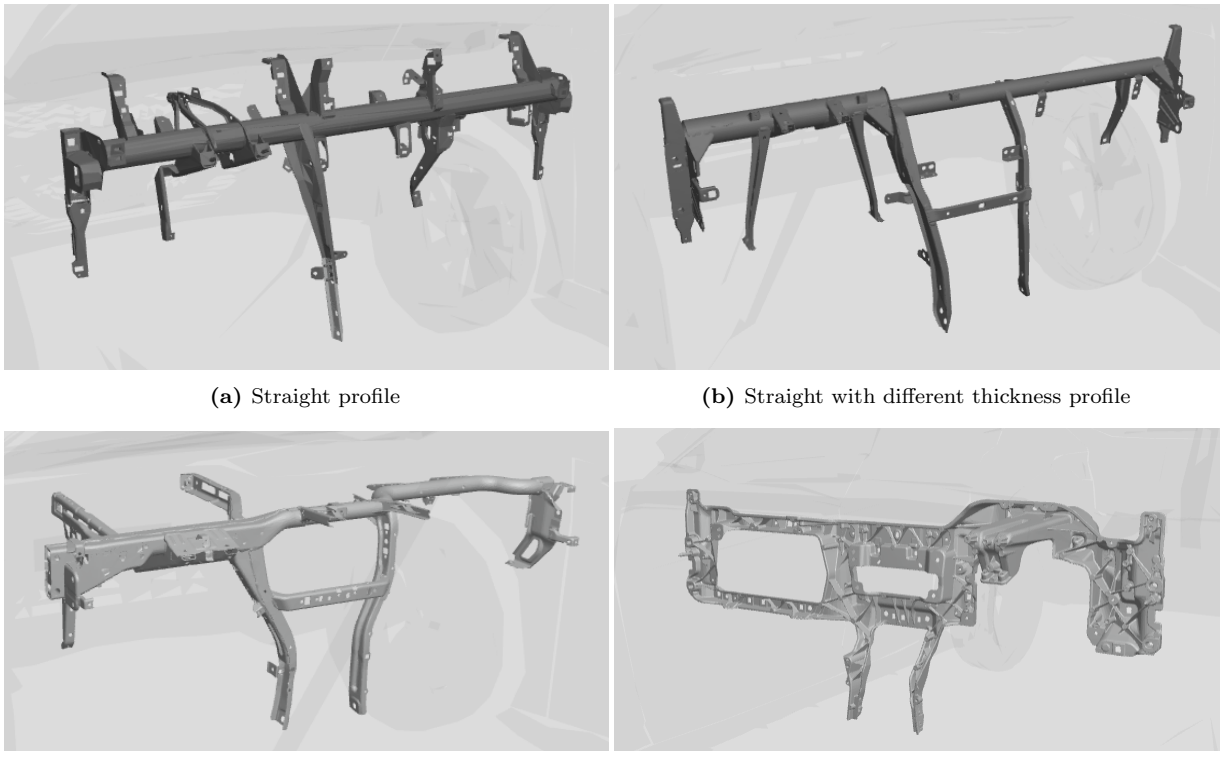

(a) Straight profile

(b) Straight with different thickness profile

(c) Multiple corners profile

(d) Die cast

Figure 2.3.1: The four main types of CCB [3]

Table 2.2: Types of CCBs in the EV database [3]

Type	Number	Percentage of total
Fully Straight	12	23%
Straight 2 diameters	9	17%
Curved	24	46%
Fully Die-Cast	7	14%

In table 2.2 the number of CCBs per type is given for the BEVs available in the database. As is clear all types can often be found, with the majority of CCBs being non-straight as the CCB is usually constrained by packaging in the car and thus the shape has to change to whatever is required.

2.3.2 Composite cross-car beams

Currently, no composite CCB can be found in a high-volume production car. The closest to this would be the half composite CCB designs seen in the BMW ix drive 50 sport 2022 and the NIO ES8 2022 [3] which have a magnesium CCB on the driver side which holds the steering wheel and are also connected to the floor. The passenger side of the CCB is made of a molded long GF PP part as can be seen in fig. 2.3.2a.

Fully composite high-volume CCBs have only been seen in the form of proof of concept such as the non-continuous fiber molded beam with metal ends by Faurecia [39], one of the major automotive part suppliers. Another option is the continuous fiber press formed CCB by Faurecia shown in fig. 2.3.2b, which has a claimed weight reduction possibility of 40% [40].

(a) Half composite CCB concept in the BMW ix drive 50 sport 2022 [3]

(b) Concept of a press formed composite CCB by Faurecia [41]

Figure 2.3.2: Composite CCB's

2.3.3 Design choice: Shape cross-car beam

For this thesis the goal is to design a continuous fiber CCB, as it has better strength and impact properties than short discontinuous fibers, see fig. 3.2.1b, thus the injection molded type beam in fig. 2.3.1d is not an option that will be investigated further. It has been decided to design the Curved CCB like the one shown in fig. 2.3.1c. This is the most difficult to manufacture out of the three variations, so if it is possible to produce this shape then the others will be producible too. The choice to not go for the straight beam does mean pultrusion is not an option as a production method, which has proven itself already in composite bumper beams for example [42], more on this in section 4.2. However, the remaining available production methods have more other uses too which makes them interesting to look into [43].

Chapter 3

Material Choice

3.1 Thermoplastics in automotive

The use of composites can offer improved strength and stiffness at a reduced weight [37, 44]. Currently in automotive most structural parts made of continuous fiber reinforced composites are made out of a thermoset in combination with braiding, pultrusion, resin transfer molding, compression molding, or other methods [45, 46], some of these production processes are described in chapter 4. TPCs can also offer a high strength and stiffness-to-weight ratio and can be better suited for high-volume production than thermosets [37, 47]. For example, significant potential is seen in making vehicle floors, battery casings, bumper beams, and support structures, usually made of steel, out of GF TPC. This is expected to enable a weight reduction of about 35% to 40% [7, 44, 47–49]. TPC products can also result in lower total life cycle emissions than steel or aluminum [26, 37].

TPCs can have different reinforcing types of fibers. The easiest to use in manufacturing and lowest cost is a short fiber reinforced thermoplastic (SFT), which is easily injection moldable. Using SFT increases the strength and stiffness substantially compared to pure plastics. These have the potential to replace metal parts at a lower weight and cost, whilst increasing energy absorption in the event of a crash [26, 44]. A commonly used technique in automotive and other industries is injection molding [49, 50]. This process allows for the rapid production of complex parts.

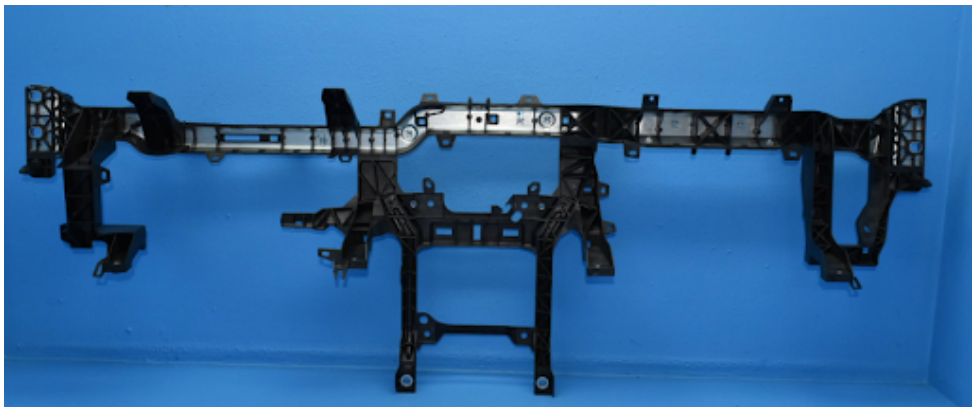

Figure 3.1.1: Steel U-shaped CCB of the Tesla Model S Plaid with function integration using injection molding[3]

Injection (over)molding gives the option to integrate a lot of functions into one part, as is shown in fig. 3.1.1 where all black parts are overmolded onto the steel beam in one cycle. Overmolding is a technique whereby additional parts are injection molded onto and often around another part. The part that is overmolded in the automotive industry is often a large flat product produced by stamp forming such as a

metal or plastic door; a beam such as in fig. 3.1.1; or an extruded part. This saves time otherwise needed for attaching multiple parts on the CCB which would have to be welded, bolted, or bonded.

3.2 Fiber length

Fibers can have different lengths, depending on the production process and cost limitations. The longer the fiber the higher the properties. However, as is shown in fig. 3.2.1b, short fibers of only about 1 mm long, such as those found in injection moldable composites, already have 90-95% of the stiffness of continuous fibers. For similar strength, the required length is higher at 7 to 10 millimeters. Impact is the property that is most sensitive to fiber length with a length required of 16 millimeters or longer to get close to the level of continuous fibers [51, 52]. Thus the required fiber length can differ based on the definition or requirement. The actual fiber lengths required can also be different for other fiber-matrix combinations as the fiber-matrix interface adhesion can differ.

Compression molding is also commonly used for composite parts, as less flow is needed fibers can be longer and their length can be better preserved, typically in the range of 10-50 millimeters [30]. These composites are usually made with GF and are known as glass mat thermoplastics, these have a random fiber orientation.

The most complex but with the highest mechanical properties are the continuous fibers. Continuous fibers are fibers that are uninterrupted and have a significant length, which could be from one edge of the product to another edge of the product. Although shorter fibers can already provide very high stiffness, their orientation is more difficult to control. Continuous fibers can be placed precisely in the orientation that is needed. Structurally demanding parts need the strength and stiffness that only continuous fibers can provide [53].

The most common form to have continuous fiber thermoplastics in before producing a part is as a pre-impregnated ply (pre-preg), which can be Unidirectional (UD) fiber tapes or a fabric of fibers which is impregnated with the matrix already. These are solid at room temperature for thermoplastics. Another but less common way is as a commingled fabric in which the structural fibers such as GF are mixed together with fibers made of matrix material such as Polyamide (PA), this fabric is easily formable as the fibers are not yet held together by the matrix. A pre-preg or commingled fabric is then usually press formed into shape, more on this in section 4.3. Although other production methods are available too, more on this in chapter 4.

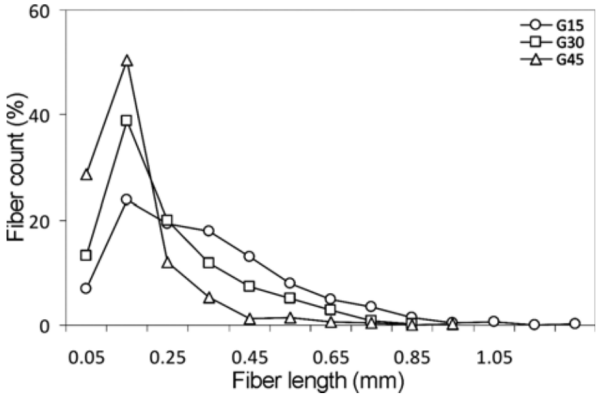

(a) Difference in the distribution of fiber length in the product with different FVF of 15, 30, and 45%. The fibers had a starting length of 6 mm. Clearly fiber breakage increases with increasing fiber volume content [54]

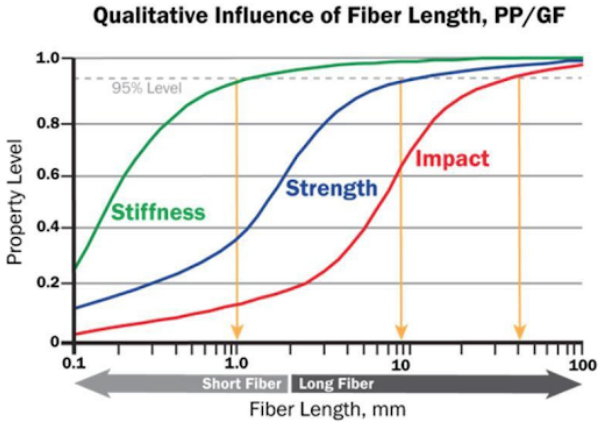

(b) The influence of fiber length on different properties [51, 52]

Figure 3.2.1: Fiber length

3.2.1 Injection molding with fibers

Injection moldable TPCs require discontinuous fibers as the composite needs to flow through the mold, thus they lack some of the benefits of the strength of continuous fiber composites such as woven or UD laminates. The fiber length in injection molding is often divided into two categories. With a distinction for short fibers with a length of less than 1 millimeter, or discontinuous long fibers with a length between 1 and 25 millimeters [51, 55]. The length of the fibers, however, is reduced by the injection molding process [54, 56]. The longer the fiber, the more difficult and thus expensive the injection molding becomes as the composite becomes more viscous. The higher viscosity causes higher shear forces during the injection molding process which causes more fiber breakage, reducing the fiber length. For randomly orientated fibers such as those produced by injection molding an upper volumetric limit has been found empirically which is given in eq. (3.2.1), where FVF the fiber volume fraction and ϕ is the aspect ratio of the fiber [57, 58]. The aspect ratio is the length of a fiber divided by its diameter. Above this limit, fiber orientation cannot be random [58]. The assumption that fibers are randomly oriented is usually valid as the fibers rotate in the flow and quickly touch each other leading to high local contact forces which lead to fiber breakage. Increasing the FVF over the limit given in eq. (3.2.1) is likely to cause further fiber breakage, which lowers the aspect ratio. For example, a 50% FVF a GF with 10 microns diameter would have a length of 108 microns, which is similar to what is found in fig. 3.2.1a.

$$FVF = 5.4/\phi \tag{3.2.1}$$

Next to the length of the fibers, the properties of a fiber-reinforced composite depend for a large part on the volumetric proportions of the fibers in the matrix [59]. An increase in FVF improves all mechanical properties, except for strain to failure, up to a limit. This reaches a maximum of mechanical properties for both SFT and Long Fiber Thermoplastic (LFT), at a fiber weight content of about 40-50% [51]. As an increase in fiber content increases the fiber breakage, leading to shorter fibers, which is shown in fig. 3.2.1a. The increase in strength due to a higher fiber content can at a point be mostly negated by the decrease in fiber length [59]. The breakdown of fiber length due to injection molding causes a loss in mechanical properties. However, this effect can be somewhat compensated by the orientation of the fibers in the flow direction. This also means that the increase in mechanical properties of a composite product made of LFT is less than might be expected as there is less orientation along the flow with the longer fibers compared to SFT [51].

3.3 Comparing polypropylene and polyamide-6

For the (semi-)structural TPC parts the two materials being used most are PP [49, 55, 60–64] and PA [3, 40, 63–66]. Of the plastics used in cars PA accounts for 8% of the plastics, and PP for 44% [60], some typical properties of the neat polymers are given in table 3.1. PA can handle higher temperatures than PP and is seen as an engineering plastic as opposed to a commodity plastic like PP [64]. This means that PA is often the preferred matrix of choice for structural applications, especially under the hood where temperatures can be higher due to the combustion engine. Different types of PA are available, of which PA6 and PA66 are the most common [67], with PA6 being the cheaper one of the two [20]. PA66 mostly has the edge over PA6 with somewhat higher temperature applications, although commonly both PA6 and PA66 are used for similar applications. The high temperature requirement, however, is not needed for the current requirements set in section 2.2.

Table 3.1: Properties of the neat material at 23 $°C$ and 50% RH [19, 20]

	PA6	**PP**	
Density	1130-1150	895-909	kg/m3
Tg	23-28	-24.2 - -16.2	$°C$
Melting point	210-220	140-150	$°C$
Yield strength	38.6-48.2	24.1-28.4	MPa
Tensile strength	68-76	26-50	MPa
Young's modulus	0.94-1.18	0.90-1.55	GPa
Elongation at break	41-59	112-483	% strain
Price	2.5-3.5	1.1-1.5	EU/kg

The average outdoor temperatures are below the glass transition temperature (Tg) of PA6, this is not the case for PP, as shown in table 3.1. Important to note is that the Tg of PA is strongly influenced by moisture. For PA6 the Tg is in the range of 60 to 70 $°C$ when dry, when conditioned at 50% RH it goes down to 20 $°C$ [6, 55, 68, 69]. If PA6 is soaked in water, the Tg can even drop to -20 $°C$ [70]. For PP the Tg is usually in the range of -25 to -10 $°C$ and it is not affected by moisture like PA is [19, 55, 69, 71].

The creep resistance of neat PA is higher than that of PP, the difference becomes smaller when these plastics are used in composite. The creep resistance of long fiber reinforced PP is higher than neat, or unreinforced, PA and even in a comparable range to reinforced PA [72]. Especially for (semi-)structural applications these plastics are reinforced with GF or Carbon Fiber (CF), more on these materials in section 3.4, usually in the form of SFT or LFT in an injection or compression molded part. Another common way to use PA or PP but with continuous fibers is by press forming, this is discussed in section 4.3.

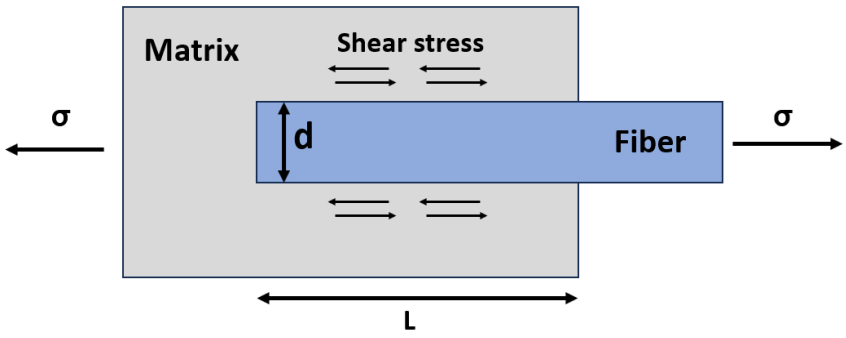

Figure 3.3.1: An illustration of the factors determining the critical fiber length

$$L_c = \frac{\sigma_f \cdot d}{2\tau_c} \tag{3.3.1}$$

One of the disadvantages of PP is that it has very low surface energy which makes adhesive bonding or painting challenging [19]. This also influences the critical fiber length, as the interfacial shear strength is lower. The critical fiber length L_c is the minimum length a fiber needs to have in a given matrix so that the fiber is broken instead of pulled out of the matrix, thus making maximum use of the strength of the fiber. The formula for it is given in eq. (3.3.1). The critical fiber length depends on the strength of the fiber σ_f, the fiber diameter d, and the maximum shear stress τ_c. The maximum shear stress can either be the matrix shear strength or the matrix-fiber bond strength. Thinner fibers also help decrease the critical length as the matrix interface is relatively larger compared to the fiber diameter. A lower critical fiber length is beneficial for the mechanical properties of the composite. For example, the critical length for GF-PP is about 3.2-4.4 mm, as adhesion to PP is challenging. Whereas for GF-PA, it is much shorter at 1.24 mm [73]. As for toughness, an important aspect in crash, the range of values varies, with the best toughness values being equal for PP and PA, but the lowest toughness values of PP are three times lower than that of PA [74].

Table 3.2: Typical mechanical properties range of PA and PP LFT [21]

LFT Material	**Fiber loading**	**Tensile strength** [MPa]	**Tensile modulus** [GPa]	**Flexural strength** [MPa]	**Flexural modulus** [GPa]
GF/PA	25-50 wt%	106-251	7.7-18	173-324	6.5-15.9
GF/PP	30-40 wt%	48-150	6.5-10.8	167-175	7.8-9.0
CF/PA	18-35 wt%	110-172	6.5-14.7	222-242	14.1-16.6
CF/PP	18-50 wt%	47-105	6.7-28.8	95-179	5.1-18.4

In table 3.2 the range of properties found in literature for LFT PA and LFT PP are given. It shows how the reinforced PP strength values are lower than that of reinforced PA, both for the tensile and flexural strength. The stiffness values can be more comparable between the two matrices, although for the flexural modulus with CF the PP matrix performs significantly worse.

It is important to note that it is common to give the dry PA values which can be much higher than the conditioned values, as shown in table 3.3, even though the values of the conditioned material at 23 degrees and 50% RH is more realistic in normal use [19]. This is especially important for matrix-dominated properties, thus the values for the LFT in table 3.2 will be impacted more than those of the continuous fibers in table 3.3 as the matrix has to transfer the force from one discontinuous fiber to the other with discontinuous fiber composites.

Table 3.3: The Tepex data sheets of a PA6 and PP GF laminate, the fiber reinforcement is the same for both. The values for PA6 given are that of the conditioned material (23 deg RH50%). To show the difference, the dry values are given in brackets [22, 23]

	PA6 GF Tepex 47% FVF	**PP GF Tepex 47% FVF**	
Density	1800	1680	kg/m3
Tensile modulus	18 (23)	20	GPa
Tensile strength	380 (390)	430	MPa
Tensile elongation at break	2.3 (2.2)	2.7	%
Flexural modulus	16 (20)	17	GPa
Flexural strength	300 (580)	370	MPa

For continuous fiber composites, however, this difference can be much smaller as the fibers determine the strength and stiffness of the laminate to a large extent [75]. The Tepex laminates by Lanxess, shown in table 3.3, are a representative automotive grade TPC. The laminates shown have the same GF reinforcement with either a PP or a PA6 matrix. It shows clearly how the dry PA6 laminate is stiffer than PP, but conditioned at 50% RH it is not. For the tensile strength, the difference between dry and conditioned PA is small, however, for the flexural strength the difference is much larger as the shear loading in bending makes the impact of the matrix larger. When comparing the conditioned PA6 to the PP laminate the values are very comparable. Opposite to table 3.2, the PP laminate is actually superior to the conditioned PA6 laminate.

3.3.1 The influence of temperature and moisture on damping and stiffness of PA and PP

The damping of a material is the dissipation of energy. This results in lower deflections when excited and the deflection dies out quicker. Metals often have very little damping with wrought aluminum having a damping factor of about 0.0011 [19]. Plastics, in this case PA6 and PP, can have a much higher damping factor, or energy dissipation, as is shown in fig. 3.3.2. This can be a significant advantage of using composites over metals, as will be shown in section 8.7.2.

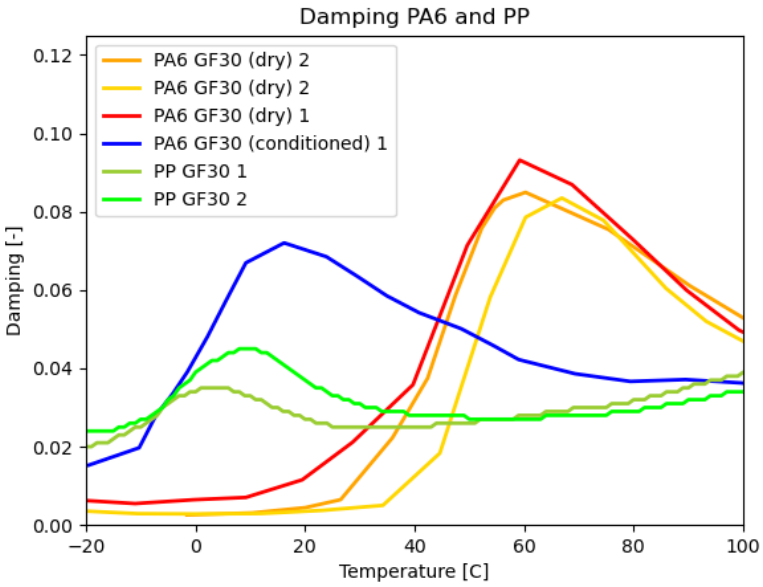

Figure 3.3.2: The influence of temperature on different fiber-reinforced PP and PA composites. As well as the influence of moisture shown by the difference between dry (red line) and conditioned (blue line) PA6 [4–6]

The damping factor of PA6 shows a very strong dependence on temperature, moisture, and loading rate, see fig. 3.3.2 and fig. 6.2.3. With the damping factor ranging as low as 0.002, only double that of wrought aluminum and steel, and with peaks higher than 0.08. Crucially this big change in damping factor occurs over a small temperature range close to or within even moderate climate temperatures. In fig. 3.3.2 the rise in damping for dry PA6 starts around 30-40 $°C$, around Tg. However, when exposed to moisture, the Tg of PA6 lowers and this also shifts the damping curve to lower temperatures, as is shown in fig. 6.2.3. At 50% RH, the shift of Tg in for PA6 is about 40 $°C$ from 60 down to 20 $°C$. Soaked in water, the Tg could even go as low as -20 $°C$ [70, 76]. The behavior of PA6 can differ strongly even under normal driving conditions as temperatures can hover around its Tg. With high damping in average driving conditions above freezing temperatures, and with a drastic reduction in damping properties below that. This can make designing with damping in mind more challenging for thermoplastics compared to metals, especially with PA6, as steel and aluminum have practically no change in damping or stiffness over the range of temperatures important here. Next to this, the damping value of a TPC depends on the fiber directions and also on the type of loading. So a large number of tests need to be done for the full picture.

Opposite to PA6, the Tg, and with that the damping too, of PP is not affected by moisture [71]. Fiber-reinforced PP mostly has a damping factor between 0.02 and 0.04 with a relatively small temperature influence compared to PA6, as PP is already above its Tg in most use cases. The influence temperature has on the loss factor, also called damping, is not straight-lined, as is visible in fig. 3.3.2 and fig. 3.3.3. In general, a higher temperature means higher damping. But there is a strong peak for both PP and PA6 around 0 to 20 $°C$ (for conditioned PA6). The Tg and the damping ratio of polymers can be influenced by the incorporation of fibers [54], this is shown in the right graph of fig. 3.3.3.

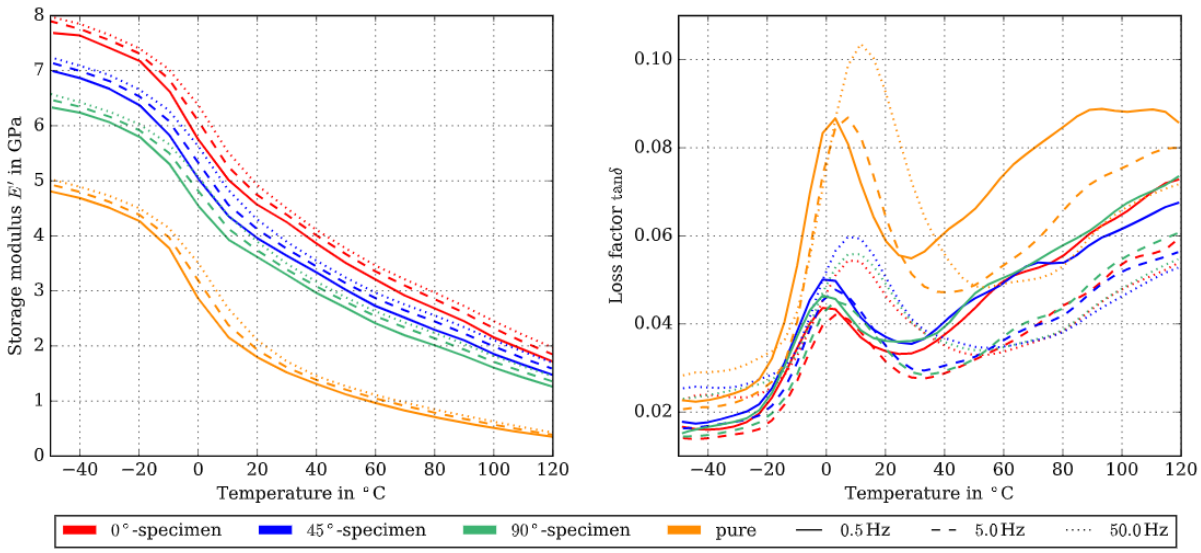

Figure 3.3.3: The influence of temperature on the storage modulus and damping of SGF PP[5]

The temperature has an impact on both the damping and the stiffness of the polymer and composite, as shown in fig. 3.3.3. As the temperature increases the stiffness decreases for both PP and PA6. In fig. 3.3.3 the drop in storage modulus, or the stiffness, above the Tg of -20 $°C$ for PP is clearly visible for both the pure polymer as well as the reinforced one. At lower temperatures, below 0 $°C$, the stiffness is usually higher but the damping is lower. At higher temperatures, above 20 $°C$, the stiffness is lower and the damping is high. With a region with much higher damping and relatively good stiffness still in between. This drop in stiffness will be less for continuous fiber composites, but it will still have an impact on the Young's modulus even in fiber direction in the range of one to a few GPa [77]. This drop in stiffness will cause the eigenfrequency of the system to lower and the amplitude to increase. The resulting change in frequency response is discussed in section 8.7.2.

3.3.2 Matrix choice

Considering all, no strong technical reason was found for using PA6 over PP given the requirements for the intended application. The current trend in automotive seems to be that PP is chosen in more and more applications [49], especially if the temperature is not a limiting factor, as it has a two to three times lower cost than PA [20]. PP has some advantages as it is cheaper, much less moisture sensitive, can be processed at lower temperatures which saves time and energy, and requires less energy in polymerization which results in a lower CO_2/kg [78]. Thus the rational choice would be to go for PP. However, as the amount of information on PA6 is much greater both in literature and from companies [4], PA6 was chosen for this project. Thus the matrix material for the CCB will be Polyamide-6.

3.4 Comparing glass and carbon fiber

3.4.1 Fiber options

The most commonly used fibers are glass and carbon fibers [3, 4, 79]. The differentiating properties of GF and two types of CF are given in the list below [80]. There are a number of types of GF, but the most widely used type is E-glass which is also what is normally used in fiber-reinforced composites [81, 82]. Intermediate modulus CF is usually limited in use to aerospace applications, with the automotive industry using the cheaper Standard Modulus CF.

- Electrical Glass (E-Glass or glass for short), low cost hence most commonly used glass fiber, relatively high strength of around 2400-3450 MPa, relatively low modulus of about 70 GPa.
- Carbon standard modulus, also known as high strength carbon, most common carbon fiber, with a high tensile strength of about 3500-4800 MPa, and a modulus of about 220-265 GPa, low impact

strength, relatively expensive and requires large amounts of energy during production [83, 84]

- Carbon intermediate modulus, a tensile strength of about 4100-5900 MPa, a higher modulus than standard modulus carbon fiber at about 265-320 GPa, also more expensive. Widely used in aerospace applications [85, 86]

3.4.2 Material indices

To compare different potential materials that can be used for the CCB the material properties of some common automotive-grade thermoplastic composites are compared to that of high-strength steel and high-strength aluminum [19, 23, 87, 88]. As the fiber angle is important too, for the cross-ply up the values of the cross-ply at a 45/-45 angle are given too, these were determined using the ABD-matrix. In table 3.4 the Young's modulus and corresponding material indices are given, and in table 3.4 the same is done for the shear modulus. The meaning of each material index will be discussed too.

A composite has the best properties in the direction of the fibers, if all the fibers are aligned, such as for a UD composite tape the properties are closest to that of the dry fibers. However, since a composite requires a matrix to hold the fibers together, the properties are a combination of that of the matrix and the fiber. If the fibers are placed in multiple directions, the properties in a single direction drop, although in other directions they improve. A common layup in automotive is a cross-ply with fibers in a 0/90 layup, this drops the properties compared to the UD material, shown in table 3.4. If the load in a part is required in every direction a quasi-isotropic layup can be used, this has fibers in the 0, 45, and 90 directions. However, this further drops the specific modulus as is clearly shown in table 3.4. Going from a cross-ply to a quasi-isotropic layup drops the specific modulus by about 10-30%. This means the weight advantage of composites is reduced if a part has to withstand large loads in all directions and shows the importance of optimization of the layup.

Table 3.4: Comparison of performance index specific properties

Material	**Density**	**Young's modulus**	E/ρ	$E^{1/2}/\rho$	$E^{1/3}/\rho$
	[kg/m^3]	[GPa]	$[\frac{Pa \cdot m^3}{kg} \cdot 10^6]$	$[\frac{Pa^{1/2} \cdot m^3}{kg}]$	$[\frac{Pa^{1/3} \cdot m^3}{kg}]$
UD PA6 CF 60 wt%	1450	100	69	218	3,2
UD PA6 GF 60 wt%	1730	30	17	100	1,8
Cross-ply 0/90 PA6 CF 50 wt% (45/-45)	1460	43 (28)	29 (19)	142 (115)	2,4 (2,1)
Cross-ply 0/90 PA6 GF 50 wt% (45/-45)	1800	21 (16)	12 (9)	81 (71)	1,5 (1,4)
Quasi-isotropic PA6 CF 50 wt%	1460	36	24	129	2,3
Quasi-isotropic PA6 GF 50 wt%	1800	19	10	76	1,5
High-strength steel	7850	210	27	58	0,8
Aluminum 6061 T6	2710	69	25	97	1,5

The specific modulus, E/ρ, of the materials given in table 3.4 is a good value to compare the stiffness between the materials quickly. However, that value is only for pure tension of the material. Different performance indices based on Ashby's work [89] are given in table 3.4. $E^{1/2}/\rho$ should be optimized for the lightest beam against bending and buckling under compression. This is the case if the shape is chosen and the section area can be changed as needed [90, 91]. Depending on what is limiting it could also be that another of the indices should be optimized [91]. If a beam is loaded in bending and can only change in height, the $E^{1/3}/\rho$ index needs optimized. $E^{1/3}/\rho$ should also be optimized against the bending and buckling of a flat plate, for example, the bodywork of a car.

The high stiffness and low density of CF give it superior material indices for most layups compared to the metals. Only the 45/-45 and isotropic layup score worse than the metal for the pure tension E/rho index. The very common cross-ply GF layup has no index in this table higher than that of the aluminum given, at best it is similar for $E^{1/3}/\rho$. The isotropic and 45/-45 GF layups perform even worse. This shows that for the bending of a beam at the lowest weight aluminum will likely be the better material choice compared to GF based on the material indices.

Table 3.5: Comparison of performance index specific properties for torsion

Material	**Density**	**Shear modulus**	G/ρ	$G^{1/2}/\rho$	$G^{1/3}/\rho$
	$[kg/m^3]$	[GPa]	$[\frac{Pa \cdot m^3}{kg} \cdot 10^6]$	$[\frac{Pa^{1/2} \cdot m^3}{kg}]$	$[\frac{Pa^{1/3} \cdot m^3}{kg}]$
UD PA6 CF 60 wt%	1450	3,8	2,6	43	1,1
UD PA6 GF 60 wt%	1730	3,4	2,0	34	0,9
Cross-ply 0/90 PA6 CF 50 wt% (45/-45)	1460	5,2 (20,3)	3,6 (13,9)	49 (98)	1,2 (1,9)
Cross-ply 0/90 PA6 GF 50 wt% (45/-45)	1800	4,4 (9,3)	2,4 (5,2)	37 (54)	0,9 (1,2)
Quasi-isotropic PA6 CF 50 wt%	1460	12,8	8,8	77	1,6
Quasi-isotropic PA6 GF 50 wt%	1800	6,8	3,8	46	1,1
High-strength steel	7850	80,0	10,2	36	0,5
Aluminum 6061 T6	2710	26,0	9,6	60	1,1

Since the CCB is also subjected to significant torsion loading, the material indices with the shear modulus are given as well in table 3.5. For composites the shear modulus is dependent on the direction as well, hence the values of the cross-plies at a 45-degree angle are given in brackets. If we assume the CCB is a hollow shaft in torsion, then $G^{1/2}/\rho$ should be optimized if the section area is free or $G^{1/3}/\rho$ if the wall thickness is fixed but the outer radius is free. In these cases, the composites can be similar or better to steel and aluminum. Especially if the 45/-45 fiber direction is included in the layup, as it increases the shear modulus of the composites is significantly. Depending on the layup aluminum can still be a better option. However, limitations might apply to certain dimensions, for example, the outer radius of the beam due to available space. If only the wall thickness can be changed G/ρ should be optimized for a hollow shaft, in which case steel and aluminum are the better choice over the composites. This shows how important it is for composite products to use larger outer dimensions to get the benefit of weight savings in certain scenarios. Again, the CF 45/-45 cross-ply and isotropic layup can often outperform the metals. However, for GF the material index is lower than that of aluminum for $G^{1/2}/\rho$ and only barely better for the $G^{1/3}/\rho$ index. Thus for torsion, it is again challenging to get a lighter beam using GF compared to aluminum based on the material indices.

The material indices show it is challenging for a GF composite beam to be lighter than an aluminum beam. However, other factors than the material indices shown have to be factored in too. An important one is material and production costs, but factors such as damping, corrosion resistance, and fatigue resistance can also play a role in material selection [90].

3.4.3 Material costs

The superior properties of CF composites come with higher material costs, as can be seen in table 3.6. In table 3.6 the costs per kg of different materials have been given. The aluminum and steel mentioned are commonly used for cross members in automotive [19, 92]. For the composites the material costs for the base materials have been given and the costs for the woven fabric composite.

Table 3.6: Material cost per kg

Material	**Costs per kg [EU]**	**Source**
High-strength steel dual-phase	0.8	[19]
Aluminum 6061 T6	2.25	[19]
PA6	3	[93]
CF (HS 3k tow) dry fiber	35	[8]
GF dry fiber	3	[9, 10]
GF PA6 Tepex woven fabric	6	[19, 43]
CF PA6 Tepex woven fabric	25	Estimated [37]

It can be challenging to get a good indication of the cost of the base materials as prices can have a wide range and the material definition of mentioned prices can differ too [94], a range of the costs are given in fig. 3.4.1. The dry CF price has been taken from a recent extensive research estimate into the costs

of CF [8] combined with the info on the type of fiber used in a common CF PA6 composite used in automotive called Tepex with 3k high strength CF tows [87]. The weight percentage of CF and PA6 has been multiplied by their respective material costs and some costs were added on top of that for production. The cost for production was estimated to be about the same difference between the raw material costs of the GF PA6 based on their weight and material costs compared to the costs of the GF PA6 Tepex laminate [19]. The estimated cost of 25 EU/kg for the CF PA6 Tepex and 6 EU/kg for GF PA6 Tepex has a similar ratio as found in the literature, stating that the material cost of CF PA6 was found to be five times higher than GF PA6 [37]. The difference in the pure fiber costs can be even higher, as seen in fig. 3.4.1.

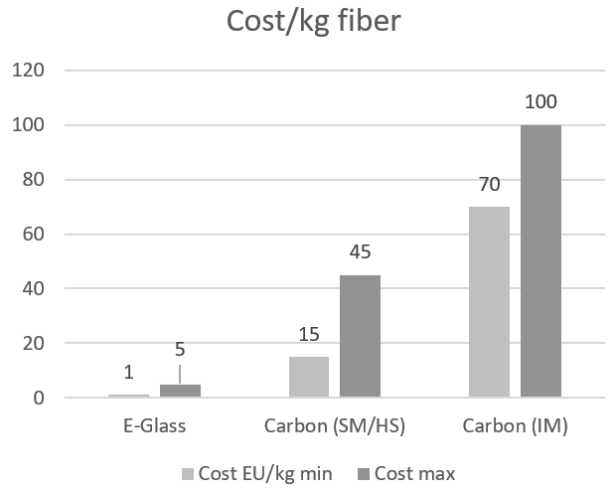

Figure 3.4.1: Cost per kg of dry fiber [7–10]

Next to the material cost, CF has about ten times higher CO_2 emissions per kg of material than GF. Using a higher-performance material such as CF or magnesium and thus reaching a lower weight does not necessarily result in the lowest environmental impact [26]. The emission reduction gained by the weight savings due to CF can for a large part be offset by the emissions of its production [26]. Thus if it is possible to fulfill the requirements using GF could be beneficial for the cost of the CCB. Although this would come at the cost of higher weight.

3.5 Costs composite products

Next to looking at the price difference between material options such as done above, it is also important to put those costs in perspective by comparing them to the current value of weight. The value of weight is the accepted cost per kg saved. Next to material costs, the manufacturing and design costs can also differ compared to metals.

The largest inhibitor of widespread use of composites for high-volume manufacturing is due to the high cost [95]. Carbon fiber composites can offer a 50% weight reduction with regards to steel, but currently at more than five times the cost. Although it is expected that the price per kilogram of a carbon fiber composite will reduce [96]. The high price of carbon fiber is acceptable in the aviation industry where the value of weight is between 500-2000 EU/kg [97, 98]. However, in BEVs, the accepted cost per kg saved is estimated at 5-17 euro, and for internal combustion engine cars it is even lower at 1-9 EU/kg [96, 97]. It is estimated that with a limited application of carbon fiber in only the most critical parts for stiffness, lightweighting would cost about 4 EU/kg saved in 2030. Whereas extensively using carbon fiber for maximum weight savings will come at a cost of 8-10 EU/kg saved [96]. If the carbon fiber price does drop like predicted it would make lightweighting by using carbon fiber in the cost range it would need to be. It is estimated that at a cost of 7-8 EU/kg for CF it would open up the possibility of mass manufacturing CF parts for automotive [7]. However, other options for lightweighting are available too, often at a lower cost [96].

Adding to the challenge of using composites is the short design cycles in the automotive industry of only 20-30 months [97]. To gather all the data needed for a new composite material extensive testing is required, estimated at a cost of 500.000 euros [97]. The cost of retooling to composite products is also a barrier as the initial investment for potentially new tooling for composites is needed [99]. However, certain processes such as stamp forming of thermoplastics need very little extra investment to make use of the already widely used sheet metal stamp forming machines [37]. Tooling costs for composites are about 40% lower or even more compared to steel-stamping tools [30, 37, 100].

A disadvantage of the versatility of composites is that they also have a much larger number of parameters that can change in the design, making design and optimization more challenging and thus costly compared to metals [101]. A solid multi-objective analysis of material choice, production method, and design strategy is needed to reduce the design cost [97].

Chapter 4

Production Methods

The CCB can be divided into two parts, the long structural horizontal beam and the branches attached to it. The branches will be injection molded onto the beam as is already commonly done, see fig. 3.1.1. For the structural part of the beam three production processes are discussed: braiding, pultrusion, and press forming. Two automated high-speed methods to manufacture the blanks that are shaped by the press forming are discussed after. As the focus of this research is on making a continuous fiber thermoplastic structural part both injection and compression molding are not an option for the main part of the beam in this work. In section 4.6 a visual overview of some of the possible production process routes is given. The chapter ends with the concept choice for the CCB in section 4.7.

4.1 Braiding

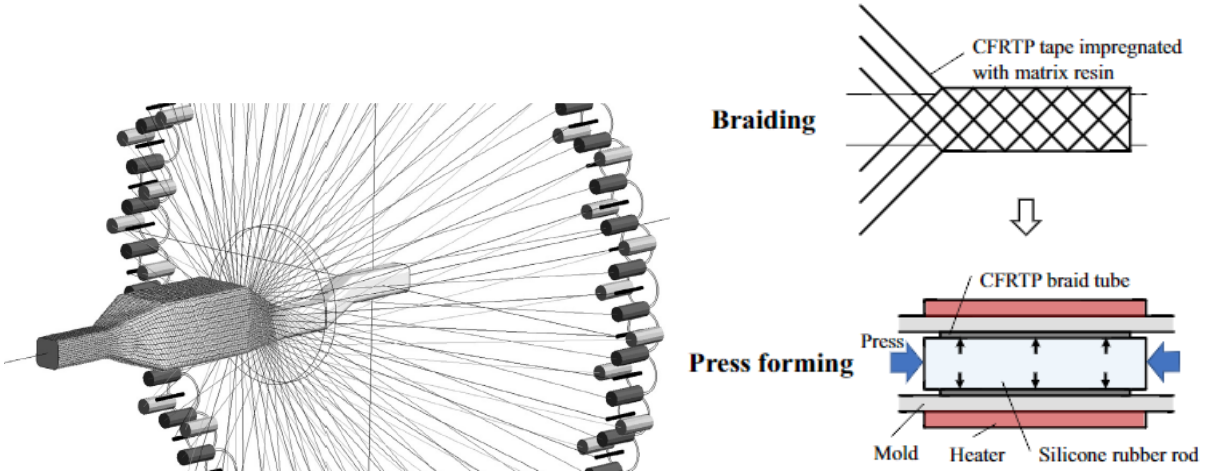

(a) The braiding of a shape similar to a CCB [102]

(b) The process of braiding and consolidation using press forming [103]

Figure 4.1.1: Braiding

Braiding is a production process that interlaces fibers around a mold as is shown in fig. 4.1.1a, creating a preform, similar to a sock. With thermoset braiding, the preform can be made up purely out of dry fibers which can later be impregnated by a thermoset matrix using resin transfer molding. However, for thermoplastics, in most cases [104], resin transfer molding is not possible due to their high viscosity [105], so their processes are different. The viscosity of molten thermoplastics is in the range of 100-5000 Pa s compared to that of uncured thermosets which are as low as 0.03-1 Pa s [4, 106, 107]. The high viscosity would also mean a longer processing time as the flow rate is substantially lower. Trying to impregnate fibers with a higher viscous thermoplastic matrix would also result in dry fibers as the matrix

penetrates slower into the fibers and voids as trapped gasses move slower through it, vastly reducing the performance of the part. Inhomogeneous temperature regulation can also cause locally increased viscosity and its subsequent issues. Although research is being done on in situ polymerization, which would allow the impregnation of dry braided products with a thermoplastic matrix using a similar process as currently used with thermoset matrices. The unpolymerized matrix has a low enough viscosity for proper impregnation after which it is heated to form the eventual polymer [105]. This would thus avoid the issues arising from the high viscosity of the conventional melting processes of thermoplastics [105, 108]. Although very promising, the current availability of monomers that are both economically viable and have feasible production processes is very limited [108].

Thermoplastic braiding is conventionally done either using commingled fibers or by using thermoplastic UD prepreg tapes [109]. Commingled fibers are dry glass or carbon fiber bundles that have thermoplastic fibers in them too. When heated the thermoplastic fibers melt and flow to fill the gaps as it becomes the matrix and binds everything together [104, 110]. With the matrix already within the fiber bundles, the distance it has to travel during melt is short, this ensures good fiber wet out.

Braiding can create quite varying shapes, from a simple straight profile to varying cross-section thicknesses and curved shapes, as is shown in fig. 4.1.1a and fig. 4.1.1b. Thus it would be capable of producing the three non-die cast beam types of CCB beams found in cars, see fig. 2.3.1. Braiding shows the potential for a high degree of automation and low-waste production, as low as 5-10% [111], compared to 10-26% in fig. 4.4.2b, for example. An advantage of braiding is that insert can be integrated [112]. Interlaced structures with a lack of seams can be produced with braiding, this gives a higher impact resistance and toughness than other composite manufacturing methods [113]. This is even better for 3D braiding with fibers through the thickness, thus greatly increasing interlaminar strength [102]. However, due to the undulation of the fibers, 2D braided composites are less stiff than laminates [113]. This is not the case for 3D braided structures which can be comparable in strength and stiffness to laminates [102]. Although, the fibers are often still loaded off-axis, limiting the mechanical properties of the braided product.

After braiding the thermoplastic preform it needs to be consolidated, this is done by applying heat and pressure to melt the matrix which flows to fill the gaps and create one solid product, an example of this is shown in fig. 4.1.1b. Usually, the preform is placed in a heated mold with a bladder inside of the preform which is blown up to apply pressure. This process is shown in fig. 4.1.1b although here a silicone rubber rod is used to apply pressure instead of a bladder. It can be challenging to achieve full consolidation and avoid voids with bladder molding as the viscosity of the matrix is relatively high and the available air pressure is usually too low, hence other options such as the press forming with the silicone rod are researched [103].

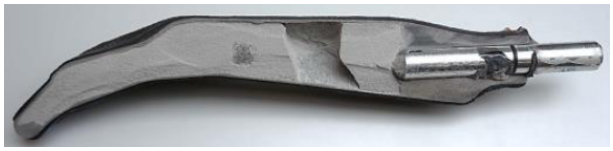

Figure 4.1.2: A soluble core for braiding and consolidating a complex hollow shape [11]

As mentioned above, usually, the preform is braided on a mandrel after which the preform is taken off the mandrel and placed inside a mold with a bladder inside the preform. Another option is to braid around the mold directly, as is shown in fig. 4.1.1a, this allows for more complex shapes [11]. The mold could be a lost core mold such as shown in fig. 4.1.2, which, after consolidation, can be easily removed by dissolving it. These cores can be manufactured cost-effectively by a pressing or casting process for high-volume [11]. It is claimed the raw material is sustainable and environmentally friendly, and the raw core material can be recycled for 98% [11]. The wash-out of the core can be done using a water-soluble, non-toxic solvent and requires no additional energy [11]. If lower volumes are needed, for prototyping for example, then machining and printing of the cores are options too. Another option is to leave the core in place, this can help support against buckling with subsequent injection molding or in general use.

Achieving proper consolidation for thermoplastic braiding remains challenging [103]. To improve consolidation multiple steps are often required, increasing production time [103]. Good consolidation quality has been achieved for thin parts, but the 10-minute consolidation time required was considered short for

thermoplastic braiding [114]. For thicker parts achieving high enough pressure for proper consolidation and short enough heating times might be more challenging.

Braiding is a mature technique for thermoset production, being used in both aerospace for landing gear for example [115], and in automotive for A-pillars [45], both structural parts. The braided structural parts are currently limited to high-end markets with limited volume production. However, TPC braiding has received much less research attention and currently sees only little use in the industry [116]. The challenges with proper consolidation due to the high matrix viscosity remain very challenging [108, 114]. Even if proper consolidation can be achieved the long consolidation times cannot reach the required cycle times for high-volume production as set in the requirements in section 2.2. In situ polymerization could be the solution, but that is currently not mature or economical enough yet [108].

4.2 Pultrusion

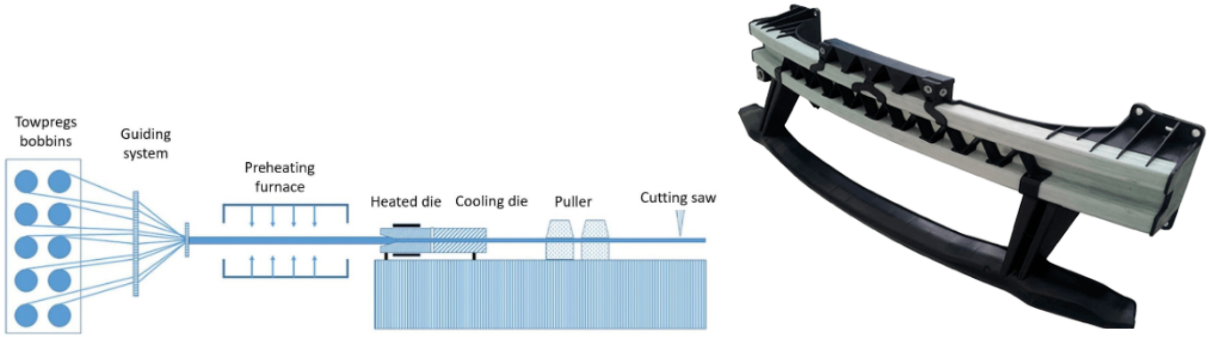

(a) A schematic overview of a nonreactive pultrusion production process [106]

(b) Injection molding of additional parts such as crash boxes, reinforcement ribs and a lower bumper [66]

Figure 4.2.1: Thermoplastic pultrusion

Pultrusion is similar to extrusion, apart from that the part is pulled through the mold instead of pushed. The process described here is for thermoplastics as that of thermosets is different. The process is shown in fig. 4.2.1a, tows, bundles of fibers, are pulled from spools and preheated. These tows could be commingled yarn, UD tape, polymer powdered fibers, or towpregs, towpregs are pre-impregnated bundles of fibers [104, 106]. Pultrusion allows very high fiber volume fractions (up to 70% [66]. A high percentage of the fibers have to be aligned in the pull direction [79]. For parts that require good mechanical properties in that direction, this is excellent, for parts that also require properties in other directions this is disadvantageous. Although, other fiber directions and even fabrics can be incorporated to improve torsional and transversal properties [112]. Pultrusion is often combined with braiding, this can also be done with TPCs using commingled hybrid yarns [112, 117]. These tows are then pulled into a heated die which melts the matrix to impregnate all the fibers. This is followed by a cooled die which solidifies the part into a solid part. After these dies the product is the puller which pulls all the material through the dies. This pultruded part is then cut into pieces.

Pultruded parts have a constant cross-section and are often straight which limits the products that can be made. Although it is possible to give pultruded parts a 2D or even 3D curvature [42, 66], such as in fig. 4.2.1b, this is not enough flexibility required for the CCB of this project, see section 2.3.3. However, if the choice was made to design a straight constant cross-sectional CCB, like in fig. 2.3.1a, then pultrusion is a good alternative as pultrusion is a good option for high-volume low-cost composite parts [112]. Pultrusion can produce parts with limited material waste, thus keeping costs low. Obtaining sufficient processing speed is one of the main challenges, heating the part at a high enough rate remains challenging, especially for thicker parts [112]. It has the potential for production speeds of 20 meters per minute for example, although the production speeds are currently limited to about 0.35 to 2 meters per minute [42, 46, 112, 118]. A disadvantage of pultrusion is that the beam is limited to a constant cross-section throughout the length of the beam, just like the aluminum hydroformed part. Thus optimization might be more challenging. As pultrusion often incorporates braiding into the process, therefore the issues with

thermoplastic pultrusion are often very similar to those for thermoplastic braiding due to the high melt temperatures and viscosity [119].

4.3 Press forming

Press forming produces parts by forming a blank between two mold halves, this process, which includes an additional step of injection molding is shown in fig. 4.3.2. It is also known as thermoforming or stamp forming. A blank is a flat laminate, or a layup, of composite plies that will be formed into the shape of the product, the manufacturing of these is further explained in section 4.4. These plies could be dry or prepregs, for thermoplastic press forming, however, the common way is to use a prepreg. The thermoplastic blank is heated, often using infrared ovens [95, 119], until it is in melt and then press formed into shape in a mold.

The mold can be made of different materials, it can be two metal halves, or one side can be a softer material such as rubber too [119, 120]. After it is formed the mold stays closed until the matrix is solidified again, called the holding time. This process is shown in fig. 4.3.2 with an optional injection molding step included. The blank can be tailored such as in fig. 4.4.3a with unidirectional and woven laminates placed where required, and thus has a large freedom in layup throughout the product too. The shape of the formed product can vary too, thus press forming is also capable of producing the three non-die cast beams in fig. 2.3.1.

Press forming is a very quick process, highly suited to large-scale economical production [37, 47]. Overall it is seen as the best process for thermoforming for high-volume, economical production of parts at a high rate [47]. A target cycle time for composite parts suitable for high-volume production was defined as 60-90 seconds [7, 37], which was able to be met with rapid-stamp forming [37], with the cycle times including layup and forming in the range of a minute to a few minutes [37, 121–123], going as low as 30-60 seconds [124]. With most of the time going to the cooling of the matrix whilst in the tool, this prevents residual stresses and warpage [119]. If too short a holding time is used, the part might become distorted as the elastic strain in the fibers might not be held properly by the matrix [47]. Next to this, longer holding times increase consolidation, thus reducing void content [47]. So a balance between this and short cycle time has to be found. This is also the case for the cooling rate, slower cooling improves the mechanical properties of the product but also increases processing time [47]. The mold could be isothermal, however, to speed up production it could be beneficial to have both heating and cooling in the mold halves [119, 123]. This could keep the temperature high enough for consolidation for longer whilst still keeping cycle times short [123].

Infrared ovens are the fastest way of heating a blank, taking one to two minutes for PEEK [119], however, the surface of the blank can get much hotter than the center, especially for thick or poorly consolidated blanks. When using poorly consolidated blanks the heating time required may increase as there is poor heat conduction through the blank [120]. Blanks made by ultrasonic spot welding required a 20% longer heating time in tests [123]. Another option than infrared ovens can be convection ovens, taking five to ten minutes, but the heating is more uniform [119].

Stamping and injection molding are already a standard in the automotive industry which makes it easier to integrate TPCs made by press forming into the existing process chain [112], only requiring low-cost extra heating equipment to preheat the blanks [37]. TPCs also require lower investment costs for press forming equipment compared to metal making them attractive for high-volume production [30, 37]. However, due to the high raw material costs, at high enough production volumes metal parts could be cheaper again [37].

Press forming has a lot of benefits, but it also comes with its challenges. The main challenges are the forming of wrinkles and buckling of fibers during forming [47, 119], an example of this is shown in fig. 4.3.1a, these can strongly reduce local strength and stiffness due to potential fiber breakage and bending. Waviness and buckling of the fibers can result in a 50% strength loss [119]. The challenging thing about the forming of fibers is that in tension the fibers are practically inextensible, but under compressive forces, they easily wrinkle. Wrinkling is especially common in double curved parts, which cause local compressive loading of fibers during forming [47]. A part could be held by grippers that hold the blank in tension at well-designed locations can aid in preventing wrinkling [119], an illustration of this is given in fig. 4.3.1b. However, using grippers does mean a part needs trimming after forming and uses

more material. Higher temperatures can also help in preventing the formation of wrinkles and improve consolidation [47].

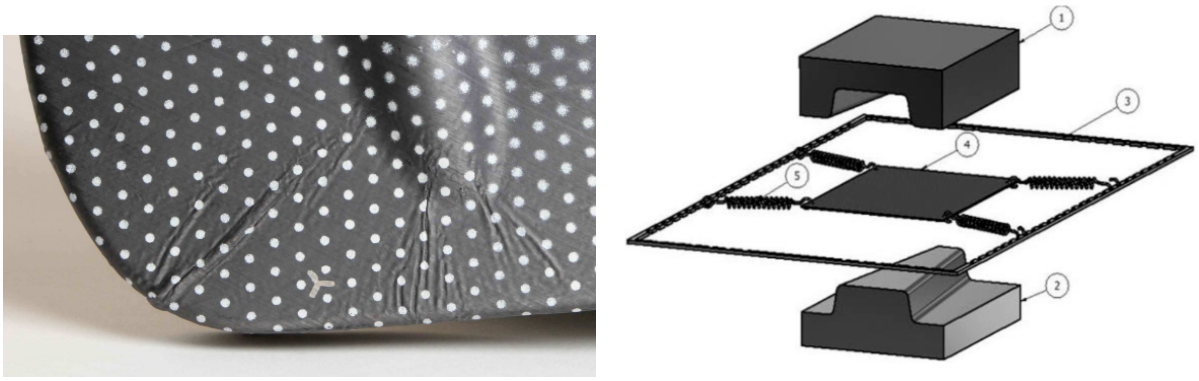

(a) Wrinkles visible in a press formed product [125] **(b)** An illustration of grippers during press forming [126]

Figure 4.3.1: Press forming products

Next to this, spring-back, spring-in, and warpage can occur after forming due to residual stresses which depend on processing temperatures and forming rates [47, 127]. Software is available to help reduce the chance of production issues, but often this assumes constant thickness fully consolidated plies [123]. More simulation software development would need to be done for the more challenging designs to have first-time right manufacturing. Otherwise, more testing could be required, with it potentially requiring expensive mold redesign and time. Especially when using tailored layups with local reinforcements forming is more challenging and currently no guidelines exist for this.

Another potential issue arises due to thickness variability in the blank. If the blank shows different thicknesses either due to the layup or variations in laminate thickness, then the local pressure could show large differences and cause issues such as voids [47, 119, 123]. Especially matrix-dominated properties, such as the flexural strength and modulus and the interlaminar shear strength (ILSS) are impacted most an increasing void content [47]. A composite with voids of 1 to 3% can already have a decreased transverse shear modulus of 15% [128]. The sensitivity to these issues depends on the compaction and flow of the material used [123]. With automotive composites often having a less tight weave and lower viscosity matrices this problem might be less than for aerospace. The use of a non-rigid mold, such as silicone rubber, on one side can improve consolidation even with some thickness variation as it provides a more equal pressure distribution [119, 120, 123]. However, such a rubber mold may have a shorter lifetime and introduce residual thermal stresses thus precision forming of parts can be challenging [127].

4.3.1 Overmolding

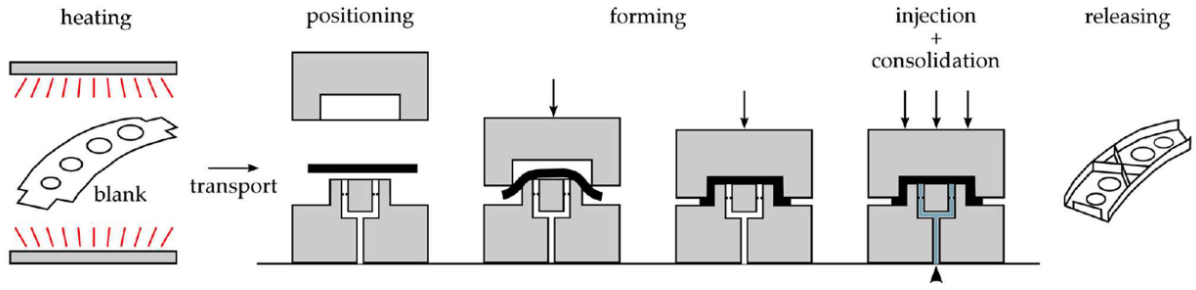

Figure 4.3.2: The process of overmolding: a combination of press forming and injection molding. Figure reproduced from Bouwman [12]

Overmolding has a number of benefits which includes a potential for a high level of function and reinforcement integration as mentioned before. The steps of the overmolding process are shown in fig. 4.3.2.

In a single-step process, the press forming and injection molding are done in one mold as shown in fig. 4.3.2. In a dual-step process, a part is first press formed, after which it is taken out of the mold and the injection molding is done in another mold.

Next to function integration, overmolding also allows for net-shape production [129, 130]. To create a net-shape product the edges of the part are injection-molded, as is shown in fig. 4.4.3b. This no longer requires subsequent trimming of the composite part by using water-jet cutting for example [37]. The net-shape molding also allows for the molding of holes and cut-outs [123]. If too little margin is kept for the edge then a slightly misplaced product could hinder the flow around the product [131]. Larger edges are therefore a safer option, as is clearly done in fig. 4.4.3b, it does add weight but it can be a good solution for mass manufacturing [131].

If a single-step overmolding process is used then it is possible the laminate under the ribs can deconsolidate before the molding takes place with matrix squeeze out and displacement of fibers into the rib cavities in the mold [131]. This fiber displacement could mean a local weakness as a bend is introduced in the fibers. On the other hand, however, it was found the interface was strengthened by the displaced fibers going slightly into the injection molded ribs [131]. This usually results in larger sink marks in the final product than the dual-step process would give. The overmolding process could cause fiber redistribution which makes predicting the actual interface strength difficult [131].

When using a dual-step process, it is important the temperature is high enough for long enough to have proper healing. This is more challenging than in a single-step process, as the heat from the injection molded plastic has to melt the surface of the press-formed part too with the dual-step process. If not designed properly the dual-step process could show micro-cracks due to improper bonding as a result of the rapid cooling [131].

Due to the faster cycle time of a single-step process and the potential for a stronger more reliable interface, the single-step process seems to be the better option for the molding of semi-structural ribs for the CCB.

(a) Press formed and over-injection molded product [132]

(b) Two press formed shell halves welded together [133]

Figure 4.3.3: Stiffening options of press formed products

4.4 Blank manufacturing

Before a part can be produced by press forming a blank is needed. A blank is a flat layup of multiple plies that can be laid up by pick and place or by Automated Tape Placement (ATP) for example, both

of these processes are discussed below. The loosely consolidated blank can be preconsolidated in a flat mold first before forming the actual part [134], although this seems to not be required [120, 123], this is discussed in section 4.4.3.

A benefit of making a composite blank is that it can be tailored so that is optimized based on the load requirements by changing the material or thickness locally. This reduces the weight of the final part and it can also reduce material usage, if done right it can reduce the scrap rate too [135]. As opposed to metals, for example, composite waste cannot be recycled to a similar quality level, at best it is downcycled into injection moldable pellets. Since material costs are a large part of the cost of composite products a reduction of scrap during production could lower the costs of composites significantly [136]. Tailored blank making has the potential to reduce material waste by as much as 60% [137], although this heavily depends on the shape of the blank.

4.4.1 Automated Tape Placement

An option for the manufacturing of the flat blank is by using ATP, this flat blank can then be shaped using press forming. The process of tape placement is shown in fig. 4.4.2a. This is currently mostly done with multi-axis robotic arms which allow tape to be placed at any angle on complex 3D surfaces. Using ATP with in situ consolidation allows for a high degree of optimization of the part by adjusting the fiber angle and amount of material throughout the product based on local requirements. Adapting the blank layup based ATP can also be used to apply local reinforcement on a blank which can then subsequently be press formed [138]. This can even be done with different material combinations. Using ATP for produced tailored load and waste-reduction optimized flat blanks shows potential for mass manufacturing [37, 123]. However, the layup rate of ATP on a three-dimensional part is too slow for a cost-effective mass-produced composite part in the automotive industry [139]. With typical layup speeds of ATP being about 5-15 kg per hour [19, 140]. Therefore, the focus here is on flat blank making.

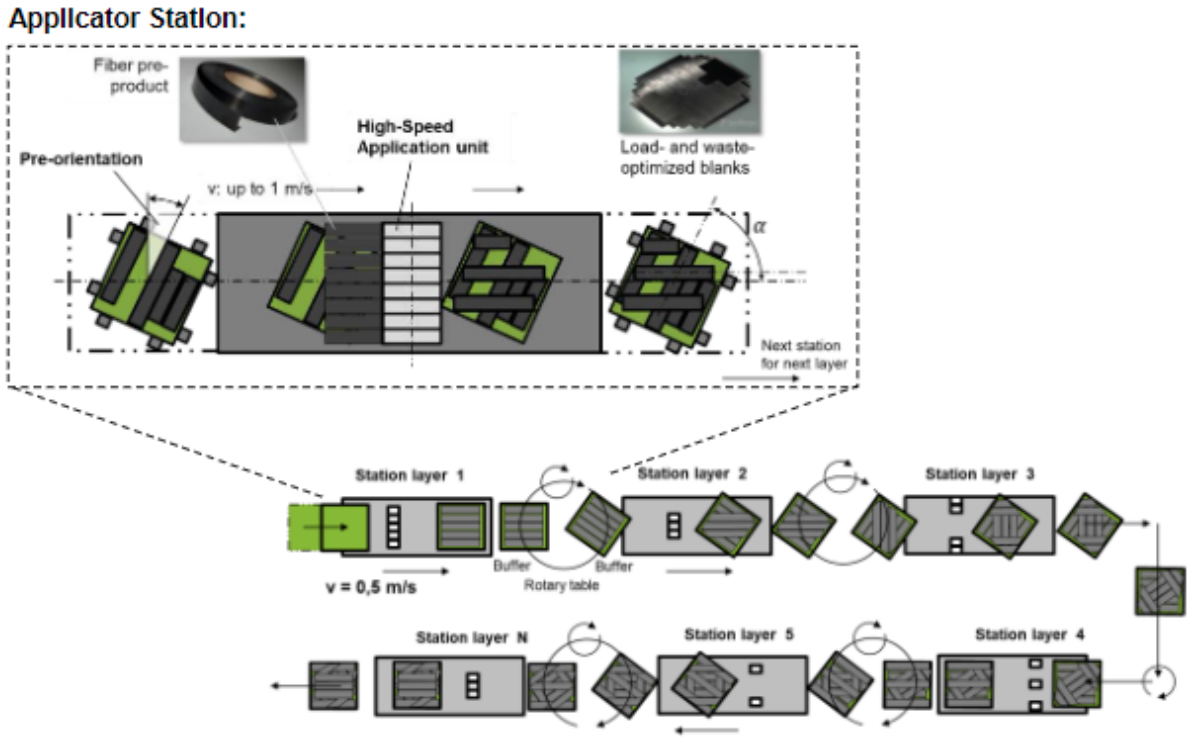

Figure 4.4.1: A production line with multiple applicator stations [13]

For a flat part, the layup rate of a multi-axis robot arm is not required and it limits the layup speeds. To achieve the high speeds of ultra-fast tape placement another system is used. Instead of moving tape laying heads, the blanks are built up on rotating tables, this allows the placement heads to only require travel in one direction [13]. Ultra-fast tape placement has been shown to be able to make a fully consolidated

thermoplastic blank with a cycle time of only five seconds [13]. This is done by using multiple applicator stations and per applicator station up to 28 applicators can be used. It is claimed that the output of this process can be over 500 kg per hour, which equals over eight kilograms per minute [13]. Another ATP machine with a single head has claimed to be able to produce 100 kg per hour [141]. This would suffice for the requirement of a cycle time of one CCB per minute, as their weight is around one kilogram.

Tailored blanks can reduce material waste substantially [13, 123, 136, 142]. Reducing material cost is one of the main inhibitors of the more widespread use of composites as the part cost is dominated by material cost [95, 136], which is especially the case for high-volume production. The waste rate of the composite material even with optimized nesting can be as high as 27%, meaning a large share of the part cost is for scrap material. Even for a relatively square example, the total material usage dropped by 12% just by using near-net-shape layup [123, 142].

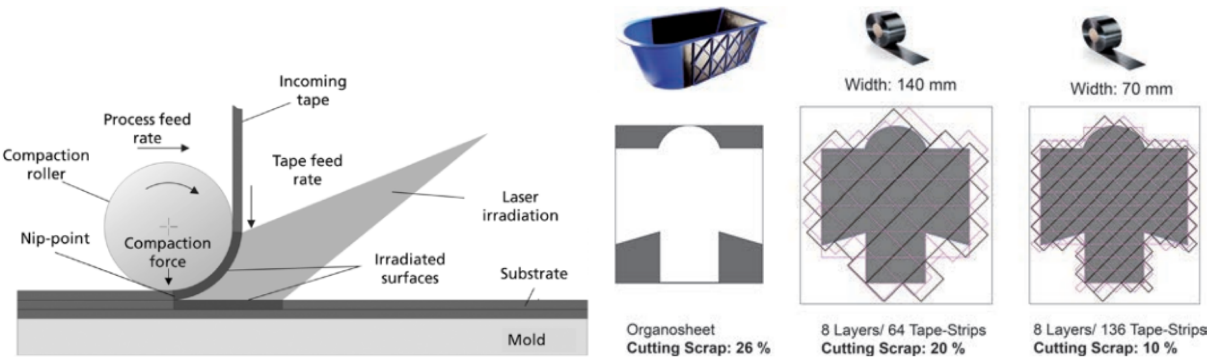

(a) An overview of the process of tape placement [139]

(b) Difference in the scrap rate of a blank production compared to different tape widths [142]

Figure 4.4.2: Automated tape placement

A disadvantage of tape placement is that at non-0 or 90-degree fiber angles a sawblade edge is created as the tape is cut, see fig. 4.4.2b. This sawblade edge needs to either be trimmed into the exact shape or the edge can be overmolded, providing the exact shape in another way. The smaller the tape width for layup the lower the potential scrap rate, see fig. 4.4.2b, although at the cost of longer cycle time.

4.4.2 Pick and place

Instead of putting down tapes of a constant width like with ATP, it is also possible to cut out net-shape plies [134], this reduces the number of loose strips that need to be placed. These plies can be cut out of a roll of pre-impregnated wide tape or out of a pre-impregnated woven fabric, both are used in fig. 4.4.3a. Just as with ATP, it is possible to have a multi-material layup, for example, the majority of material being glass fiber with some carbon fiber reinforcements. As the shape is cut it is also an option to include holes in the plies [143].

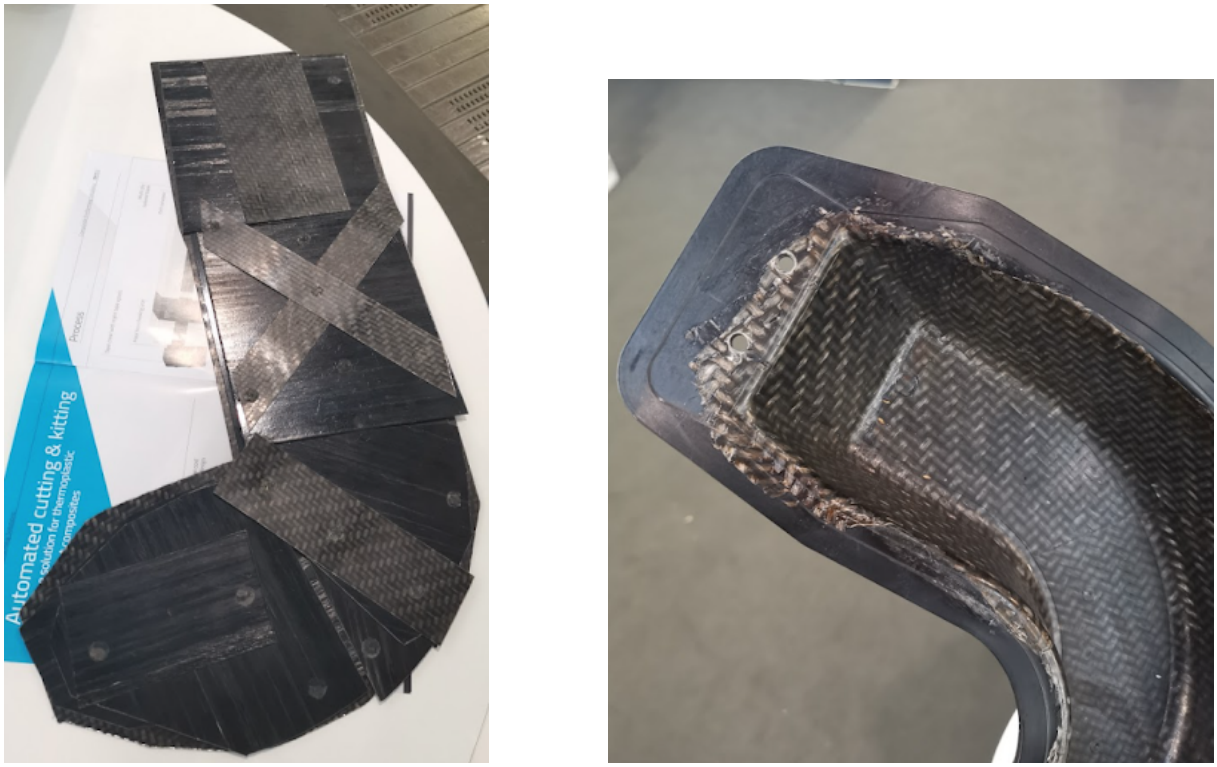

(a) A tailored blank [121]

(b) Net-shape using injection molded edges [121]

Figure 4.4.3: Pick and place layup followed by overmolding

The cut TPC plies are then stacked using a robot arm with attached vacuum grippers [144]. The first ply is put on a stacking table, this often uses a vacuum to keep the ply in place [134]. The following plies are often laid down in place and spot welded to the layer below it whilst still held by the vacuum grippers, see fig. 4.4.4. This way the ply stays in place and does not buckle [14]. The marks from the spot welding are also visible in fig. 4.4.3a. The stacking of a single cutout can be done in under 4 seconds [134], thus with large net-shape cutouts the stacking of a full part can be done within the cycle time of the press forming.

The blank shown in fig. 4.4.3a can be manufactured with pick and place and single-step overmolded with a cycle time of only one minute and an output of five kg per minute [129]. The total time spent on a single product is longer, but since the part moves through the production line only the slowest process is limiting. The actual time required depends on the number of separate plies, but probably mostly on the thickness of the product as the heating of the product is the limiting factor. For example, the part shown in fig. 4.4.3a with 13 loose patches requires 40 seconds for preforming. This is followed by 50 seconds in a conduction oven for slower heating through the whole product, then 60 seconds in an infrared oven. The final step is overmolding which takes another 60 seconds [135].

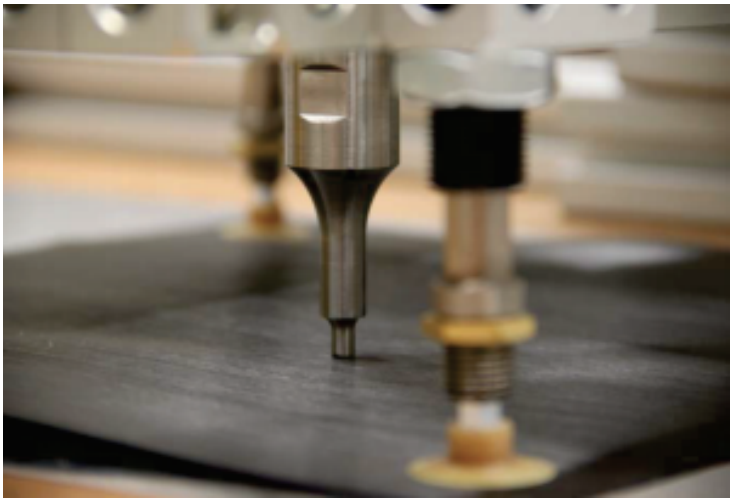

Figure 4.4.4: Spot welding after placement by vacuum grippers [14]

4.4.3 Preconsolidation of blanks

After the different plies are placed either by pick and place or by ATP the plies can have a large number of air gaps between them, or even be mostly loose apart from the welded points. In the final product, it is important to have a low void content. Voids are trapped pockets of air or other gasses and can significantly lower the mechanical properties of a composite. One way to lower the voids in the blank is by preconsolidation, which is the process of turning the separate plies into a single laminate before the press forming process of the actual part. Preconsolidation can be done by press forming the blank in a flat mold, this process melts the matrix and presses the different layers together, pressing out the air and bonding the plies together. This leaves fewer voids in the blank which might not be able to be pressed out during the rapid pressing and cooling of the material during the press forming of the part. However, this preconsolidation after layup is an expensive process as it adds another production step.

Research has shown though, that press forming can deliver similar consolidation quality in the final product with a large difference in the consolidation quality before press forming [120]. The product after press forming with blanks with very little consolidation, such as those made by ultrasonic spot welding with pick and place and rapid ATP, showed no noticeable difference with preconsolidated blanks, both achieving a void content of below 1% [120, 123]. To further increase the chance of proper consolidation, matrix-rich prepreg surfaces can be used [123]. Thus potentially the expensive press-consolidation step can be left out.

4.4.4 ATP vs Pick and place

Pick and place has some benefits over ATP as it can place large woven fabrics in a single step and the cutouts can be more complex without the sawblade edge. Next to this, the size of cutouts is easier to change with pick and place than with ATP where tape width determines what shapes can be made. As for the speed of production, it depends on the shape, the more complex shapes the slower ATP will be. However, ATP could be quicker if a large number of fiber angles are needed such as for a very tailored layup with fibers along the load paths. This could also result in ATP having a lower material scrap rate. The cutouts of pick and place, despite optimized nesting, could still result in a higher material scrap rate than that of ATP.

The choice between ATP and pick and place depend on the design of the part and the production volume. As for the CCB in this research, pick and place is deemed to be the better-suited process as it can quickly place the large 45/-45 plies with the length of the CCB. As described in section 4.4.2, pick and place combined with overmolding likely has enough material output within the required cycle time for the composite CCB.

4.5 Creating a closed profile from press formed parts

A drawback of press forming is that the products cannot be made hollow, and are thus limited to open U shaped-profiles. This limits the torsional stiffness when compared to a closed-box product. This drawback could be resolved by closing the box with another half or by molding ribs. It is common to press form and injection mold ribs and branches in one step, an example of this is shown in fig. 4.3.3a.

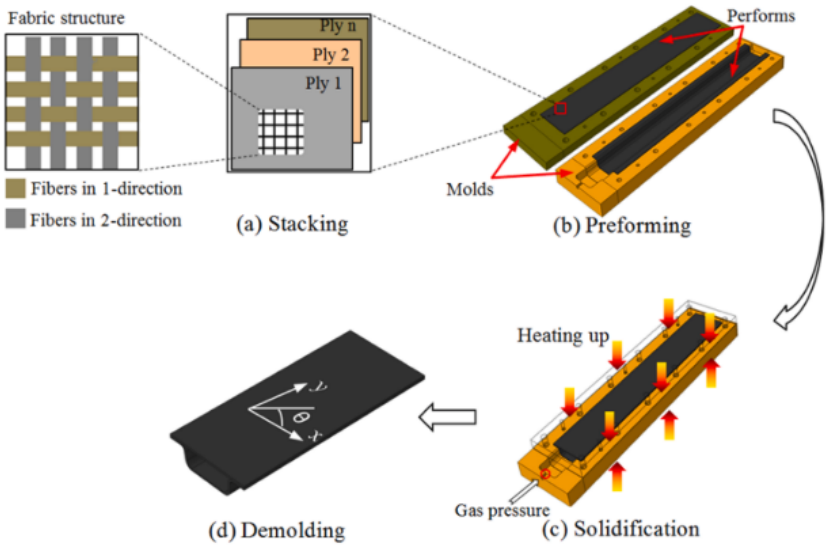

Figure 4.5.1: Thermoforming of a top-hat shape [15]

In automotive steel open hat channels are often closed with a plate that is joined by spot-welding [145] or a combination of adhesive and rivets [37]. These shapes are commonly used to resist bending loads [15]. In fig. 4.5.2a the potential dimensions for the CCB top hat shape are shown. These techniques could be used for TPCs too. However, having holes for a mechanical connection like rivets introduces the risk of stress concentration or bearing failure. Next to this, making these holes is likely to produce dust, which needs to be dealt with as it is harmful to humans and machines, especially carbon fibers. So if it can be prevented that is a big advantage. Using adhesive can also be challenging, especially with a plastic-like polypropylene which does not bond well with adhesive without proper treatment [19].

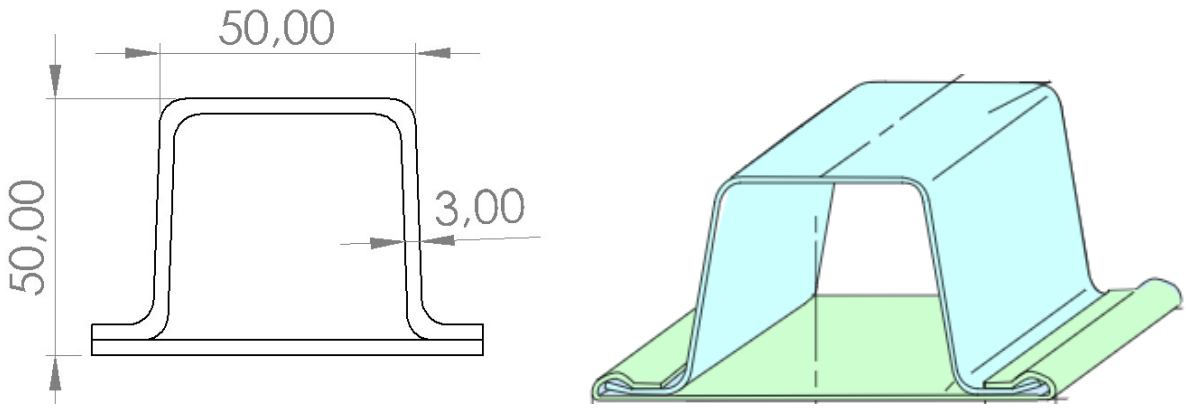

(a) The dimensions of the top hat channel with the plate

(b) Hemming the edges to connect two parts

Figure 4.5.2: Top hate shape

Another option, made possible by the use of thermoplastics is to weld two halves together as is shown in fig. 4.3.3b [119], or to melt the two parts together using two mold halves and internal pressure [15].

Although both of these options do add another production step. The use of press forming with overmolding and welding allowed function integration and a weight reduction of 30% [133]. An advantage of welding over using adhesives is that it can join thermoplastics that might be hard to bond an adhesive to, and it does not introduce another material, making recycling easier. On top of this, it can provide stronger bonds at an improved speed [146]. A shear strength equal to the shear strength of the continuous fiber composite can be achieved with PP [147], an otherwise challenging material to use adhesives on.

Another option that is more conceptual for composites, but is commonplace for sheet metal is hemming [148]. Hemming, or folding, one part around the other part, as is shown in fig. 4.5.2b could create a very strong bond not based purely on adhesion but by form locking the parts together. For composites this hemming would require bringing the material in melt to fold it, this could also have the added benefit of welding the two parts together in this hemming process. To also lock the parts in the lengthwise direction indentations could be molded in the blue part into which the green part can lock along the length of the top hat shape. Hemming and welding are not exclusive, so the parts could be welded together after they have been formed in case a stronger connection is required.

4.6 Overview production routes

An overview of the discussed production processing routes for thermoplastic composites is illustrated in fig. 4.6.1. For clarity, only the options discussed are shown. Other steps such as welding, applying adhesives, or using other connections are possible with all routes and are left out for clarity too.

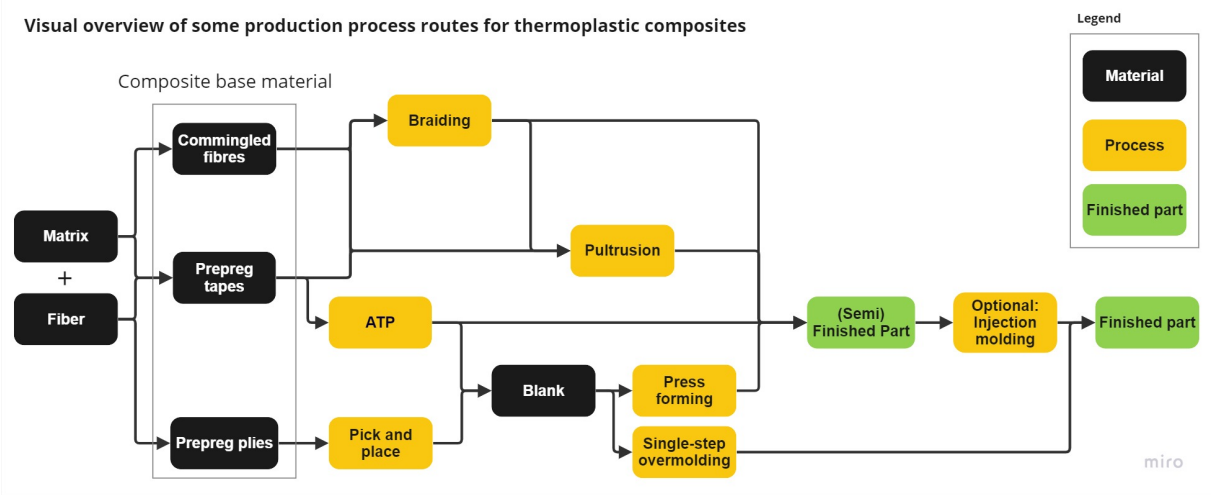

Figure 4.6.1: Visual overview of some of the discussed production process routes for thermoplastic composites

4.7 Concepts: Overmolding and braiding

Two production methods were deemed most suitable for the production of the proposed design of the CCB: overmolding and braiding. Two concepts were drawn up for comparison. The general shape is based on the CCB of the Skoda Enyaq shown in fig. 2.3.1c and in fig. 4.7.1a, as mentioned in section 2.3.3. This shape was chosen as it was the most challenging of the 3 non-die-cast shapes found for CCBs. It has both the bend in the beam on the passenger side and the thicker part of the beam on the driver's side. Using the estimate from the beam formulation in table 5.1 the first designs of the beam were made and simulated, see fig. 4.7.1.

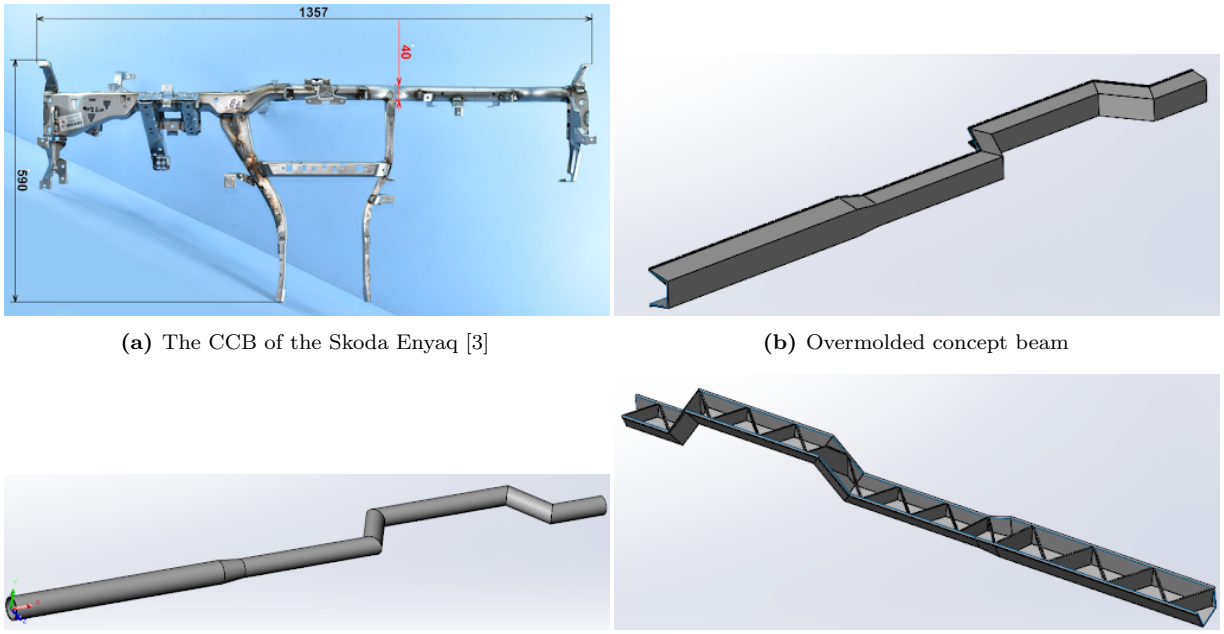

(a) The CCB of the Skoda Enyaq [3]

(b) Overmolded concept beam

(c) Braided concept beam

(d) Ribs on the inside of the overmolded concept

Figure 4.7.1: The braided and overmolded concept

4.7.1 Overmolding supports

Both beams would also have the center support like in fig. 4.7.1a. This would most likely be over-injection molded. For the braided concept that means an extra processing step and possibly requires inner support against buckling under the injection pressure. The overmolded beam could be made with both the press-forming and the molding of the ribs and center support in a one-step process.

The biggest challenge for using overmolding in structural parts is the predictability of the strength of the interface between the press-formed parts and the injection molded ribs [149]. This is mostly the case for the press-formed beam which relies on the ribs to not buckle. The center support and ribs could be molded around the beam so it is not purely relying on the adhesion of the interface, this is done for example by Tesla also visible in fig. 3.1.1 [50].

4.7.2 Concept choice: Overmolded beam

On a production basis, both the braided and the overmolded beam concepts are considered valid options. The main advantages of the braided beam are the higher torsional stiffness as a hollow closed profile can be manufactured and it does not rely on an overmolding interface for the beam itself. Next to this, braiding offers higher impact resistance as mentioned in section 4.1. Braiding itself is mature, but for TPC the consolidation times required for proper consolidation are too long for the required cycle time for high-volume manufacturing, which is its main disadvantage. TPC braiding also has received relatively little attention compared to TPC press forming.

Therefore, the choice was made to continue with the overmolded concept. Next to this, it is thought that it has more potential uses in cars [43]. As mentioned in section 4.3.1 using a single-step overmolding process is likely the better process. Press forming and overmolding have garnered a lot more interest in research than thermoplastic braiding. Stamp forming is already widely used in the automotive industry, and in some cases, the existing infrastructure can be used for press forming TPCs, only requiring extra inexpensive heating stations [37, 150]. Although commonly TPC forming is done using more complex heated tools. On top of that overmolding is already in use for some parts in the automotive industry today [43, 50, 130, 133], showing its maturity. Overmolded parts can also have a much shorter cycle time making them more suited for high-volume production needed for the automotive sector [37].

Chapter 5

Design

In chapter 3 it was determined that a PA matrix with continuous fibers will be reinforced with either CF or GF. To compare those two options against each other and some common metals a simplified CCB will be modeled analytically as a fixed-fixed beam shown in fig. 5.1.1. Using the dimensions from the Skoda Enyaq CCB in fig. 4.7.1a and the Tesla Model 3 CCB in fig. 8.2.1b as a first estimate of dimensions. These estimates can then quickly be adapted for each material with little work required, this aids in the initial design of the beam in CAD which will be modeled and simulated more accurately in chapter 7 and chapter 8. By having a good start less time consuming iterations are needed. On top of this, the initial estimation gives valuable insight into the potential weight and cost differences between the material options as is shown in table 5.1.

Two production methods seem suitable for the production of the continuous fiber composite CCB. Two concepts based on each production method were compared in section 4.7. Based on multiple factors the overmolded beam was deemed the better concept. Further modeling and analysis will be done on that concept. The overmolded composite beam will be compared to an aluminum beam such as in the Tesla Model 3, see fig. 8.2.1b, as it is a lightweight cheap option.

5.1 Initial dimension approximation

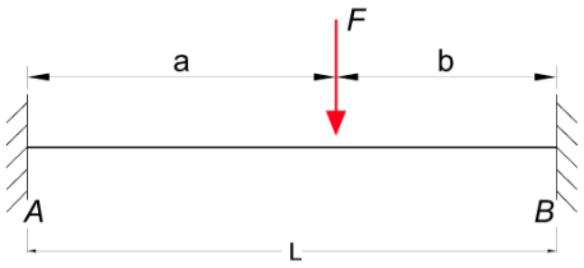

Figure 5.1.1: Free body diagram of the CCB as a fixed-fixed beam [16]

The benchmarking of CCBs gave a good range for the dimensions of steel and aluminum CCBs. To make a good initial guess of the dimensions of a carbon and glass CCB with equivalent stiffness a program was written with simple fixed-fixed beam equations for the deflection and the second moment of inertia for the torsional stiffness. This allows for a quick approximation and iteration of the dimensions needed for the lower-stiffness composite beams. The approximate required dimensions are given in table 5.1, with the diameter (diam) and thickness (t) of the hollow circular beams. The cost shown is purely the material costs, this disregards any potential cost benefits the TPCs can have during production.

Combining this with representative material data, most material datasheets give limited data, so if more is required the U20MM micromechanics modeler tool [151] was used to easily get a good estimate of the

missing values for the composite beams. The carbon and glass fiber materials are based on a Tepex twill weave used in automotive [4], with the fibers either at a 0/90 angle (0deg) or a 45/-45 (45deg) angle. The values for the metals are for high strength steel, aluminum 6061 T6, and magnesium AM50A respectively [19].

$$I = \pi \frac{d_o^4 - d_i^4}{64} \tag{5.1.1}$$

$$\delta = \frac{F \cdot a^3 \cdot b^3}{3 \cdot L^3 \cdot E \cdot I} \tag{5.1.2}$$

Using the fixed-fixed beam equation given in eq. (5.1.2) together with the area moment of inertia of a hollow cylinder given in eq. (5.1.1) the deflection δ at the location of the point load can be determined. The outer diameter d_o, E modulus are given in table 5.1. The inner diameter can be determined, when the thickness is known. The free body diagram of the beam is given in fig. 5.1.1, with the length of the beam L being 1300 mm, which is similar to that of the CCB in fig. 4.7.1a. A point load F of 150 Newtons is placed halfway the beam, this deflection should not exceed 1 mm, as is one of the requirements in section 2.2.

$$Ipolar = \frac{\pi \cdot (d_o^4 - d_i^4)}{32} \tag{5.1.3}$$

$$T = G \cdot I_p \tag{5.1.4}$$

The more challenging requirement is the movement of the steering wheel due to a downward load. This loads the beam in torsion, thus the torsional rigidity values should be roughly equal to compare the beams. The shear modulus is given in table 5.1 and the formula for the second polar moment of inertia I_p is given in eq. (5.1.3), multiplying these gives the torsional rigidity T or the resistance against rotation around the length of the beam, given in eq. (5.1.4).

$$f_n = \frac{22.4}{2\pi} \sqrt{\frac{E \cdot I \cdot 9.81}{w \cdot L^4}} \tag{5.1.5}$$

As the natural frequency of the beam also has to comply with a requirement it is calculated using eq. (5.1.5) by [152] for the natural frequency of a fixed-fixed beam including its own weight w as load per length. This leaves out the weight of the steering wheel and other attachments which will lower the natural frequency substantially. However, the natural frequency values here are just for comparison between the beams.

Table 5.1: Beam formula approximation

Material	E [GPa]	G [GPa]	d_o [mm]	t [mm]	δ [mm]	T [Nm^2/rad]	Weight [kg]		Cost [EU]		f_n [Hz]
Steel	210	80	40	1.0	0.35	3730	5.0	+11%	3.00	0.3x	236
Aluminum	69	26	45	2.4	0.34	3801	4.5	-	10.15	-	252
Magnesium	45	16	55	2.0	0.33	3747	3.1	-30%	7.70	0.8x	310
GF PA6 45deg	14.3	8.5	60	3.0	0.55	3719	5.0	+11%	30.17	3.0x	188
CF PA6 45deg	17.3	14.4	60	1.7	0.75	3813	2.4	-47%	59.10	5.8x	234
GF PA6 0deg	18	4.4	60	3.9	0.35	2364	6.4	+42%	38.60	3.8x	208
CF PA6 0deg	39	5.2	60	1.6	0.35	1302	2.2	-51%	55.72	5.5x	353

The results in table 5.1 already show some interesting differences. Despite the advantage the composite beams have with a higher diameter compared to the metal ones, the glass fiber beam is already slightly heavier than the aluminum beam, even though it has a higher deflection and is slightly less stiff. The natural frequency is a lot lower due to the similar weight and much lower stiffness. Even though it shows

no clear weight or stiffness benefits, the material costs are three times higher. The material costs of carbon fiber are clearly a lot higher than the metal options too.

5.2 Design composite beam

The design of the composite beam is very similar to that shown in fig. 4.7.1b, with a bigger and thicker part on the driver side as this side has the most impact on meeting the requirements. Next to this, the corners have been rounded to aid production and prevent excessive stress concentrations. For the composite beam the open side was chosen in this direction to load the side walls in tension rather than compression as much as possible to prevent buckling, this has markedly better performance [153]. The Tesla Model S Plaid has the open side of the U shape towards the front of the car too, see fig. 3.1.1. To further prevent buckling of the side walls the open sides flare out, which is clearly visible in fig. 5.2.1a.

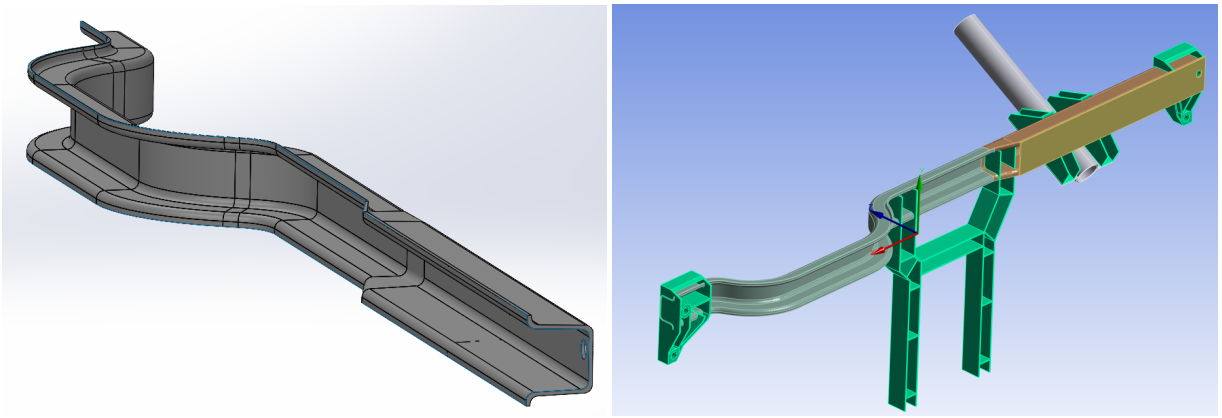

(a) Side view of the composite CCB

(b) In green are the overmolded parts

Figure 5.2.1: Composite CCB overview

In fig. 5.2.1b all the parts in green are the overmolded parts. These are almost the same as the overmolded parts shown in fig. 8.2.1a. The design of the overmolded parts has largely been inspired by the overmolded parts of the Tesla Model 3 CCB shown in fig. 8.2.1b. The design might need adjustment if a forming analysis with software such as Aniform [154] shows that this design is very challenging to produce without production issues. However, the choice was made to not include such an analysis in this work.

Part II

Modeling and Simulation

In the first part, a design has been chosen including the material and production processes. This part will focus on the modeling and simulation of the composite CCB. First mechanical testing was done to gather data for the simulations. The testing consisted of relaxation tests of bolted connections and Dynamic Mechanical Analysis (DMA) testing to measure the Tg and damping. For the modeling, simple simulations were done first which could be checked by analytical calculations to determine the best element for the model. The influence of different reinforcements is compared. After which the dimensions and material layup of the beam have been optimized to comply with the requirements set for the CCB. Different material options are given that comply with the requirements but come with different weights and costs. These are all compared to a reference aluminum CCB, the current standard in high-volume low-cost lightweight CCBs. An important benefit composite materials can have over metals is the high material damping, but this damping is strongly dependent on multiple factors. It is shown how this high material damping could mean lower eigenfrequency requirements could suffice for composite CCBs.

Chapter 6

Mechanical Testing

6.1 Relaxation testing of bolted connections

TPC parts in automotive often use metal inserts to reinforce bolted connection points [3]. This is clearly visible in the example thermoplastic composite front-end module carrier of the Lucid Air in fig. 6.1.1 which has 37 metal inserts [155]. These connections are usually produced by injection molding around a through-the-thickness metal insert. Inserts can increase the strength of the connection, although a wrongly designed insert can decrease the strength too [156].

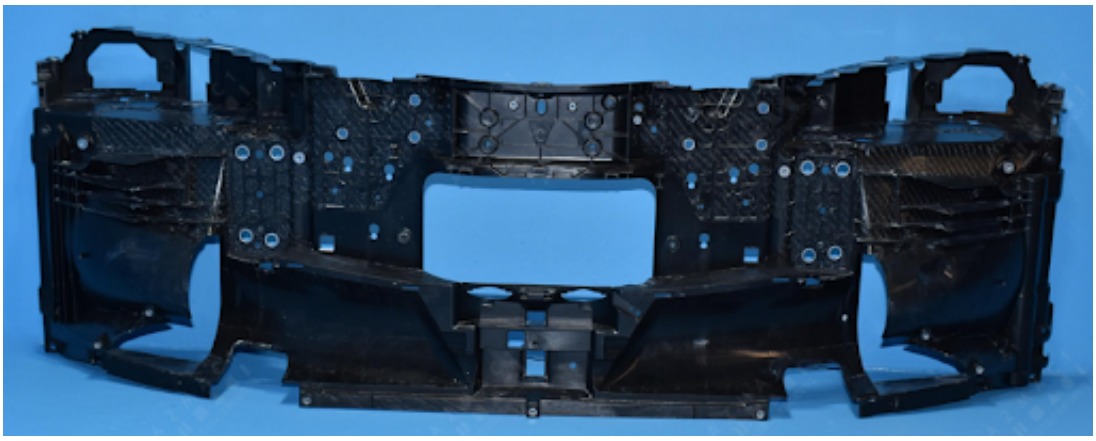

Figure 6.1.1: The TPC front-end module carrier of the Lucid Air with 37 metal inserts [3]

Additionally, an important reason for using metal inserts is to prevent a reduction in clamping force. The clamping force is desirable as it creates friction between the two joined parts which can then transfer shear loads. It can also increase fatigue resistance and prevent the separation of parts [157, 158]. Holes are commonly designed oversized which helps to prevent tolerance issues [156], but it means the bolts hold parts in place purely by clamping force. Therefore, it is important the preload applied for this clamping force does not decrease too much over time due to the relaxation of the material under the bolthead. The clamping force generally loads a composite through-the-thickness in which is dominated by the visco-elastic matrix properties [158, 159]. Thermoplastics like PP and PA6 are close to or even above Tg in the majority of their service life. This combination of materials being above Tg and subjected to high forces has a high potential for problematic relaxation, leading to a reduction in clamping force [160, 161]. Using a metal insert can avoid this problem.

However, using metal inserts has a number of disadvantages. Inserts can increase the weight of parts and make the recycling of the part more challenging. Next those this, it increases part count and requires advanced molds, increasing the cost of logistics and production. A misaligned insert can also cause expensive mold damage.

To limit the use of inserts it should be clear during the design phase which connections require inserts and for which it is unnecessary. This requires tools to predict the long-term behavior of composite joints under load. Although bolted joints are widely used for composites, they are not fully understood yet and research into the best design procedures is still required [158, 159, 162, 163]. One aspect of that is the prediction of clamping force reduction due to relaxation and determining the influence of factors such as the initial preload and environmental conditions. A lack of validated data for through-the-thickness properties of composites is also hindering the design of bolted connections [160]. To this end, relaxation tests have been done to attempt to gain insight into the relaxation behavior of the chosen material for the composite CCB, being GF PA6, under a simulated clamping force of a bolted connection. However, these tests failed as it was found that the change in temperature of the room where the testing machine was situated influenced the results significantly, and thus the results cannot be used for this thesis. The setup of the test and an explanation of the influence of the room temperature is given in appendix A.

6.2 DMA Testing

As mentioned previously in section 3.3.1 an advantage composites can have over some metals is their higher damping. This can dampen vibrations that occur in the car before they reach the driver, thus increasing the comfort of the occupants [35]. The damping of composites depends strongly on the fiber angle, the temperature, and in some cases the moisture content of the material, especially for PA, shown before in section 3.3.1. The influence of these variables on the damping coefficient was tested with a DMA test. The damping can also depend on the frequency of the vibration, however, that is out of the scope of this research.

In the test, a specimen was put in a 3-point bending DMA test and was oscillated up and down through a range of temperatures. By looking at the input and output force measured, the elastic modulus and the damping was determined over a temperature range. Multiple specimens were tested, changing the fiber angle and the moisture content. Both of these variables can strongly influence the damping factor thus it is important to test the different combinations of these variables. These test results were then used in a simulation to compare the vibration of the steering wheel between an aluminum and a composite CCB in section 8.7.

6.2.1 Method

Materials

The material for the tests was kindly provided by Royal DSM N.V. [164]. The consolidation of the plies into a laminate was done at the ThermoPlastic Composites Research Center, Enschede, the Netherlands [165]. The material is a 40% FVF continuous UD GF tape in a PA6 matrix [164]. This tape was stacked 8 layers thick and consolidated into a cross-ply laminate, giving a $[0/90]_{2s}$ layup.

Specimen preparation

The DMA specimens were cut out of a 2 mm thick laminate with a length of 54 mm and a width of 10 mm using a diamond-coated water-cooled saw blade either into a 0/90 or ± 45 fiber orientation, see fig. 6.2.1. Both dry and conditioned specimens were required for the DMA tests. Part of the specimens was then conditioned in a conditioning chamber at 70 $°C$ and 62% RH according to the ISO standard for accelerated conditioning of PA test specimens [166]. According to the ISO standard, the specimens were conditioned if the weight change was within 0.1% for three consecutive days. This accelerated conditioning will result in a similar moisture content as the equilibrium in standard atmosphere at 23 $°C$ and 50% RH. The conditioning took about seven days. The other specimens were dried in an oven at 110 $°C$, which took less than two days, after which the weight did not further decrease.

The damping of PA6 can depend strongly on the humidity level of the material, therefore both dry and conditioned specimens were tested. To determine the impact of the fiber angle on the damping, two different layups were tested. One of the two specimens per humidity level has the fibers at a 0/90-degree angle (90 for short), with the 0-degree fibers along the length of the specimen, see fig. 6.2.1. The other has the fibers at a 45/-45-degree angle (45 for short), this makes the behavior less fiber dominated. Thus in total four different specimens were tested.

Test setup

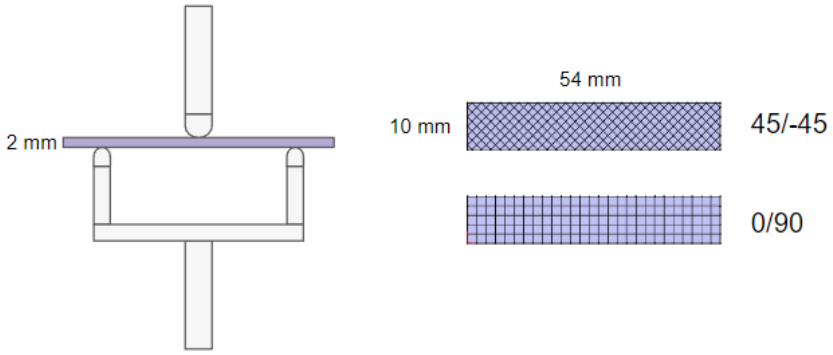

Figure 6.2.1: The 3-point bending setup is shown on the left, with the PA6 GF specimen dimensions and layups on the right

The test was done using a 3-point bending test with a 40 mm span width, this is shown in fig. 6.2.1, as this is most common in literature and the standard according to ASTM [167]. The specimens were tested on a DMA Eplexor 2500 at 1 Hz. The specimens were oscillated with a static and dynamic amplitude of 0.25% of the thickness of the specimen. The specimen was enclosed in an oven which regulated the temperature. The temperature range tested was -30 to 110 $°C$ at a heating rate of 2 $°C$/min. The heating rate can also influence the results, for the greatest precision a heating rate of 2 $°C$/min is recommended, but it could lead to drying out of wet specimen [167]. In literature, a range of 2 to 5 $°C$/min is commonly found [167–170]. The loading frequency and heating rate were the same regardless of whether the dry or conditioned specimens were tested. The humidity was not controlled. The output measured is the force required to follow the prescribed oscillation at different temperatures.

6.2.2 Results and discussion

Data analysis

The DMA test measures the stiffness and the damping of the specimen [171]. The test machine applies a sinusoidal strain to the specimen and measures the resulting force. This resulting force is then split into two waves of the same frequency [172]. The in-phase part of the measured force, or storage modulus, is a measure of how elastic the specimen is. The out-of-phase delayed response, or loss modulus, is the measure of how much energy the viscous part of the specimen dissipates as heat. The ratio of the loss modulus over the storage modulus is the damping of the material, or tan δ. The Tg can be determined in multiple ways from the DMA results giving slightly different results [173]. It was decided to use the peak of the damping curve for the determination of the Tg here, see section 6.2.2 for the results.

The damping was supposed to be measured every 5 $°C$, however, due to an unknown problem most specimens were sampled less frequently, as visible in the different amount of sample points in fig. 6.2.2a and fig. 6.2.2b. To get a proper estimate of the full damping curve the data was interpolated using a modified Akima piecewise cubic Hermite interpolation function in MATLAB, these interpolations are plotted with a solid line in the figures below.

Storage and loss modulus

The results of the DMA tests are shown in fig. 6.2.2a and in fig. 6.2.2b. In fig. 6.2.2a the storage modulus is given, which shows a downward trend in elasticity for all specimens as the temperature goes up. The storage modulus changes a lot depending on the fiber angle, with the 0/90 layup the elastic fibers dominating the response, this is seen most clearly in the storage modulus of the 0/90 layups which is significantly higher in fig. 6.2.2a.

As for the loss modulus in fig. 6.2.2b the conditioned specimens have a higher peak at a lower temperature than the dry specimen. The difference between the layups is smaller for the loss modulus. The red line of the dry 45 specimen in fig. 6.2.2b does show a smaller peak just under 0 $°C$, the cause of this peak is

unknown and more tests should be done to see if that peak shows consistently, as only one measurement point defines the peak, so it could be an outlier. If it is not a measurement error then it could be a mechanical relaxation of another phase in the material [174], but this is out of the scope of this research.

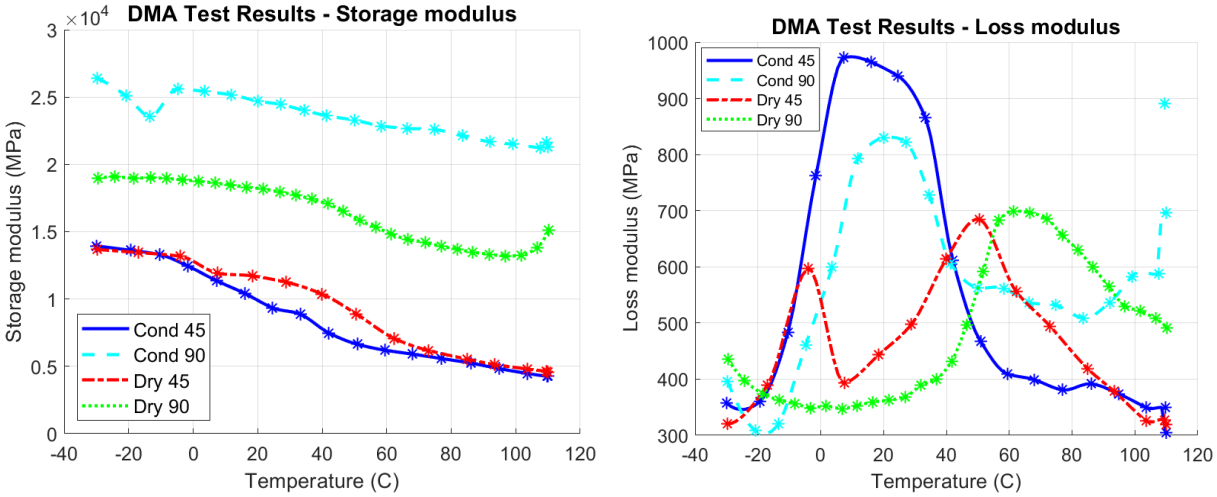

(a) The storage moduli for the GF PA6 specimens

(b) The loss moduli for the GF PA6 specimens

Figure 6.2.2: Results from the DMA from dry and conditioned GF PA6 specimens with either a 45/-45 or a 0/90 fiber angle

Damping and glass transition temperature

Table 6.1: Results DMA for the Tg and damping

Specimen	Tg ($°C$)	Max Damping at Tg (-)	Damping at 20 $°C$ (-)
Cond 45	26.5	0.10	0.10
Cond 90	23.9	0.03	0.03
Dry 45	73.3	0.08	0.04
Dry 90	69.3	0.05	0.02

In fig. 6.2.3 the damping is plotted which is the ratio of the loss modulus to the storage modulus which is plotted in fig. 6.2.2. As mentioned before, the Tg is determined by the peak of the damping curve, the results of which are given in table 6.1. The peak of the damping factor is also dependent on the decrease of the storage modulus, hence, this usually results in a slightly higher Tg than when using the peak of the loss modulus [167]. The Tg is the temperature at which the material goes from a glassy state to a rubbery state as the amorphous regions of the material gain higher chain mobility due to the increased temperature [70]. The values of Tg for the dry and conditioned specimens are clearly distinct, with the values also similar to what is found in literature and datasheets [4, 70]. The Tg for wet specimens is lower as the absorbed water increases the distance between the polymer chains and thus decreasing the intermolecular forces. This increases the chain mobility and thus water acts as a plasticizer, lowering Tg [70]. There is a slight spread in Tg between similarly conditioned specimens. The Tg seems not to be dependent on the fiber angle in the tests, this is to be expected as the matrix material does not change. For a more precise estimation of the Tg, multiple tests should be done. Next to this, it could be that the crystallinity is slightly different between specimens which could affect the Tg as well, however, this has not been tested.

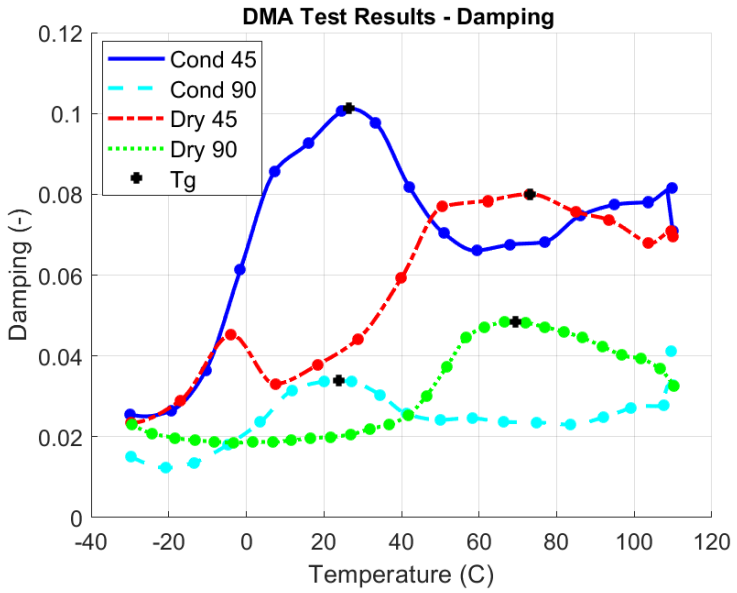

Figure 6.2.3: The damping ratios over a wide temperature range for the GF PA6 specimens

The damping shown in fig. 6.2.3 is clearly different between the different layups. As the storage modulus of the 90-degree specimens is much higher than the 45-degree specimens, the damping is much lower for the 90-degree specimens. The damping is a matrix-dominated property and is therefore strongly temperature dependent, this is clearly visible too. The damping is highest around Tg, which is clear with the damping peaks of the conditioned specimens around 25 $°C$ and the dry specimens having the peak around 70 $°C$. The absorbed water in the conditioned specimens increases the chain mobility so it has a similar effect as increasing the temperature, this results in higher energy dissipation and thus damping for the conditioned specimens in the range of -5 and 45 $°C$ compared to the dry specimens. At temperatures further above Tg, the mobility increases too much, with both the loss and storage moduli decreasing rapidly. As PA6 in the common climate for cars will be around the conditioned state as opposed to the dry state the damping peak around 23 $°C$ is placed very well with it covering most common temperatures with good damping properties. The damping curves plotted in fig. 6.2.3 are the data most of the interest as this gives the material damping over a range of temperatures. The range of the expected damping values for this material can be used for simulating the vibrations at the steering wheel in chapter 8.

Chapter 7

Preliminary Study On Modeling

In table 5.1, a first rough comparison was made between beams of different materials. To make a more accurate comparison a simulation will be done with the actual shape of the beam and the supports around it in chapter 8. Before this simulation can be done it is important to make sure the beam is modeled correctly so that the results are correct too, this will be discussed in this chapter.

To make modeling quicker and less prone to error the following was done. Before larger simulations of whole parts are done, first the material model and elements are checked. An overview will be given of the different element types after which they are compared on the basis of accuracy for a torsional loading simulation of a thin-walled cylinder, a shape closely resembling the dimensions of the CCB. The cylinder is compared to analytical calculations. Here different element sizes and types are used to determine their influence and what level of detail is needed for accurate results without increasing the computation time too much. These initial models are easy to check for any errors as they are simple to understand and check with hand calculations. This can prevent a more time-consuming search for the cause of error in bigger models, or prevent using results based on bad material models or elements.

7.1 Material parameters

To model a material its material parameters are required, such as those for strength and stiffness. The number of these parameters differs substantially depending on the type of material. For materials that can be assumed mostly isotropic, meaning that the material parameters are independent of the direction, such as steel, aluminum, and plastics the modeling is relatively simple. For stiffness only two material parameters are required, usually, the Young's Modulus E and the Poisson's ratio ν [175]. Using Hooke's Law these two can determine the shear modulus G. For strength again only two material parameters are needed, the tensile strength and the shear strength. Thus metals and unreinforced plastics require only four material parameters in total for strength and stiffness [175]. This isotropic assumption might not hold for all metals as there can be differences in material properties due to for example drawing of high-strength steel [176]. But in general, metals can be assumed to be isotropic [176].

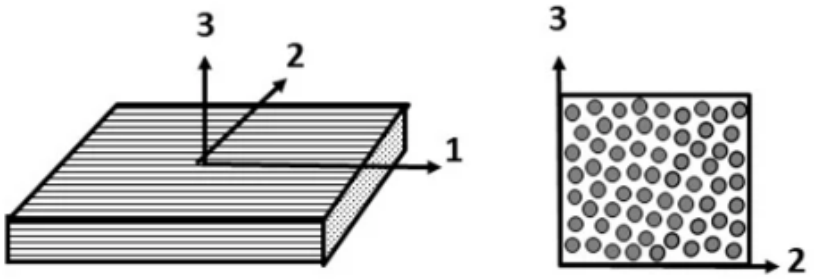

Figure 7.1.1: A schematic overview of a UD composite

Composites are made up of fibers and a matrix, a schematic overview of a UD composite is shown in fig. 7.1.1. The material properties vary strongly depending on the direction and therefore composites require more parameters. For a UD composite such as shown in fig. 7.1.1 the material properties align along three principal axes, with 1 being the longitudinal direction along the fibers, 2 the transverse direction, and 3 the thickness direction. In Ansys these directions are often given in X, Y, and Z respectively. This is called an orthotropic material and requires nine independent stiffness constants and another nine strength constants [175, 177]. The assumption is often made that the thickness direction (3) has the same properties as the transverse direction (2), in which case the material is called transversely isotropic. This reduces the stiffness material parameters required to five and those for strength to six. Getting all the material parameters required for composites can be challenging as some values are harder to test. The amount of information needed makes testing and modeling cost more time and money. In practice, composites are often still modeled as isotropic to save time and costs.

For this report, the composites are modeled in Ansys Composites as orthotropic on a ply level. The fibers of the cross-ply composite commonly used are both along the 1 and the 2 axes. Most common weaves have the same amount of fibers along those two axis, so then the properties are the same. However, it is also possible to have more fibers along one axis. The material parameters required for a ply for this research to model the stiffness and harmonic response are given below. Each ply is defined as an orthotropic layer, which can then be stacked at different orientations to make a laminate. In Ansys Composites each ply, and thus the fiber direction, is defined by a certain angle in a local coordinate system.

Material parameters required on a ply level:

- Density
- Damping Ratio
- Orthotropic Elasticity
  - Young's Modulus X, Y, and Z direction
  - Poisson's Ratio XY, YZ, and XZ
  - Shear Modulus XY, YZ, and XZ

7.2 Element types

Ansys uses different element types with the standard options using Ansys Workbench and Ansys Composites Preppost. The options are defined by either a shell, solid shell, or solid element, each of which can be either a linear or quadratic element. The different options are discussed in more detail below.

7.2.1 Shells

Composite parts are often thin shell-like structures and shell elements are the computationally the most efficient. Hence composites are often modeled using shell elements. Next to this, meshing with shell requires fewer elements and usually is easier to mesh and less likely to result in negative Jacobian errors. For linear shell analysis Ansys uses the 4-node shell 181 [178]. For quadratic elements, the 8-node shell 281 element is used [179]. For good quality shell elements it is important to have the smallest dimension of a shell at least 10 times that of the thickness of the shell [180, 181]. Next to this, the edges of the quadrilateral elements should also stay as close to 90 degrees as possible [182].

In simulation software using shells, it can be the default that the maximum stress is only stored for the top and bottom layer of the shell as the bending stress is at a maximum here [180]. However, for composites failure might occur in any layer of the layup, depending on the orientation or material of the layer. Therefore a layer-by-layer analysis needs to be carried out in case of failure analysis. If only the displacements, a modal analysis, or buckling analysis is required, then using a homogeneous equivalent shell with only the laminate stiffness suffices [181], and layer-by-layer analysis is not needed.

However, shells do have their limitations. They are unable to capture through the thickness stresses and strains, which always are zero for shell elements [178, 179]. Due to the low shear modulus of composites, they should always be modeled as thick shells, as opposed to thin shells, to take into account the shear

deformation [181]. In addition, thin shell elements assume the transverse shear stress to be zero. Transverse shear is important for accurately capturing bending cases [183]. An example of the transverse shear stress occurring during the bending of a plate is shown in fig. 7.2.1. Neglecting the transverse shear deformation can underestimate the shear deformation if the laminate is thick or the difference in shear moduli between the laminas is large [181], such as in a laminate with a core as shown in fig. 7.2.2. Thus the shell elements can be overly stiff and thus underestimate the amount of bending. The stiffness of the layers in the laminates should also not have more than two orders of magnitude difference [180, 181]. This makes shells unsuitable for many sandwich constructions. Some shell elements can also underestimate the stiffness if the laminate is thick and curved, especially under torsional loads [178]. Hence it is advised to check the accuracy of shell elements by first modeling a simpler model with 3D solid elements. This is shown in section 7.3. And as shell elements have no thickness, it can be hard to model adhesive joints for example [184].

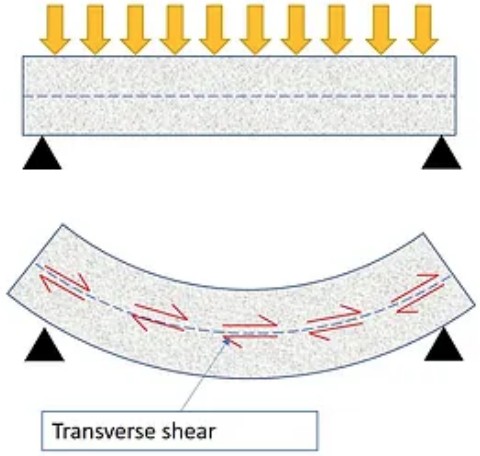

Figure 7.2.1: Transverse shear due to bending [17]

7.2.2 Solid Shells

Ansys Composites Preppost has to option to make a solid model using solid shell elements. For linear elements, it uses the 8-node solid shell SOLS190 [185]. However, for quadratic elements it just uses the quadratic Solid 186 [186] element. Compared to solid elements solid shell elements are quicker to mesh and simulate, although they are slower than shell elements [187]. An advantage over shell elements is that solid shells are also capable of through-thickness stresses and strains. Next to this, solid shells can also be stacked through the thickness as opposed to standard shells. Making it more precise for thicker parts [180]. Solid shells have been found to generally be stiffer than shell elements [188]. Solid shells are also easier to connect to other continuum elements than shells [185]. Although boundary conditions, especially simply supported, are more difficult to apply [188].

Compared to solid elements it is better at handling transverse shearing stress in bending dominant load cases [180, 183, 185, 188], not being prone to shear locking such as especially linear solid elements are [187]. It also has improved formulations for in-plane bending, preventing thickness locking. Although it is recommended to also use at least 3 elements through the thickness for plates with solid shells as otherwise they can be very stiff in bending [188]. The aspect ratio of an is defined as the ratio of the longest edge to the shortest edge of an element [182]. In general, as the aspect ratio increases, so does the inaccuracy [182]. Solid shells have no aspect ratio problems that solid elements can have, thus the thickness can be very thin [181]. This allows for modeling of a sandwich with at least three elements three elements through the thickness at least, one for each face and one for the core. Using different elements for each material with potentially very different moduli improves the accuracy of the results [181].

7.2.3 Solids

Solid elements can model 3D geometries. And if no analytical solution is available a solid element can be used to check the performance of shell and solid shell elements [188]. With quadratic solid

elements typically being the safest choice for most simulations [189]. Solid elements are, however, usually computationally more expensive. Especially for shell-like parts as solid elements should not be very thin compared to their length, resulting in a bad aspect ratio [190]. Thus for thin parts, a short element length is needed with solids to improve the aspect ratio, resulting in an increase in elements and thus computation time. To model 3D structures with solids Ansys uses the 8-node solid 185 for linear elements [191], and the 20-node solid 186 for quadratic elements [186]. If the laminate is made of a woven fabric or is very thick then a solid element should be used [181]. Solid elements are also important to use when looking at very localized phenomena with high differences in stress and strain. For both solid, solid shell and shell elements large errors in the estimation of the stress at edges can occur due to stress flattening [188].

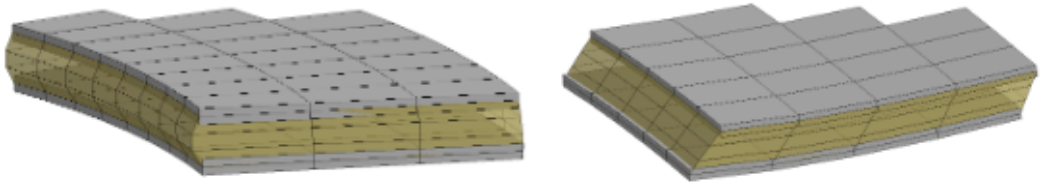

Figure 7.2.2: Realistic modeling of a sandwich plate is possible with three solid elements through the thickness. Under compression on the left and large shear deformation on the right [18]

With both linear and quadratic solid elements it is important to use multiple elements through the thickness, at least 3 to 4, for more accurate transverse shear results [186, 191, 192]. For through the thickness behavior, it is also important to use multiple layers of elements [183, 186, 189]. This makes it possible to realistically model through the thickness behavior as is shown in fig. 7.2.2 for compression and shear loading. Shear locking can occur during bending for linear elements as the edges cannot bend, this is generally not a problem for quadratic elements [189]. Shear locking results in excessively stiff elements or false stresses under bending [192]. If the quadratic elements are distorted, a gradient occurs in the bending stress, or under very complex stress states even quadratic elements can show some locking [189]. To reduce the chance of shear locking elements can be used with a reduced integration scheme. However, this introduces the potential for hourglassing during bending [192]. Hourglassing causes the element to be excessively flexible. Hourglass mode could propagate through the model if there is only one layer of elements in any direction [186, 192]. Sufficiently fine meshes prevent most propagation of hourglassing for each type of solid element [189, 192].

7.3 Elements for torsional loading

Due to the high weight of the steering wheel and the application of force on the steering wheel, the CCB is subjected to torsional loads mostly. It is important to check whether the simulation of the CCB can model this accurately. Especially for torsional loads the element choice can have a strong influence on the deformation results. For example, shell elements used for torsional loading of a cylinder or wind turbine blade were found to give a 35 to 5% lower stiffness than solid elements [184]. The main cause of this problem was identified as a too low drilling stiffness (rotation normal to the plane of the element), especially for shell elements that are offset from the nodal plane [184]. For bending, however, the shell elements were able to accurately predict the stiffness.

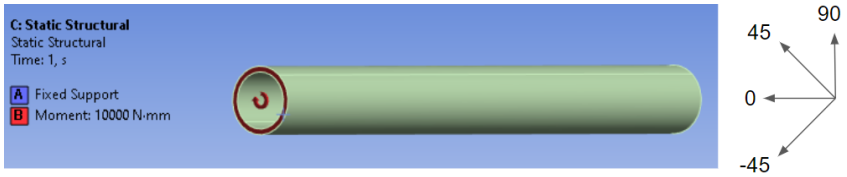

Figure 7.3.1: Setup simulation torsional loading of a cylinder

In order to check the accuracy of the different elements described section 7.2 a hollow cylinder with

dimensions similar to that of the CCB has been modeled which is subjected to torsional loading, see fig. 7.3.1. The cylinder has an inner diameter of 40 mm, a thickness of 4 mm, and a length of 500 mm. The thickness is put at 4 mm to match the thickness of the CCB with the GF layup, see estimates for thickness in table 5.1. The advantage of using such a simple cylinder is that it allows for an analytical solution to verify the simulation results. The analytical solution is found by using the polar moment of inertia, the shear modulus, the applied moments, and the dimensions of the beam, as shown in eq. (7.3.1) [193]. With δ the maximum deformation at the endpoint of the beam, r the radius, T the applied moment, L the length, J the polar moment of inertia, and G the shear modulus. The shear modulus used for each material is given in table 7.1. The shear modulus of the 0/90 degree layup is chosen to have a representative value for a GF PA6 composite. The shear modulus of the 45/-45 layup is determined using the classical lamination theory ABD matrix with the values of the 0/90 ply rotated to a 45/-45 ply. This value was also confirmed to be the same as the value for the shear stiffness engineering constant given by Ansys Composites after rotating the 0/90 layup. This way the value for the shear modulus is the same for the analytical calculation and the simulation.

$$\delta = \frac{r \cdot T \cdot L}{J \cdot G} \tag{7.3.1}$$

Table 7.1: The shear modulus used for each material for the analytical calculation

Material	**Shear Modulus [GPa]**
Steel	76.92
GF PA6 0/90	4.35
GF PA6 45/-45	9.29

Table 7.2: Difference between the analytical solution of eq. (7.3.1) with the simulation results of an isotropic material cylinder under torsional loading with different elements

Steel tube 4 mm thick Element size 5 mm Isotropic material Compared to: analytical		
	Linear	Quadratic
Shell	+13%	+11%
Solid	+1%	0%

Steel tube 0.5 mm thick Element size 5 mm Isotropic material Compared to: analytical		
	Linear	Quadratic
Shell	+3%	+1%
Solid	+2%	0%

First a cylinder made of an isotropic material, steel with a shear modulus of 77 GPa, is simulated under torsional loading. This avoids using Ansys Composites which might introduce unknown differences and also avoids composites that could add some more assumptions. Thus making it easier to identify the cause of the differences. In table 7.2 the difference in deformation between the analytical solution in c7.3.1 and the simulation of the isotropic steel cylinder is shown. The solid quadratic elements model deformation most accurately with the solid linear elements not far off. The shell elements, however, overestimate the deformation by more than 10%. Part of the reason is the sub-optimal ratio of element thickness compared to the shortest length which is below the advised 1:10 ratio, as mentioned in section 7.2.1. When this aspect ratio is improved, as is done by decreasing the thickness of the cylinder to 0.5 mm, shown in the right part of table 7.2, the shell elements perform much better. But still, the solid elements give a more accurate result. So the isotropic cylinder with the approximate dimensions of the CCB with a thickness of 4 mm, shows that shell elements underestimate the stiffness of the cylinder under torsional loading.

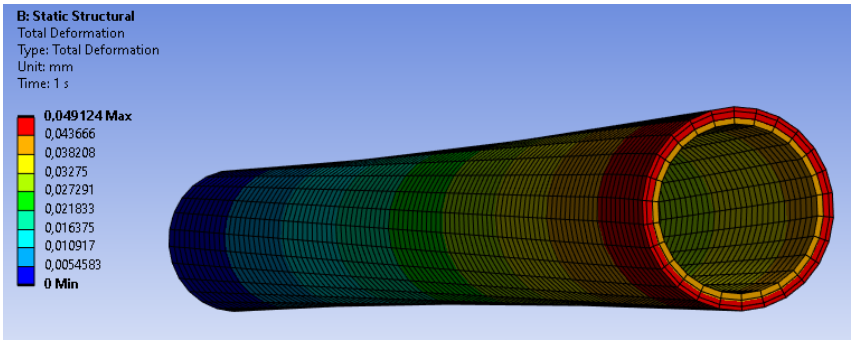

Figure 7.3.2: Element validation with cylinder

Having compared the elements using an isotropic material, the elements are checked for two composite cylinders, one with the fibers in a 0/90 orientation with the fibers running in the length of the cylinder and orthogonal to that, see fig. 7.3.1 for the definition of the fiber angles. The other cylinder has the fibers in a 45/-45 layup, which is better against torsion. The material parameters required and the modeling of the composite parts are described in section 7.1. The cylinder has the same dimensions as the isotropic cylinder in fig. 7.3.1 with 4 mm thickness. For models with the solidshell and solid elements three elements through the thickness have been used, see fig. 7.3.2, the exception to this is table 7.5 with only one element through the thickness.

Table 7.3: Difference between the analytical solution of eq. (7.3.1) with the simulation results of a composite material cylinder with the fibers in a 0/90 layup under torsional loading with different elements

Composite cylinder 0/90 Element size 10 mm Orthotropic material Compared to: analytical		
	Linear	Quadratic
Shell	+20%	-15%
Solidshell	+8%	-
Solid	+6%	-1%

Composite cylinder 0/90 Element size 5 mm Orthotropic material Compared to: analytical		
	Linear	Quadratic
Shell	+27%	-16%
Solidshell	+2%	-
Solid	+1%	0%

First, the cylinder with the 0/90 layup has been modeled with two different element sizes, see table 7.3. To see the difference with a larger element size, the results of 10 mm elements are shown too in the left part of the table. The sorting of which element is most accurate is the same for both element sizes and the same as with the isotropic cylinder, with the linear shell worst and the quadratic solid most accurate. When reducing the element size the shell elements actually perform worse, similar to before the ratio of the thickness compared to the shortest edge length nears 1:1 instead of the advised minimum of 1:10. Another difference is that for the isotropic cylinder, both the linear and the quadratic shell underestimated the stiffness of the cylinder, but for the composite cylinder the quadratic shell is actually stiffer than the solid elements. With the element size of 5 mm, see the right part of table 7.3, the solidshell and solid elements get almost the same results. The error is similar to the isotropic cylinder results seen in table 7.2. Seeing that a linear solidshell gets almost the same result as the quadratic solid shell is good as it is computationally less demanding.

Table 7.4: Difference between the analytical solution of eq. (7.3.1) with the simulation results of a composite material cylinder with the fibers in a 45/-45 layup under torsional loading with different elements

Composite cylinder Element size 5 mm Orthotropic material Compared to: analytical	45/-45	
	Linear	Quadratic
Shell	+66%	-14%
Solidshell	+3%	-
Solid	+3%	+1%

The formula for deflection as stated in eq. (7.3.1) on page 47 gave the same results as the quadratic solid for the isotropic cylinders in table 7.2 and the 0/90 composite cylinder in the right half of table 7.3. As shown in table 7.4, for the 45/-45 degree the difference between the simulation and the analytical calculation was similar, only being one to two percent worse for most elements. However, the linear shell element performed worse, underestimating the deflection 66%, up from 27% for the 0/90 layup. The absolute difference between the linear shell the other elements and is quite similar for both the 0/90 and 45/-45 results, although the absolute difference is still 20% higher for the 45/-45 degree case. Thus the higher stiffness only partly explains the high relative difference.

Table 7.5: Difference between the analytical solution of eq. (7.3.1) with the simulation results of a composite material cylinder under torsional loading with only one element through the thickness for different elements

Composite cylinder Element size 5 mm Orthotropic material Compared to: analytical	0/90 1 through	thickness
	Linear	Quadratic
Solidshell	+2%	-
Solid	+2%	0%

Composite cylinder Element size 5 mm Orthotropic material Compared to: analytical	45/-45 1 through	thickness
	Linear	Quadratic
Solidshell	+3%	-
Solid	+3%	1%

As mentioned in section 7.2, for better transverse shear results it is best to use multiple elements through the thickness. However, for the torsional loading on the cylinder, it seemed to have very little influence on the results. table 7.5 shows that both the 0/90 and the 45/-45 cylinders show good results for all elements tested. Thus for the mainly torsional loading, it seems to have little influence. The shell elements are not simulated again as they always had only one element through the thickness in the table 7.3 and table 7.4.

7.3.1 Element choice

The most accurate modeling would be with multiple through-the-thickness quadratic elements of course. However, this does increase simulation time and thus makes the process slower. Next to this, the license limited the number of elements and nodes, so with quadratic elements the mesh could not be that small. This could lead to problems where elements were becoming very big but thin, shell-like, which can cause issues for solid elements. The linear solid and solidshell elements seem to perform equally well for the torsional loading as shown above. It was found, however, that the solidshell elements gave more difficulties with contact definitions between parts, causing unwanted separation. Therefore, it was decided to do most modeling with three elements through the thickness of linear solid elements.

Chapter 8

Simulation

To give an indication of the performance of a composite CCB, it will be compared to an aluminum CCB based on the dimensions of the Tesla Model 3, as shown in section 8.2. The composite CCB will be optimized to two of the most challenging requirements set for the CCB in section 2.2. These are the eigenfrequency of the CCB and the displacement of the steering wheel when a load is applied to it, the setup of these simulations is shown in section 8.3. The goal is to meet the requirements at the lowest weight, as summarized in table 8.9. As costs are important too, the cost per weight saving of the different options for the composite CCB will be determined too and compared to the value of weight saving in automotive.

First, different reinforcement options are compared to see the impact and weight of the different options, see section 8.4. The best reinforcement is chosen for the following simulations. Secondly, a number of fiber angle combinations are simulated in section 8.5 to see what angle would be best for the driver and passenger side. The optimal angle is used for the final round of simulations. The last round of simulations is done to determine the number of plies needed per side of the beam with different material combinations for the driver and passenger side, the results of this are given in section 8.6.

It can be argued that the requirement for the eigenfrequency can be lowered for composite beams due to their superior damping, this is explained and simulated in section 8.7. In section 8.6 a GF beam is already simulated with a lower requirement for the eigenfrequency to show the potential impact. As the setup of the simulation is different it is kept separate.

8.1 Boundaries of the optimization

The focus of the optimization is put on the beam itself as this is the main part of the CCB. To give a representable simulation some parts are attached to the beam such as the end and center supports. These are not optimized, however, they are almost identical for the composite and the aluminum beam shown in fig. 8.2.1a.

The number of design variables that can be optimized for composites is much higher than that for metals or pure plastics and no robust automated optimization tools are available at the moment [101]. To limit the number of variables requiring optimization and thus simulating time, the number of parameters is limited. The beam is divided into two parts, the driver side, and the passenger side. The passenger side is the part of the beam that is green in fig. 8.3.1. For each side, the fiber material and angle can be changed, as well as the number of ply layers. For the plate reinforcement, see fig. 8.4.1d, the number of layers and fiber angle has been set already to reduce the number of variables. Similarly, the matrix is already determined to be PA6 as mentioned in section 3.3. The range of the parameters simulated has been based on the results seen during the setup of the simulations and is wide enough so that the optimization is not limited by it whilst keeping the number of options to a minimum to limit simulation time.

There are other parameters that could be optimized such as the width and height of the beam, the length of the reinforced driver side, and many other things. However, the choice was made to leave out those

parameters as that is not part of this research. Instead, the dimensions were chosen to be similar to CCB currently used in automotive, such as fig. 2.3.1c and fig. 8.2.1b.

8.2 Aluminum reference beam

The composite CCB has the potential for weight saving but has a high material cost. Therefore, it is compared to the current standard of lightweight CCBs which is the hydroformed aluminum beam with overmolded branches such as the one in the Tesla Model 3 shown in fig. 8.2.1b. It is assumed the beam is made of aluminum 6061 which is often used for cross members in automotive [194, 195], the material properties used in the simulation are given in table 8.1. The CCB as shown in fig. 8.2.1b weighs about 4.3kg in total with the estimated total material cost of 15 dollars [196]. The aluminum CCB gives a good benchmark weight and cost for the composite designs.

Table 8.1: The properties used for the simulation of the aluminum beam

Aluminum 6061 T6		
Density	2713	kg/m3
Isotropic elasticity		
Young's Modulus	69	GPa
Poisson's Ratio	0.33	
Shear Modulus	26	GPa

A magnesium CCB might be lighter, and more expensive, but it is produced very differently which makes comparison more difficult. So when comparing the aluminum and the composite CCB, it is good to keep in mind that the weight of the aluminum CCB is already very low, especially compared to the standard CCB made of steel. An important thing to note is that for the hydroformed beam thickness and circumference are the same over the whole length. So it is not possible to have the driver's side more reinforced than the passenger side as is often done for CCBs, shown in section 2.3.1.

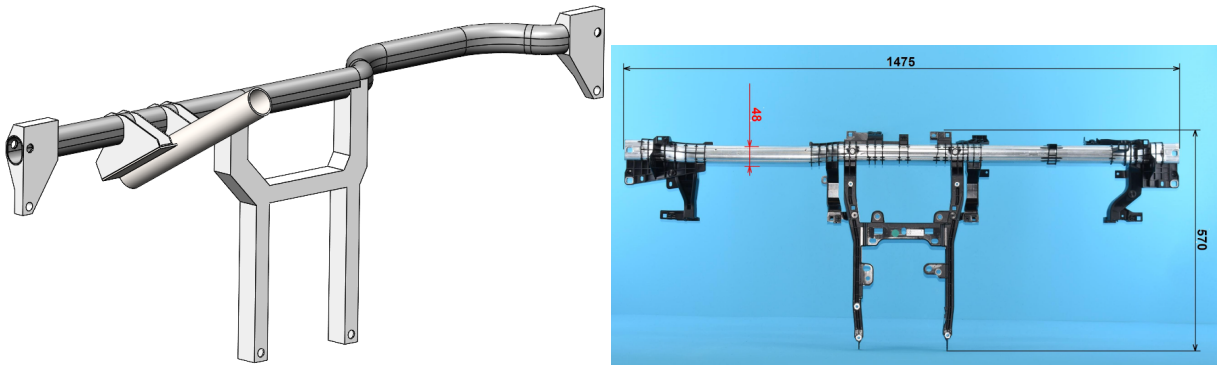

(a) The aluminum CCB as base level

(b) CCB of the Tesla Model 3 [3]

Figure 8.2.1: An aluminum CCB as a cost-effective lightweight reference beam

The dimensions of the beam closely resemble that of the beam of the Tesla Model 3 in fig. 8.2.1b. However, the path of the beam is the same as the composite CCB, which is based on the shape of the CCB of the Skoda Enyaq in fig. 4.7.1a. As for the dimensions, the aluminum beam and the composite beam are similar. The aluminum beam shown in fig. 8.2.1a has a height of 50 mm with a depth of 38 mm. The thick part of the composite beam, shown in brown on the left side in fig. 8.3.1 is 50x50 mm, and the green part of the beam is 50x35mm. The most efficient beam for stiffness would have the largest outer dimensions with the lowest thickness, however, this is limited by manufacturing capabilities and local buckling for example. GF and CF composites have a similar limit to this so-called shape factor as aluminum 6061 [197]. Thus the comparison with similarly dimensioned beams is a realistic one. The injection molded supports on both ends, in the center, and for the steering column support are all the same as well for the composite CCB to keep it comparable.

8.3 Simulations setup

For each round of simulations the following two load cases are simulated: the displacement of the steering wheel shown in section 8.3.1 and the eigenfrequency of the CCB shown in section 8.3.2.

8.3.1 Steering wheel displacement

Next to the forces experienced during crash, the highest force applied on the CCB during normal use is introduced through the steering wheel. The toughest requirement to be met is the one shown in fig. 8.3.1, which is a 600 N applied in a downward direction, negative y, whilst keeping the displacement below four mm, as set by the requirements in section 2.2. The boundary conditions are defined at the six bolt holes marked by the yellow circles visible in fig. 8.3.1, two on either side of the beam, and two on the bottom in the center, are all set as fixed support.

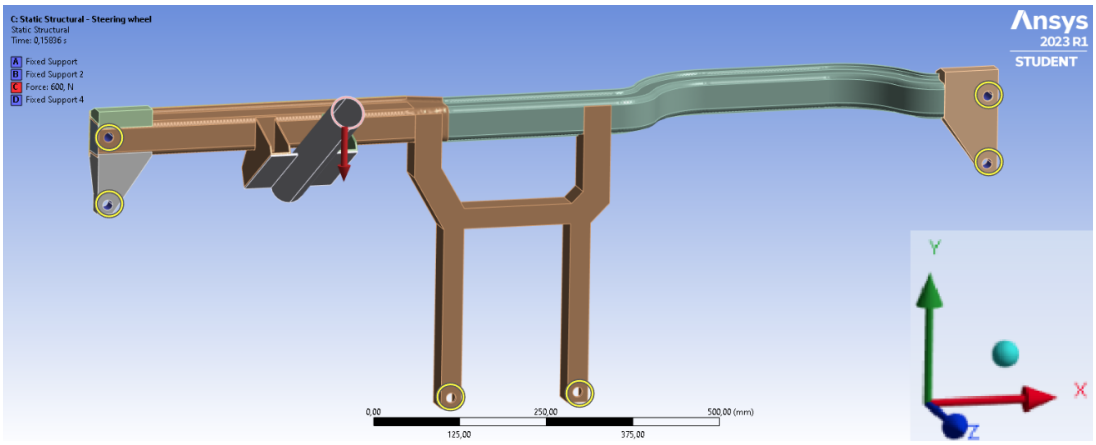

Figure 8.3.1: The deformation simulation setup in Ansys

8.3.2 Modal analysis

The most challenging requirement is that of the minimum eigenfrequency the CCB must have. To optimize for this a modal analysis is set up. For the modal analysis the force on the red circular area is replaced by a mass of two kilograms which is attached to the end of the steering column, the red circle in fig. 8.3.1, to simulate the weight of the steering wheel [3]. The other boundary conditions are the same as for the displacement simulation.

8.3.3 Material

The materials for the simulations are based on the values of Tepex, which is a woven laminate with two fiber directions orthogonal to each other [22, 23, 87]. To ease the comparison between the CF and GF, each layer is given the same thickness of 0.25 mm. The material data is based on the datasheets of Tepex laminates in combination with the estimates given by the U20MM modeler [23, 87, 151]. As mentioned before the plies are modeled as orthotropic in Ansys, the material parameters used in the simulation are given in table 8.2. For other fiber angles than 0/90, such as 45/-45, the properties are rotated by Ansys using the classical laminate theory. For all simulations that follow a biaxial material with the two fibers directions at 90 degrees apart is used. For ease of reading the main fiber angle will be mentioned only in the text, so 0 degrees (0/90) and 45 degrees (45/-45).

Table 8.2: The properties used for the GF and CF plies in the simulations

	GF PA6 Twill 0/90 47% FVF	**CF PA6 Twill 0/90 51% FVF**	
Density	1800	1460	kg/m3
Orthotropic Elasticity			
Young's Modulus			
X	21	43	GPa
Y	21	43	GPa
Z	10	8.6	GPa
Poisson's Ratio			
XY	0.13	0.057	
YZ	0.32	0.139	
XZ	0.32	0.139	
Shear Modulus			
XY	4.35	5.21	GPa
YZ	4.33	5.25	GPa
XZ	4.33	5.25	GPa

8.4 Influence of cross ribs and plate reinforcement

A big disadvantage of an open hat channel is the low torsional stiffness. To improve on this four different options for reinforcement of the CCB are simulated, as shown in fig. 8.4.1. The base level is an open hat channel without any reinforcement as shown in fig. 8.4.1a. A common reinforcement for open profiles is to add ribs, which can be done with overmolding for example, as explained in section 4.3. This is done in two ways, either cross ribs all along the beam as shown in fig. 8.4.1b. Or with cross ribs only on the driver side, as is shown in fig. 8.4.1c, as it is the most loaded section. The fourth option to overcome the low torsional stiffness of an open hat channel is to close it with a plate, as discussed in section 4.5, the design is shown in fig. 8.4.1d. In the simulation with the plate, no cross ribs are used under the plate.

Table 8.3: The objectives of simulations with different reinforcements

Objectives
Minimize displacement steering wheel
Maximize eigenfrequency
Minimize weight

Table 8.4: The parameters and range for the simulation of the influence of the different reinforcements

Driver side	
Material	GF, CF
Amount of layers	12 CF or 16 GF
Fiber angle	45

Passenger side	
Material	same as Driver
Amount of layers	8
Fiber angle	0

Plate	
Material	same as Driver
Amount of layers	8
Fiber angle	45

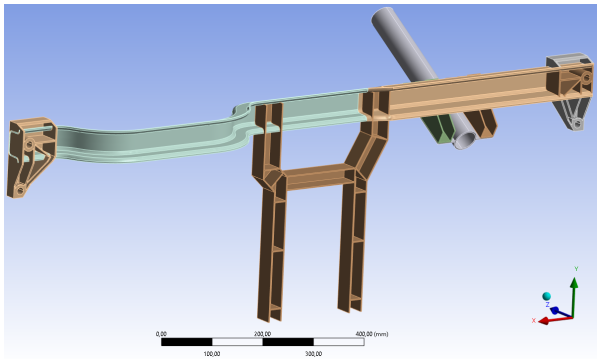

(a) Simulation with no reinforcement of the beam

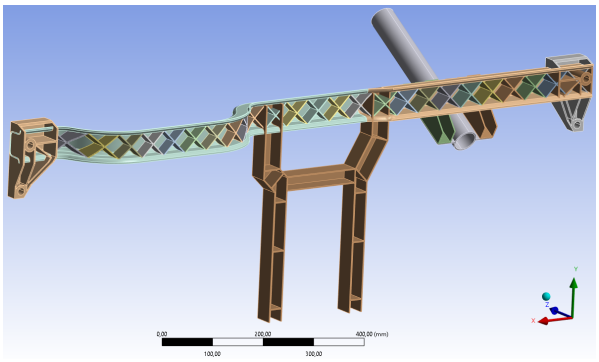

(b) Simulation with cross ribs all along the beam

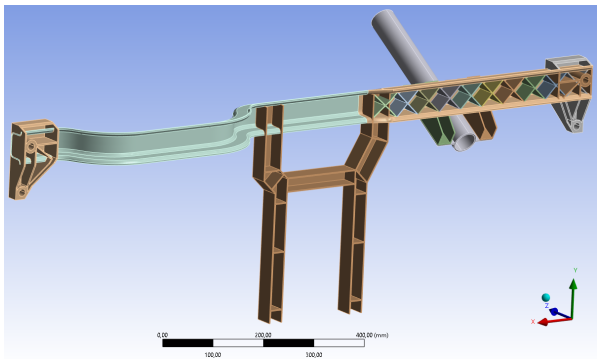

(c) Simulation with cross ribs only on the driver side of the beam

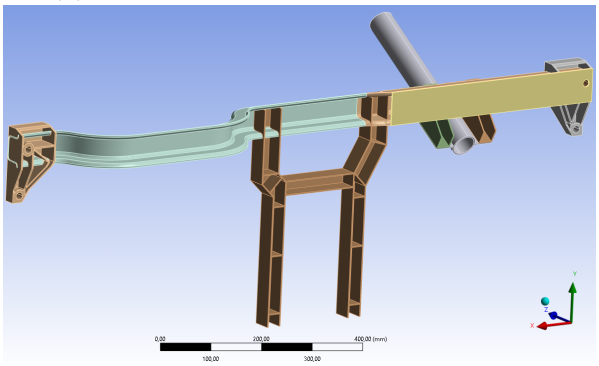

(d) Simulation with a plate on the driver side instead of cross ribs

Figure 8.4.1: The different reinforcements tested that have been simulated

Table 8.5: Comparison different reinforcements

Reinforcement	**Weight [g]**		**Displacement [mm]**		**Eigenfrequency [Hz]**	
Open hat channel	872	-	16.05	-	15.79	-
Partial ribs	1002	+130	6.10	-9.95	24.54	+8.75
Full Ribs	1132	+260	6.00	-10.05	24.82	+9.03
Plate	962	+90	3.22	-12.83	32.89	+17.10

In table 8.5 the results of the simulations for the displacement, see section 8.3.1, and the modal analysis, see section 8.3.2, with the different reinforcement configurations are given. The weight given is purely of the beam and the cross ribs or plate, so without the other parts. It clearly shows the strong influence any of the reinforcements have on the results. Most of the deformation occurs on the driver side around the steering wheel, therefore adding ribs or a plate there is important. The difference in deformation and eigenfrequency between the partial ribs and the full ribs is very little, showing how little the reinforcement does on the passenger side. Even though the added weight of the extra cross ribs next to the partial ribs doubles the reinforcement weight.

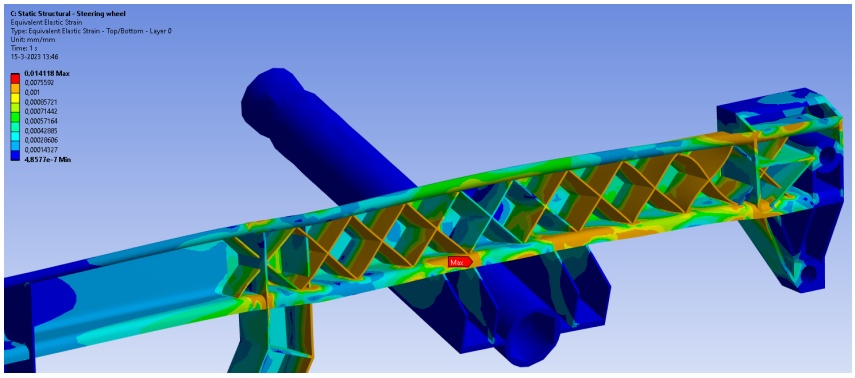

Figure 8.4.2: Strain in the cross ribs

The plate reinforces substantially more than either of the rib configurations and does so at a lower weight. The main reason is most of the material of the plate is far from the axis of rotation and thus most material is where the highest deformation is. Whereas for the ribs this is not the case, as is visible in fig. 8.4.2, there is quite a gradient in the strain through the ribs. This means not all the material is being used to its full potential. The other reason is that the plate consists of continuous fibers which have a higher stiffness than the injection molded fibers. It is clear that the plate offers the most benefit at the lowest weight. However, the production of it might be more challenging. Given the potential benefit that is shown in these simulations, it would be good to investigate the use of a hat channel combined with a plate to close it off. The options for making this are given in section 4.5.

For further simulations of the composite beam, the plate instead of the overmolded ribs will be used, as it has clear advantages shown in table 8.5.

8.5 Fiber angle

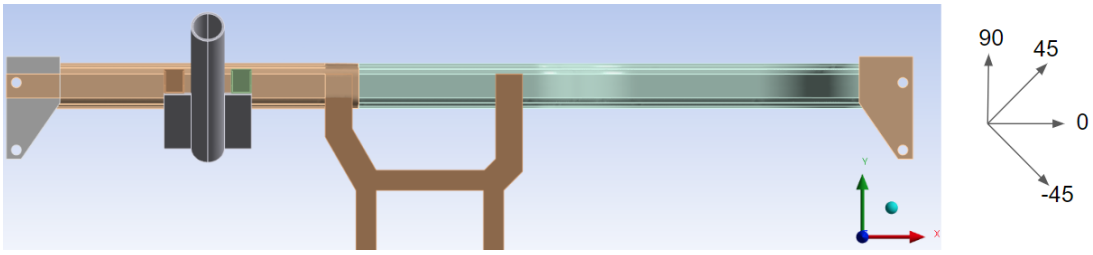

Figure 8.5.1: Definition of the fiber angles mentioned in relation to the CCB

A round of simulations was run with the fiber angle options of 0/90, 15/-75, 25/-65, 35/-55, and 45/-45 degrees for both the drivers and the passenger side separately, see table 8.8. The fiber angle with regards to the CCB is shown in fig. 8.5.1. The angle between the fibers is 90 degrees at all angles as a 0/90 woven fabric is used which is rotated, as mentioned before. If braiding or UD layers are used other fiber angle combinations such as 35/-35 would have been options too, this has not been simulated. The simulations were done for both a full CF as well as for a full GF beam, the latter is shown in table 8.8, to check if the large difference in stiffness mattered for the optimal fiber angle. Both the eigenfrequency and the steering wheel displacement have been simulated as the best layup for each might be different or even conflicting.

Table 8.6: The objectives of the optimization for the composite CCB

Objectives
Minimize displacement steering wheel
Maximize eigenfrequency

Table 8.7: The parameters and range for the optimization of the fiber angle of the composite CCB

Driver side		**Passenger side**		**Plate**	
Material	GF, CF	Material	same as Driver	Material	same as Driver
Amount of layers	12 CF or 16 GF	Amount of layers	8	Amount of layers	8
Fiber angle	0, 15, 25, 35, 45	Fiber angle	0, 15, 25, 35, 45	Fiber angle	45

Table 8.8: Results of the simulations with different fiber angle combinations for the full GF beam, sorting based on lowest deformation first. The colors are for providing a quick easy to see overview only

Driver ply angle	**Passenger ply angle**	**Deformation [mm]**	**Eigenfrequency [Hz]**
45/-45	0/90	2.4	37.3
45/-45	15/-75	2.4	37.2
45/-45	25/-65	2.4	37.1
45/-45	35/-55	2.4	37.1
45/-45	45/-45	2.4	37.0
35/-55	0/90	2.5	37.6
35/-55	15/-75	2.5	37.5
35/-55	25/-65	2.5	37.4
35/-55	35/-55	2.5	37.4
35/-55	45/-45	2.5	37.3
25/-65	0/90	2.7	37.0
25/-65	15/-75	2.7	37.0
25/-65	25/-65	2.7	36.9
25/-65	35/-55	2.7	36.9
25/-65	45/-45	2.7	36.8
15/-75	0/90	2.9	36.0
15/-75	15/-75	2.9	36.0
15/-75	25/-65	2.9	35.9
15/-75	35/-55	2.9	35.9
15/-75	45/-45	2.9	35.9
0/90	0/90	3.0	34.9
0/90	15/-75	3.0	34.9
0/90	25/-65	3.0	34.8
0/90	35/-55	3.0	34.8
0/90	45/-45	3.0	34.8

The deflection of the steering wheel in section 8.3.1 is a torsional load for the beam and thus the optimal fiber angle is expected to be 45 degrees. This is also clear in the results in table 8.8, with 45 degrees having the lowest deflection. For the passenger side in this case it is actually the opposite, with 0 degrees causing the least deflection. The rotation of the steering wheel and subsequently the movement of the center support in the middle might load the passenger side more on bending than torsion. For the driver side, the fiber angle has a big impact, with the highest deformation being almost 25% worse than the lowest. The fiber angle on the passenger side barely has an impact on this.

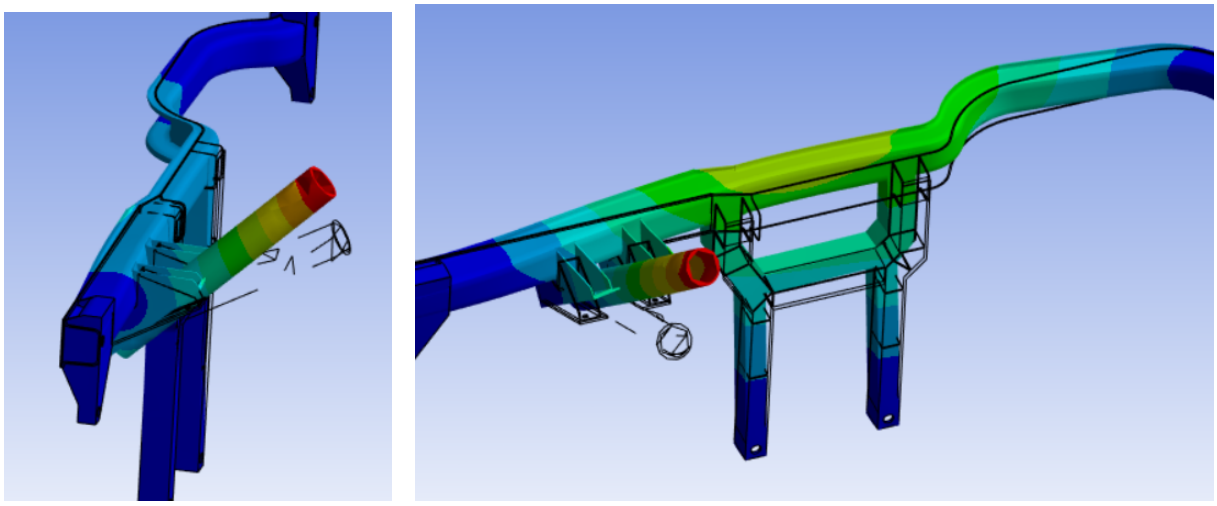

(a) The CCB with all fibers at 0 degrees in the modal analysis results in a rotation around the length of the CCB with the steering wheel going up and down

(b) The CCB with all fibers at 45 degrees in the modal analysis results in the center of the CCB going back and forth, which results in the steering wheel moving left to right

Figure 8.5.2: The influence of the fiber angle on the results of the modal analysis. The original position is given by the black outlines

For the modal analysis, the fiber angle determined the direction of deflection of the steering wheel strongly for the first eigenfrequency, as is shown in fig. 8.5.2. With the layup at a 0-degree angle, the fibers along the length of the beam, the beam rotated around its length, with the steering wheel going up and down. illustrated in fig. 8.5.2a. When a 45-degree angle was used, however, the deformation of the beam was different with the center part going backward and forwards, illustrated in fig. 8.5.2b, in z-direction in fig. 8.3.1. This made the steering wheel move sideways. So the fiber angle not only changes the eigenfrequency, which differed a few Hz between these two examples, but also the mode shape. It could be that the CCB in the car is more restricted in certain directions than others. Then the less stiff directions could be compensated for by choosing a certain fiber angle. A support strut in the center of the CCB towards the front, which prevents the movement back and forth, is also commonly found on CCBs [3].

The difference between the highest and lowest frequency for GF is almost 3 Hz, from 34.8 to 37.6 Hz. This difference is even larger for the CF which sees a change of 7 Hz, from 35.6 to 28.6. The best fiber angle for the driver side with the highest eigenfrequency is either 35 or 45 degrees, having very similar results. For the passenger side, again the lower angles are best in this case. The reason why a lower angle is better for the passenger side seems to be that the passenger side is not rotated around its axis as much as the driver side. However, it does support the center support from moving back and forth too much, which is stopped better with the 0-degree fiber angle preventing sideways deflection of the beam better.

The results shown table 8.8 are of the full GF beam, the results of the CF beam were very similar. A 45-degree fiber angle for the driver side and a 0-degree fiber angle were the best for both the CF and GF beam. A slight difference in results was found for the eigenfrequency, here for the GF the 35-degree angle has slightly better results than the 45-degree angle. For the CF the 45-degree angle was best again. So in short, the material choice seems to not influence the optimal fiber angle strongly in this case.

8.6 Ply material and thickness

In section 8.5 the optimal fiber angle for both the GF and the CF seems to be 45 degrees for the driver side and 0 degrees for the passenger side, therefore these angles can be set constant for the more precise layer and material optimization. As the stiffer CF requires fewer layers than the GF, the options are specified per material to reduce unnecessary simulations. This leaves just the material and thickness, or amount of layers, as a variable for the driver, passenger, and plate part of the beam. As with the previous

round of optimizations the plate will be used as reinforcement. The objectives are given in table 8.9 and the range of parameters is given in table 8.10.

Table 8.9: The objectives of the optimization for the composite CCB

Objectives	
Maximum displacement steering wheel	4 mm
Minimum eigenfrequency	35 Hz
Minimize	Weight

Table 8.10: The parameters and range for the optimization of the ply material and thickness for each part of the composite CCB

Driver side		**Passenger side**		**Plate**	
Material	GF, CF	Material	GF, CF	Material	GF, CF
Amount of layers	CF: 8, 9, 10, 11, 12 GF: 12, 13, 14, 15, 16	Amount of layers	8, 10, 12	Amount of layers	8
Fiber angle	45	Fiber angle	0	Fiber angle	45

In simulations done so far, it was noted the passenger side of the beam carries very little load with the current requirements. However, a requirement for a side crash, as would be common in real-world applications, or the deployment of the passenger airbag would require the passenger side to carry a significant load too. Hence, the minimum amount of layers the passenger side could have was chosen to be 8 layers. This should give a more realistic comparison to the aluminum CCB.

As shown in table 8.10 different material combinations can be made for the beam. A selection of these options is given in table 8.11. After simulating these combinations with different numbers of layers for each side, the optimal layup that still meets the requirements is given in table 8.11. The results of each material combination are given in table 8.12 and compared to the results of the aluminum reference beam shown in section 8.2.

Table 8.11: The layup of the different options for the composite CCB, the results are given in table 8.12, the fiber angles used are given in table 8.10

Material	**Driver material**	**Driver layers**	**Passenger material**	**Passenger layers**	**Plate material**
Full CF	CF	10	CF	8	CF
CF Driver&Plate, GF Passenger	CF	10	GF	8	CF
CF Driver, GF Plate&Passenger	CF	11	GF	8	GF
CF Plate, Rest GF	GF	14	GF	8	CF
Full GF	GF	16	GF	8	GF
Full GF lower requirements	GF	11	GF	8	GF

Table 8.12: Reference aluminum and composite beams, the layup of the beams is given in table 8.11

Material	**Material cost [EU]**		**Weight [g]**		**Deformation [mm] <4**		**Eigenfreq. [Hz] >35**		**Cost per kg saved <17**
Aluminum 6061 T6	2.35	-	1043	-	2.9	-	36.1	-	-
Full CF	17.19	7.3x	688	-34%	2.8	-1%	35.6	-1%	42
CF Driver&Plate, GF Pass.	11.67	5.0x	761	-27%	2.8	0%	35.0	-3%	33
CF Driver, GF Plate&Pass.	10.75	4.6x	810	-22%	2.7	-4%	35.2	-3%	36
CF Plate, Rest GF	7.56	3.2x	965	-7%	2.6	-10%	35.9	-1%	67
Full GF	6.34	2.7x	1056	+1%	2.4	-15%	37.3	+3%	no saving
Full GF, lower requirement	5.30	2.3x	883	-15%	3.8	+33%	30.7	-15%	18

In these simulations, just as is found in literature [35], the eigenfrequency of the beam is the limiting factor in the design, as is shown in table 8.12. As expected, due to the low loading on the passenger side, the minimum amount of 8 layers suffice for each option. The results show that the composite CCBs can have a substantial weight advantage of about 30% over the aluminum beam. The eigenfrequency is limiting for all beams apart from the lower requirement GF beam. The weight savings and their costs as given in table 8.11 will be discussed further in section 8.6.1.

It is interesting to see that the earlier results in table 5.1, duplicated in short here in table 8.13, already paint a remarkably accurate picture of the weight and cost differences. Even though those calculations are quite rudimentary and take a lot less effort. The big difference is that the beams in those calculations are all hollow circular tubes and the outer dimensions vary somewhat. Despite this, the estimate that the GF beam will be somewhat heavier and have almost three times the material cost is rather accurate. Just like the CF beam which has a weight saving of around 40% but at six to seven times the material cost.

Table 8.13: Summary of table 5.1 'Beam formula approximation' for ease of reading

Material	**E** [GPa]	**G** [GPa]	**Diam** [mm]	**t** [mm]	**Tors rigidity** $[Nm^2/rad]$	**Weight** [kg]		**Cost** [EU]		f_n [Hz]
Aluminum	69	26	45	2.4	3801	4.5	-	10.15	-	252
CF PA6 45deg	17.3	14.4	60	1.7	3813	2.4	-47%	59.10	5.8x	234
GF PA6 45deg	14.3	8.5	60	3.0	3719	5.0	+11%	30.17	3.0x	188

8.6.1 Weight and cost

Table 8.14: Summary of table 3.6 'Material cost per kg' for ease of reading

Material	**Cost per kg [EU]**	**Source**
Aluminum 6061 T6	2.25	[19]
GF PA6 Tepex woven fabric	6	[19]
CF PA6 Tepex woven fabric	25	Estimated [37]

The cost and weight in table 8.12 is the material cost or weight for the beam only. The material cost has been determined by multiplying the weight of each material by the material cost per kg for the aluminum 6061 or the Tepex composites mentioned in table 3.6, the summary of which has been given in table 8.14. A visual overview of the weight and material cost results of the different beams in table 8.12 is given in fig. 8.6.1.

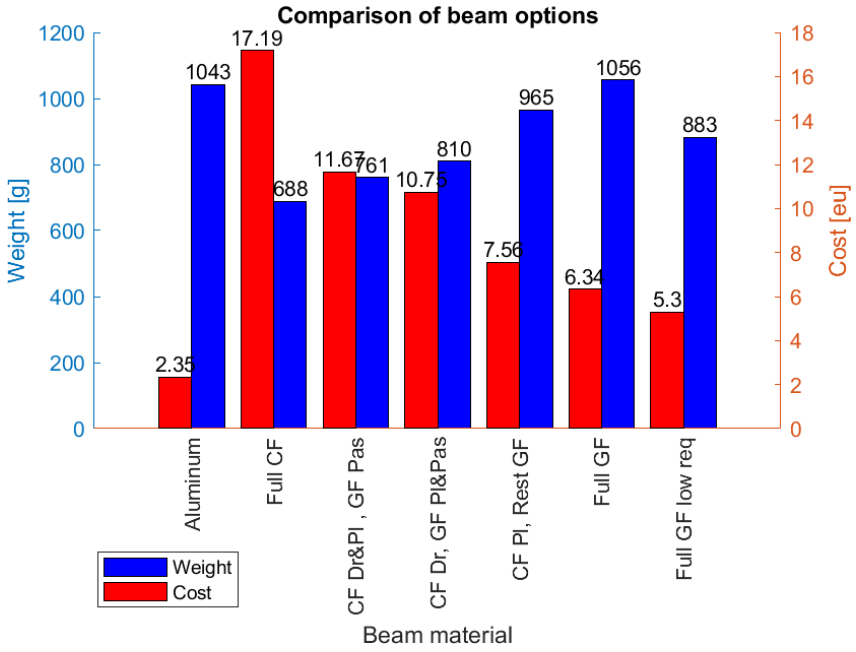

Figure 8.6.1: Comparison of the simulated beam options

A weight saving of 30% was only possible with the use of CF, which is very expensive, despite using automotive-grade CF. Replacing the long, but structurally less important passenger side with GF has a strong influence on the costs, but hardly changes the deformation or eigenfrequency. Also replacing the plate with GF gives similar results but at a slightly higher cost per kg saved. Having only the plate in CF has a much higher cost per kg saved so can be neglected.

Since low costs are very important in the automotive market options with only GF are simulated as well, significantly reducing the costs. The full GF beam comes in at about the same weight as the aluminum beam due to the low stiffness of the GF, which makes it challenging to satisfy the eigenfrequency requirement. Despite having only a slightly better deformation and eigenfrequency, the GF beam still has more than double the material cost of the aluminum beam.

The eigenfrequency requirement is limiting, lowering this requirement would allow for a lighter beam. This allows for a weight and cost saving of at least 15%. The reason for the lower requirement for the composite CCB is given in section 8.7. The lower requirement of 30 Hz in table 8.12 is possibly even on the conservative side. Although the deformation does start to become limiting too. However, even with the weight saving of the GF beam with the lower eigenfrequency requirement, the cost of weight saving is still 18 EU/kg. Which is just over the maximum of the estimated value of weight for BEVs as described in section 3.5 of 5-17 EU/kg.

The high material cost of composites is a big disadvantage for high-volume production, where material costs are a large part of the cost of the product [94]. To put the numbers given in table 8.11 in perspective, the material costs of the CCB of the Tesla Model 3 made of aluminum with overmolded GF-PA6 branches and a magnesium steering column support, shown in fig. 8.2.1b, amounts to almost 15 dollars, at a total weight of 4.3 kg. This is about half the cost of the product, excluding the tooling, R&D, and logistic costs [196]. The real cost-saving of overmolding is due to the part integration which saves on logistics and assembly costs. Although the CCB of the Tesla Model 3 already incorporates those benefits with the overmolded ribs. Thus increase in cost due to the composite CCBs given in table 8.11 is significant.

8.7 Damping

For CCBs, NVH is the most challenging requirement which determines the stiffness required. The NVH requirements are set for the comfort and feeling of quality for the occupants [198]. To ensure the steering wheel does not vibrate too much, the CCB should have an eigenfrequency higher than the vibrations that

occur from driving, such as by the motor and suspension, which would be higher than 34 to 38 Hz usually [34]. This prevents the high displacements that can occur when a part with low damping is excited close to or at its eigenfrequency. However, the dynamic damping of composites can be much higher than that of metals such as steel and aluminum [199], as mentioned before in section 3.3.1. The higher damping means that the displacement is lower when vibrating at the eigenfrequency, and the displacements dampen out quicker. Thus it could be possible to lower the eigenfrequency requirements possibly by as much as 20-35% for composites and still stay under the limits set for NVH [35].

8.7.1 Damping vibration simulation setup

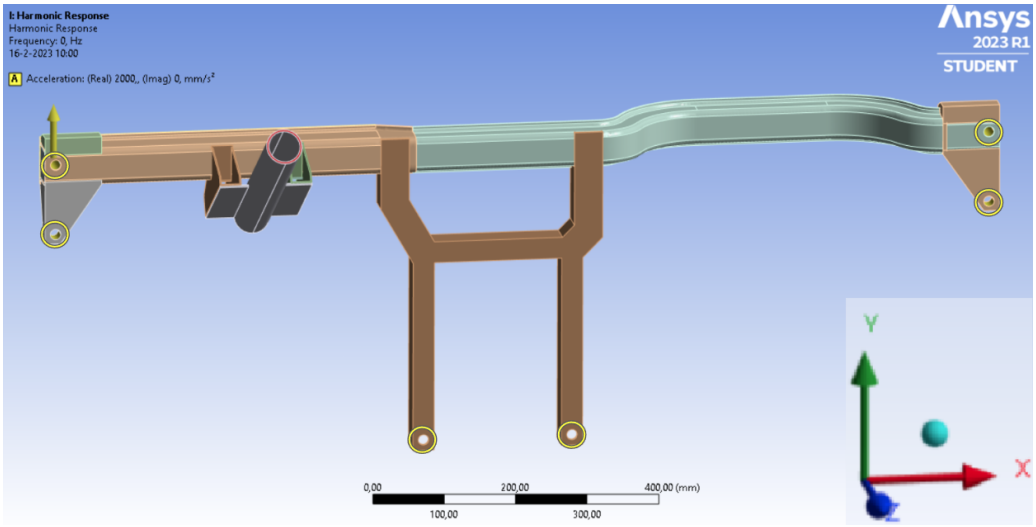

Figure 8.7.1: The vibration simulation setup in Ansys

The displacement of the steering wheel is simulated for both the aluminum and the composite CCB with the harmonic response analysis in Ansys, see fig. 8.7.2. The vibration is introduced at the six fixed base points of the model, which are the two bolt holes on either side of the beam, and the two bolt holes at the bottom of the center support, all are marked with yellow circles in fig. 8.7.1. The vibration is a harmonic acceleration orthogonal to the ground, see the upwards yellow arrow on the left in fig. 8.7.1, and the acceleration set at 2000 mm/s^2, which is based on values of the steering wheel acceleration for road vibration found in literature [200]. This could be different than the actual acceleration at the base points of the CCB like in this simulation, however, the actual value of displacement is not of interest, only the relative difference between the different materials and damping values. Just as with the modal simulations, a mass of two kilograms is attached to the end of the steering column, the red circle in fig. 8.7.1, to simulate the weight of the steering wheel [3]. To calculate the harmonic response, first, a modal analysis is done to determine the mode shapes and natural frequencies of the CCB. For the harmonic response, the mode superposition method is used. This method linearly combines different mode shapes found in the modal analysis to determine the displacement in the frequency domain and includes the material damping [201]. The damping is assumed to be constant for all frequencies. To see the dependency of damping on the frequency, a DMA test should be done over a frequency range.

8.7.2 Frequency Response steering wheel

In fig. 8.7.2 the amplitude of the vertical (Y) vibration of the steering wheel is given over a range of frequencies. Different damping factors δ have been simulated to show the influence damping has, which for the TPCs is influenced by temperature and moisture. For the GF composite parts, this change in damping factor is for the whole part. For the aluminum (ALU) part only the composite support parts have a change in damping factor, those parts are the center support, attachment to the steering column, and the supports at both ends of the beam. The damping values and temperatures are given in the legend table after the material name. For the aluminum beams first, the damping of aluminum (0.0011) is given after which the damping of the composite supports is given.

It is clear in fig. 8.7.2 that the maximum displacement of the aluminum beam at its eigenfrequency is much higher than the maximum of the composite CCB. This clearly shows why for a material with low damping, like the aluminum CCB, it is important to stay below the eigenfrequency. The peak is also very sharp, which means that just below the eigenfrequency the displacement of the aluminum beam is at a much lower level. This allows to set the eigenfrequency requirement just higher than the resonance of the rest of the car body. Putting the eigenfrequency higher than required would increase the weight of the part.

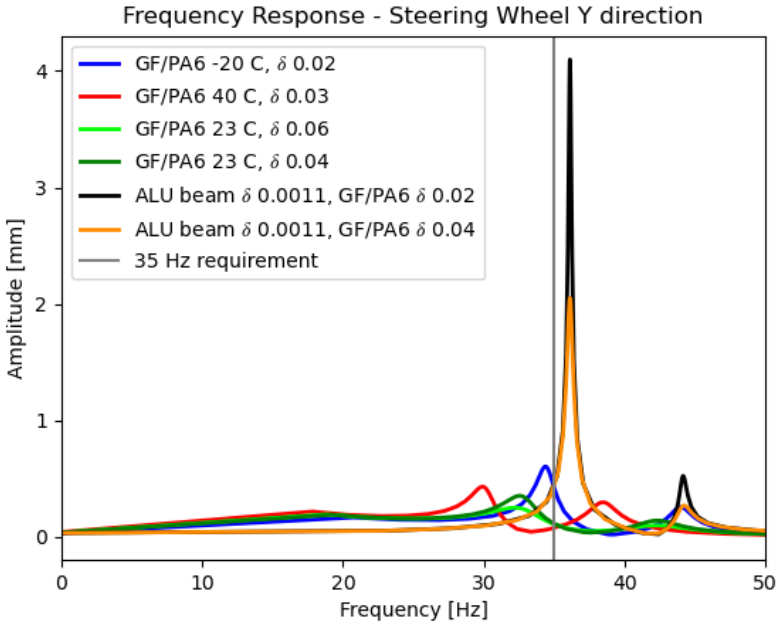

Figure 8.7.2: The Frequency Response Plot of the steering wheel due to a road-like vibration

For the composite CCB different curves can be seen, due to the lower stiffness, especially of GF, it is more challenging to get a high eigenfrequency, thus the peaks occur earlier. However, due to the damping, the peaks are generally much lower. Even if excited at its eigenfrequency the displacements are still relatively low compared to the aluminum beam. This is especially true for the damping PA6 can have, with the damping value of 0.06, or even higher, there is barely a peak visible. These damping values are well within what can be expected for a 45/-45 layup under a wide range of conditions, as is shown in fig. 6.2.3. Although as mentioned before, the damping depends strongly on the fiber direction and loading type too. This is not taken into account in this simulation which just has a general material damping value.

However, as mentioned before, the stiffness and damping of TPCs can change with temperature and moisture. If it is a dry PA6 and the temperatures are low, below 10 $°C$, then the damping is really low, see fig. 3.3.2, and thus the peaks become much higher. To show the impact of this the frequency response of the composite CCB at -20 and 40 $°C$ has also been simulated. This takes into account the change in damping and also the change in shear and tensile stiffness in both the short and continuous fiber composite parts. The estimated change in stiffness is given in the legend in fig. 8.7.2 and is estimated on literature and using the Rule-of-Mixtures [5, 77]. However, in outdoor conditions it is unlikely PA6 will reach such a dry state, so the damping will usually be better.

The change in damping does not change the eigenfrequency, but only the height of the peak, as is shown clearly by the peak of the aluminum and GF parts at 23 $°C$ fig. 8.7.2. The change in stiffness does change the eigenfrequency. fig. 8.7.2 shows how at -20 $°C$ with higher stiffness and lower damping the peak is higher and shifted to higher frequencies. The increase in stiffness is likely positive, but whether it balances out the resulting increase in amplitude due to the decrease in damping is difficult to say. The opposite is also true for the higher temperature simulation. Whether these changes in behavior due to temperature and moisture are of significance needs further research. What is clear, is that even in these scenarios

the peak is still relatively low compared to the aluminum beam. An exception to this is dry PA6 at low temperatures.

It is possible that the vibration of the steering wheel is still within NVH requirements using a composite CCB, even if the eigenfrequency is below the usual limit set for it, as already shown by [35]. Therefore, for composite CCBs the requirement for the eigenfrequency could potentially be set lower. In table 8.12 the potential benefit of a lower eigenfrequency requirement for composites is shown for the full GF beam. With a more than 15% weight saving compared to the full GF beam with the higher requirement, with the same drop in material cost. Alternatively, the focus of the requirement could be on the actual vibrations felt at the steering wheel. Having a better requirement means composites can be used to their full potential making use of their superior damping qualities to make up for the lower stiffness, thus reducing weight.

Part III

Final Design and Conclusions

Chapter 9

Final Design and Future Research

9.1 Final design

To conclude, the final design of the CCB, shown in fig. 9.1.1, and its compliance with the requirements set in section 2.2 will be discussed. In section 9.2 the advances that are required for easier adoption of TPCs in structural applications in automotive are discussed.

For the required high-volume production, the following processes show the most potential. To produce the blanks for the CCB at high volumes both pick and place and ultra-fast tape placement are viable options. For the CCB, pick and place seems to be the better option given the long thin shape of the beam with a 45-degree fiber angle which would result in short bits of tape, reducing layup speed. Single-step overmolding seems to be the most promising technique for high-volume manufacturing of the continuous fiber TPC CCB and similar parts including the functional parts around it. This technique is easily integrated into existing automotive manufacturing processes and is highly automatable. A flat plate is welded on the profile, as illustrated in fig. 9.1.1, to increase the torsional stiffness of the beam. Combining these techniques can reach the required cycle time of only minutes for the whole product including layup and forming.

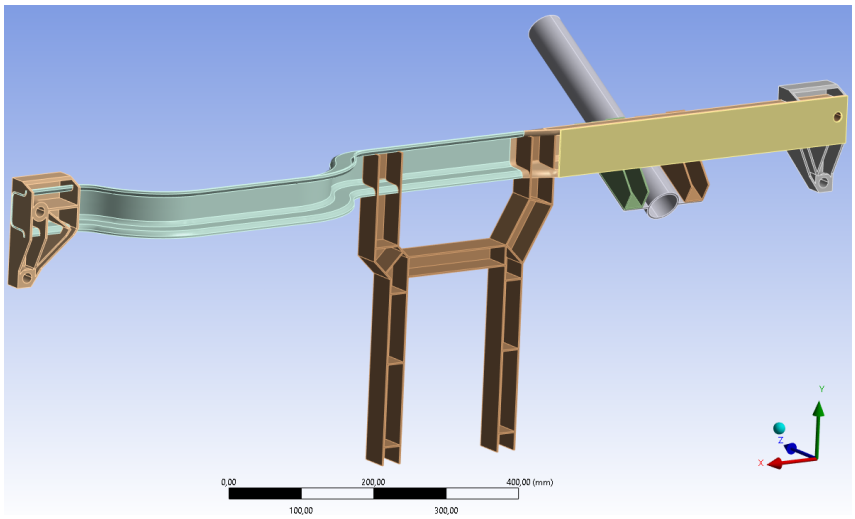

Figure 9.1.1: Final design of the composite CCB, including the attached plate in yellow

Due to the limited availability of openly accessible data for PP, the choice was made for PA for this thesis. However, on most metrics, PP can compete with PA at a lower cost. Therefore, PP is used increasingly for automotive and might have been a better option for the CCB. Both materials can handle the required temperature and humidity range, although their properties are not constant within that range, which can

complicate the design process.

A summary of the simulation results of the composite CCB is given in table 9.1. The requirements state more stiffness load cases than have been shown in the report. Simulations were performed for these load cases too, and it was found that all requirements were met. Some of these results were left out for clarity. The full GF beam with the lowered eigenfrequency requirement shows the most potential for implementation. The weight savings due to the high stiffness-to-density ratio of CF could not be justified due to its high material cost, however. The GF CCB was found to be lighter than the aluminum beam only when the requirement for the eigenfrequency was lowered, made possible by its superior damping properties. Despite the lower material cost of GF, the cost per kilogram weight savings is above the acceptable range for automotive of 5-17 EU/kg, as is shown in table 9.1.

Table 9.1: Summary of the comparison of the aluminum and GF composite beams of table 8.12

Material	**Material cost [EU]**		**Weight [g]**		**Deformation [mm] <4**		**Eigenfreq. [Hz] >35**		**Cost per kg saved <17**
Aluminum 6061 T6	2.35	-	1043	-	2.9	-	36.1	-	-
Full CF	17.19	7.3x	688	-34%	2.8	-1%	35.6	-1%	42
CF Driver&Plate, GF Pass.	11.67	5.0x	761	-27%	2.8	0%	35.0	-3%	33
Full GF	6.34	2.7x	1056	+1%	2.4	-15%	37.3	+3%	no saving
Full GF, lower requirement	5.30	2.3x	883	-15%	3.8	+33%	30.7	-15%	18

Design improvements could potentially reduce the cost to the upper end of the acceptable range, but this would limit its application to high-end vehicles. One of those improvements could be the use of local reinforcements such as tape. This could enable the bulk of the beam to be constructed out of the cheaper glass fiber while locally reinforced carbon fiber tapes are applied for stiffness [95]. Despite this, other potentially more cost-effective improvements could be implemented in average cars, such as using better steels or switching to aluminum [96]. This applies to the CCB too, as most are still made of steel, see table 2.1.

The optimization of the fiber angle in the simulations was done mainly for torsional stiffness. However, the side crash requirement might mean a much stronger beam is needed with additional fibers along the length of the beam. This could mean the GF beam has no weight or cost advantage over an aluminum beam. Having only one clear load direction in a part increases the potential for lightweighting with composites, as discussed in section 3.4.

9.2 Future research

Simulations so far have only been performed for stiffness. Extending these to strength and crash requirements will add other challenges. Composites require more comprehensive material data than metals due to their anisotropic nature, multiple failure mechanisms, and numerous caveats or unknowns. For example, the modeling of the interface between the overmolded ribs and the press-formed part can require multiple material models [153]. Especially when using cross-ribs with overmolding, the interface strength of the overmolded parts can be crucial for the structure of the part. It is possible to give a qualitative prediction of the strength of that crucial interface, but predicting the actual strength is still challenging [12, 131].

With interest in using TPCs in structural applications, further advances must be made in the modeling of their crash behavior too. Currently, it remains challenging and requires extensive testing as damage and energy absorption in composites is a combination of several individual failure mechanisms and can be strain rate dependent too [202]. The current crash models available require extensive parameter tuning using extensive material characterization tests and thus cannot predict an arbitrary layup reliably [202]. As long as crash simulations with composites remain a large barrier, the focus could be put on replacing metal parts with composites that are not part of the crash structure. This could include parts that could improve the experience in the car due to the damping of the composites reducing NVH levels.

Since composites have such a high design freedom with the possibility of local reinforcements, robust and quicker optimization tools would greatly reduce the design time. By tailoring the layup, the material

usage can be reduced, which allows further weight savings and cost reduction of composite parts. To make full use of the properties of composites it is important that weaknesses such as fiber breakage, fiber waviness, voids, or other defects that can be caused by the forming process are minimized. Reliable forming simulations are required to prevent a trial-and-error approach and thus save design time and costs [101, 150, 203]. Even with good simulation capabilities, a well-designed production process and quality control are needed to ensure the safety of a part.

Another important topic for the use of structural composites in automotive is the joining and modeling of the interface of composites and metals. An example is the extensive use of metal inserts in thermoplastic composites [49, 155], they can help prevent clamp force reduction due to relaxation and can handle higher local loads. However, the inserts make production and recycling more challenging [204], and they add weight and costs. They all require extra time and data, which is one of the big hurdles for composites in automotive [101]. Better insight into the joining of metal and composites could help reduce the use of reinforcements.

Although all these aspects were beyond the scope of this research, addressing these challenges is essential for the safe implementation of structural composite parts in the automotive industry.

Chapter 10

Conclusions

The aim of this thesis was to design a thermoplastic continuous fiber composite high-volume ready structural cross-car beam and to provide an overview of the challenges in the analysis and implementation of a thermoplastic composite structural part.

Press forming and injection molding combined with blank making using pick and place have demonstrated the capability to produce composite parts with a high degree of automation and within the required cycle time for high-volume manufacturing of automotive parts. When utilizing composites for parts, the lead time for part design can significantly increase. There are numerous variables that can be optimized, such as fiber angles and local reinforcements. Additionally, simulating a composite part is more challenging and thus costly, especially when it comes to strength and crash simulations, which require extensive testing. The orthotropic nature of composites necessitates a larger number of material parameters. Moreover, production-related issues can arise, significantly affecting the strength of the part. These factors pose particular challenges for structural parts. So more research and simulation tools are required.

Simulations based on stiffness requirements have been done to compare a composite CCB with different layups to an aluminum CCB, the current standard for lightweight CCBs in automotive. The use of CF enabled weight reduction, however, this came at a high cost. Achieving weight reduction with GF was challenging due to its relatively low stiffness. Substantial weight savings with GF were only achieved by lowering the eigenfrequency requirement for composites, leveraging the high damping characteristics of thermoplastics. Next to potential weight saving, the damping of composites can decrease vibrations in the car. However, even with using GF, the cost per kg of saved weight exceeded what is acceptable in the automotive industry.

The high material cost of composites, along with the challenges related to recycling scrap materials and products, present a large barrier to widespread adoption in the automotive industry. Additionally, the longer design time for composites and the associated lead time for product development, due to design complexity and testing requirements, often do not align well with the fast-paced design cycles of the automotive world [101]. It is important to improve design and optimization tools, as well as reduce material costs. In conclusion, a metal CCB with composite overmolded ribs offers the advantage of function integration provided by the overmolded ribs, while benefiting from the properties of metal for the structural part of the beam. These benefits include lower material costs, easier design optimization, and easier strength and crash modeling.

Appendix A

Fluctuating Temperature Influence On Relaxation Tests

If the degree of relaxation of the composite with the simulated bolted connection can be found, the drop in clamp force can be determined. As a certain clamp force is required against slippage and fatigue, the limit of what load is acceptable without insert can be determined. This could help prevent unnecessary use of inserts, thereby decreasing costs and potentially saving weight.

A.1 Method

A.1.1 Specimen preparation

The material and conditioning of the relaxation specimens have been done in the same manner as the DMA specimens in section 6.2.1.

A.1.2 Test setup relaxation test

The relaxation tests are done using a Zwick Roell testControl II tensile machine with a 10 kN load cell. A SH-242 climate chamber was placed around the sample as is shown in fig. A.1.1b to control the temperature and humidity during the tests. The specimen is placed on a flat head, the lower half, with the washer centered over the hole in the specimen as is seen in fig. A.1.1 and in fig. A.1.2a. From the top another head then presses down on the washer, this simulates the clamping of a bolt in an oversized hole in which the bolt will not touch the sides of the hole.

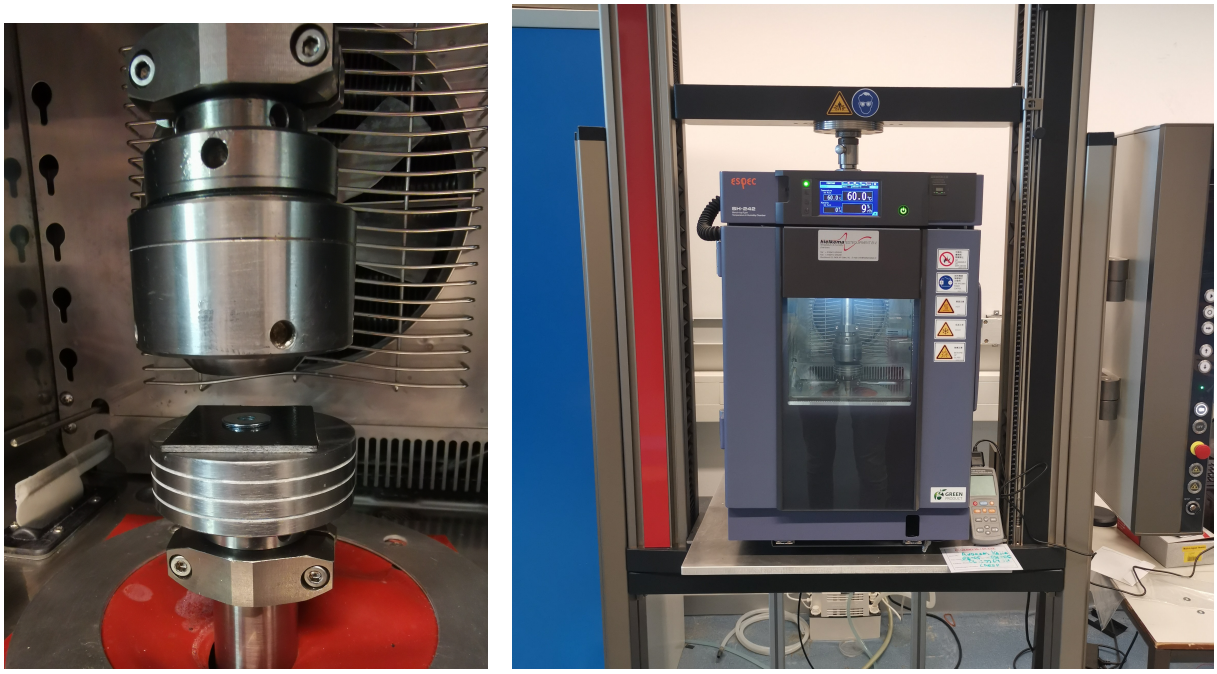

(a) The relaxation setup with the specimen and washer between the heads of the tensile testing machine

(b) The climate chamber regulating the temperature and relative humidity around the sample and the H-like frame of the tensile machine around it

Figure A.1.1: The relaxation test setup

For this test, a M5 bolt is simulated as opposed to a M8 bolt, which is the standard bolt size used to connect a CCB to the body of a car [3]. An M5 bolt has a maximum preload of about 9000 N. This results in the same pressure under the washer as the M8 preload of 25000 N which would use a bigger washer. The smaller M5 washer has enough distance from the edges of the specimen to prevent any edge effects whilst keeping the outer dimensions of the specimen within the circular lower support head of the tensile machine as is seen in fig. A.1.1.

Before the test starts the climate chamber is kept at the conditions for the test for some hours to get the tensile machine up to a constant temperature and prevent a force increase during testing due to the rods still thermally expanding. The specimen is placed in the climate chamber an hour before the test is started to get it up to an equilibrium temperature too, according to the ISO standard [166]. When all is at temperature the test is started by lowering the top head which presses on the washer until a force of 9000 N is reached, which takes about 100 seconds. When 9000 N is reached the movement of the head is stopped, this marks the start of the relaxation test itself.

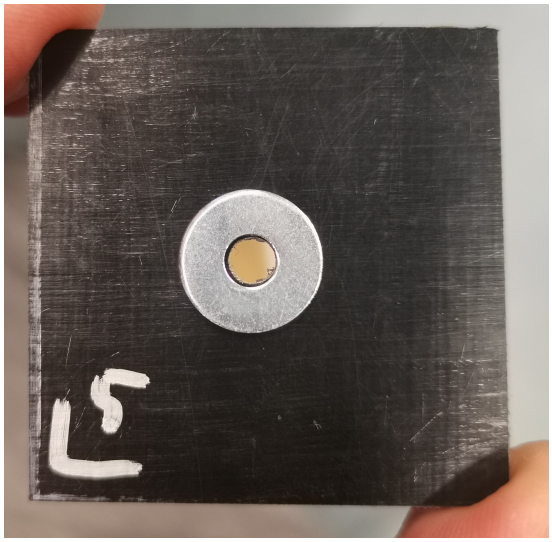

(a) The specimen with the washer over the hole

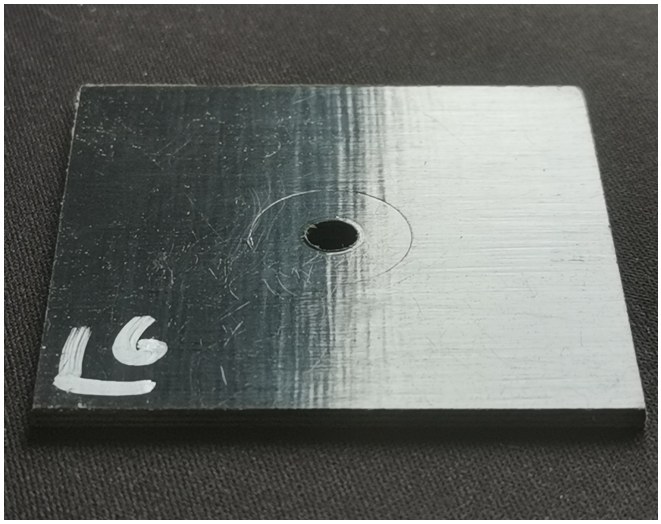

(b) A visible indentation mark of the washer in the specimen after the test

Figure A.1.2: The specimen and washer

A.1.3 Testing conditions

The dry and conditioned to 50% RH samples have different Tg's as is shown in table A.1. The samples will be tested at three different testing temperatures of 23, 40, and 60 $°C$, and at different humidities. The conditioned specimen will be tested at 50% RH and the dried specimen in a dry atmosphere. With different testing temperatures and Tg's, the distance to Tg for each of the testing conditions falls into three categories. Either well below Tg, just around Tg, or well above Tg, with two conditions in each category, as is shown in table A.1. The Tg values were determined by a dynamic mechanical analysis, see section 6.2.2.

Table A.1: Distance to Tg for each sample

Testing conditions	**Above/around/below Tg**	**Tg** $[°C]$	**distance to Tg**
23 $°C$ dry	below	69-73	-48
40 $°C$ dry	below	69-73	-31
60 $°C$ dry	below	69-73	-11
23 $°C$ RH 50	around Tg	24-27	-2
40 $°C$ RH 50	above	24-27	15
60 $°C$ RH 50	above	24-27	35

A.2 Results and discussion

The results of the relaxation tests are plotted on a linear scale in fig. A.2.1a with the measured force on the y-axis and the test time on the x-axis. It is immediately clear that the results are not as expected, which would be a smooth curve declining rapidly at first after which the force relaxation gradually smooths out [158, 159]. The basis of the relaxation behavior is there, but strong fluctuations in measured force during the tests makes the results unusable. Also on a logarithmic scale the force deviations are significant, as is illustrated in fig. A.2.1b. In fig. A.1.2b it is clear that the load applied does cause some permanent deformation, as the washer clearly left an indentation.

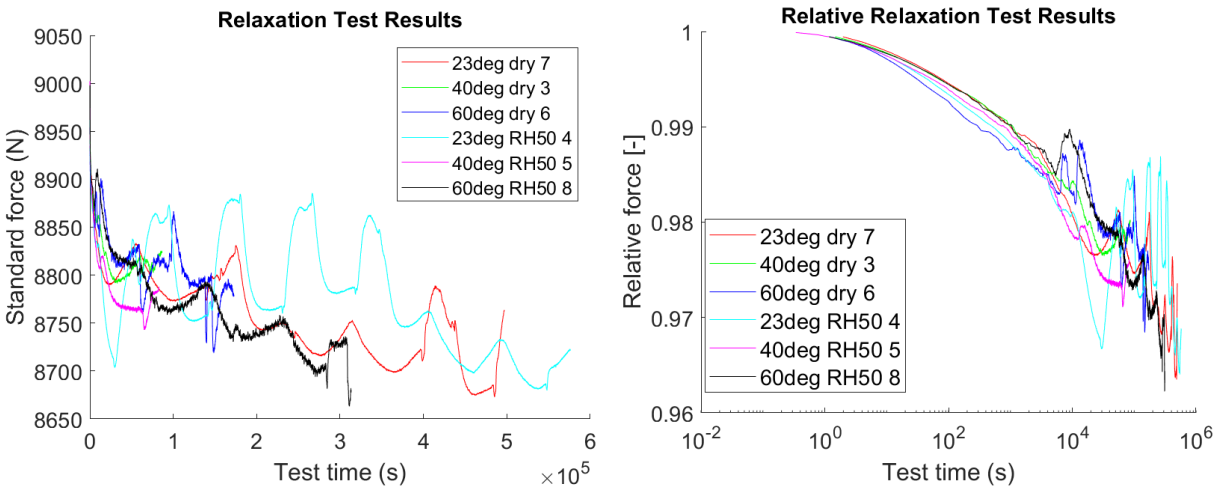

(a) The relaxation results of the six specimens at different temperatures and humidity on a linear scale with the actual force

(b) The relaxation results normalized to the max force at the start on a log x-scale

Figure A.2.1: The relaxation results

A.3 Temperature fluctuations

The relaxation results were also plotted on clock time instead of test time. This revealed that every weekday morning just after 08:00 the force would show a valley and just after 18:00 a small peak, also visible in fig. A.3.1, this effect was not visible on the weekend. So it seemed likely the climate control of the room was responsible for the disturbance of the measurements. To figure out where the problem lies the temperature was measured at different places. First inside the climate chamber to check whether it overcompensated for changes in the room temperature. It was found that the temperature next to the specimen was very constant with only a maximum difference of 0.1 $°C$. Then the temperature was measured right next to the climate chamber. This did show large deviations, similar to the inverted force deviations, this is plotted in fig. A.3.1, with the measured room temperature given by the red dashed line.

In the setup of the relaxation test the testing machine ramps up the force to 9000 N. Once that is reached the displacement of the heads is kept constant for the remainder of the test. This displacement is kept constant by not moving the spindles inside the two vertical beams in fig. A.1.1b which move the horizontal beam in between up and down. However, this does not take into account, or compensate, any change in length of any part of the H frame of the machine or the rods inside the climate chamber. This shows the importance of preheating the tensile machine with the climate chamber.

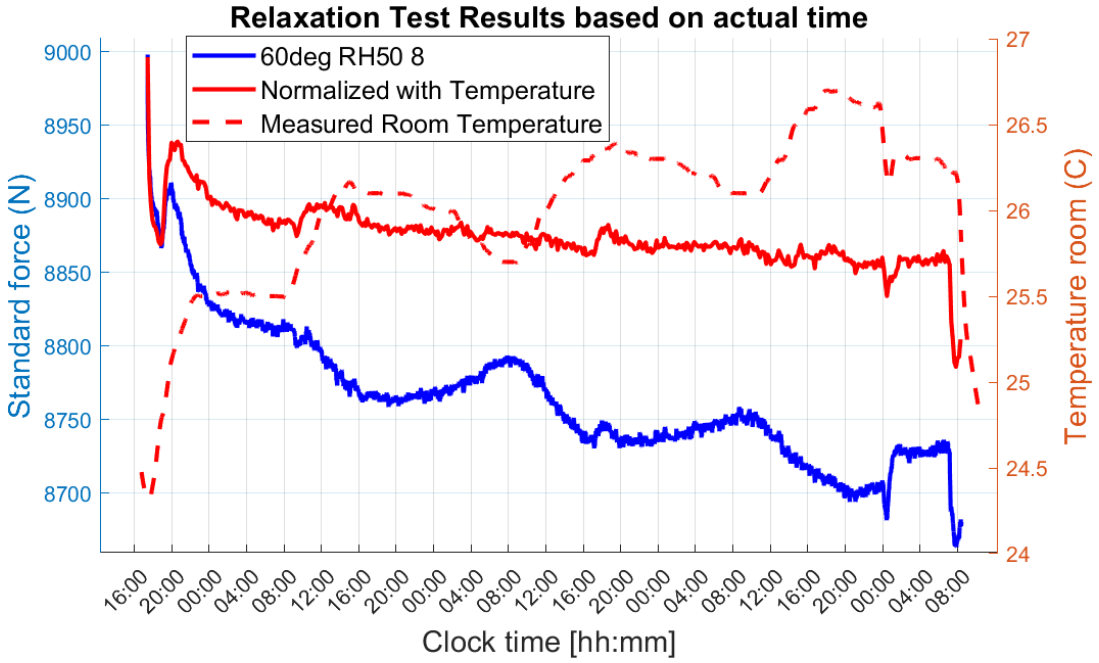

Figure A.3.1: Results from a relaxation test along with the measured room temperature which show similar behavior

An increase in temperature causes the H frame to increase in length. An increase in length in the H frame causes a decrease in force on the specimen as the horizontal bars that are attached to the rods inside the climate chamber are pushed further apart. However, an increase in temperature also causes the rods to increase in length, which increases the force on the specimen. To some degree these effects cancel each other out, although the H frame outside the climate chamber has a longer length affected by the room temperature. The influence of temperature on the force change due to the temperature change is given in eq. (A.3.1) and eq. (A.3.2). With Δd being the change in distance between the upper and lower head inside the climate chamber, with a positive value meaning a smaller distance between the heads. This movement is caused by the thermal expansion, which is the thermal expansion coefficient α times the length of the H frame L_o and the length of the part of the rods that stick out of the climate chamber L_i. Especially for the latter the exact impact of the change in temperature is more difficult to quantify as it is kept stable at a certain temperature inside the chamber but the temperature outside changes, so the actual length change of the rods is hard to estimate.

$$\Delta d = \Delta T \cdot \alpha \cdot (L_i - L_o) \tag{A.3.1}$$

$$\Delta F = E \cdot A \cdot \Delta d / t \tag{A.3.2}$$

For the change in force due to the change in temperature, given in eq. (A.3.2), it is assumed that the steel rods and H frame are much stiffer than the TPC specimen, thus their stiffness is neglected. This means that any change in distance between the clamps needs to be taken up by the deformation of the specimen over its height t with a stiffness E. The stiffness is assumed to be equal to that of conditioned neat PA6 at 60 $°C$ [205] as it is loaded through the thickness which makes the properties more matrix dominant. It is assumed only the specimen under the washer area A takes that force.

These two formulas combined can estimate the change in force due to the change in temperature from the reference temperature, which was set at the temperature measured at the start of the test, being 24.5 $°C$. However, as a number of assumptions had to be made it still requires a multiplication factor of about 0.4 times ΔF to get a relatively smooth relaxation line. The actual force measured, given in blue, combined with $0.4 \cdot \Delta F$, gives the much straighter temperature normalized line, illustrated by the solid red line in fig. A.3.1. This show how strongly the room temperature and the fluctuations in the measured test force are correlated. A correlation between the outside temperature and the change in force was also found

although less strongly. Only some of the tests have good temperature data from the room, so not all tests could be normalized like this.

The conclusion was that the setup of these tests does not give good-quality results, hence the tests were discontinued. One solution is to do creep tests, which are force controlled. Then an increase in force due to thermal expansion is compensated for by the machine. The change in length can be taken out of the equation by also measuring the actual distance between the heads inside the climate chamber. Another option is to use a type of force measuring bolt. With this setup the whole specimen and force application part can be kept inside the climate chamber, which has been shown to give a stable temperature. However, this was outside the scope of this thesis.

During these tests, the temperature difference was relatively minor with only a few degrees, but the forces generated were already significant. In a desert environment, for example, the difference between day and nighttime temperatures can be over 40 $°C$ [206]. Especially in the scenario of a metal car frame surrounding a more brittle TPC CCB, this could result in significant stresses.

Bibliography

[1] Cross car beam kirchoff. https://www.kirchhoff-automotive.com/products/cars/cross-car-beam. [Online; accessed 16-06-2023].

[2] Cross car beam aluminum extruders council. https://aec.org/page/cross-car-beam#:~:text=The%20cross%20car%20beam%20is%20the%20backbone%20of%20the%20instrument,both%20safety%20and%20driver%20comfort. [Online; accessed 04-08-2023].

[3] A2mac1. https://www.a2mac1.com/. [Online; accessed 19-09-2022].

[4] Campus plastics - a material information system for the plastics industry. https://www.campusplastics.com/. [Online; accessed 04-10-2022].

[5] Loredana Kehrer, Daniel Wicht, Jeffrey T. Wood, and Thomas Böhlke. Dynamic mechanical analysis of pure and fiber-reinforced thermoset- and thermoplastic-based polymers and free volume-based viscoelastic modeling. *GAMM Mitteilungen*, 41, 4 2018.

[6] Eniko Soós and Tibor Goda. Mechanical behavior of glass fiber-reinforced bosses: Experiments and fe simulations. *Periodica Polytechnica Mechanical Engineering*, 55:3–14, 2011.

[7] Interview christophe aufrere chief technical officer faurecia. https://www.automotiveworld.com/articles/interview-christophe-aufrere-chief-technical-officer-faurecia/. [Online; accessed 19-05-2023].

[8] Srinivas Nunna, Patrick Blanchard, Derek Buckmaster, Sam Davis, and Minoo Naebe. Development of a cost model for the production of carbon fibres. *Heliyon*, 5, 10 2019.

[9] S. V. Joshi, L. T. Drzal, A. K. Mohanty, and S. Arora. Are natural fiber composites environmentally superior to glass fiber reinforced composites? *Composites Part A: Applied Science and Manufacturing*, 35:371–376, 4 2004.

[10] Erica R.H. Fuchs, Frank R. Field, Richard Roth, and Randolph E. Kirchain. Strategic materials selection in the automobile body: Economic opportunities for polymer composite design. *Composites Science and Technology*, 68:1989–2002, 7 2008.

[11] Jens Kaerger, Lukas Atz, and Jens C Kaerger. Water soluble mandrels for lost core applications in manufacturing of hollow composite structures coconut eu project-hybrid water-soluble mandrel view project water-soluble cores for hollow structures view project water soluble mandrels for lost core applications in manufacturing of hollow composite structures. In *SAMPE Europe Conference 2019*, 2019.

[12] Mark Bouwman, Thijs Donderwinkel, Jeroen Houwers, Sebastiaan, and Wijskamp Moldflow. Overmolding: An integrated design approach for dimensional accuracy and strength of structural parts. In *3rd Annual Composites and Advanced Materials Expo, CAMX 2016 - Anaheim, United States*, 2017.

[13] Michael Emonts, Kai Fischer, Alexander Peitz, and Thomas Weiler. Ultra-fast consolidator machine development – individualized mass production of thermoplastic tailored blanks based on laser-assisted tape placement with in-situ consolidation. *Technologies for Lightweight Structures (TLS)*, 3, 1 2019.

[14] Michael Kühnel, Alfons Schuster, Andreas Buchheim, Mildred Kießig, Tobias Gerngross, and Michael Kupke. *Automatisiertes endkonturnahes Preforming Carbonfaser-Verstärkter Thermoplaste mittels*

robotischer Halbzeugablage. Deutsche Gesellschaft für Luft-und Raumfahrt-Lilienthal-Oberth eV, 2015.

[15] Dongdong Chen, Guangyong Sun, Xihong Jin, and Qing Li. Quasi-static bending and transverse crushing behaviors for hat-shaped composite tubes made of cfrp, gfrp and their hybrid structures. *Composite Structures*, 239, 5 2020.

[16] The engineering toolbox - beams - fixed at both ends - continuous and point loads. `https://www.engineeringtoolbox.com/beams-fixed-both-ends-support-loads-deflection-d_809.html`. [Online; accessed 05-06-2023].

[17] Transverse shear due to bending. `https://www.si-eng.org/post/shear-1-transverse-shear-and-composite-action`. [Online; accessed 28-06-2023].

[18] A new feature to model shell-like structures with stacked elements - tobias erhart. `https://lsdyna.ansys.com/wp-content/uploads/attachments/02-Erhart-DYNAmore-P.pdf`. [Online; accessed 28-06-2023].

[19] Ansys granta edupack software, ansys, inc., cambridge, uk. `www.ansys.com/materials`. [Online; accessed 09-02-2023].

[20] Plasticportal polymer prices. `https://www.plasticportal.eu/en/polymer-prices/lm/14/`. [Online; accessed 04-10-2022].

[21] Haibin Ning, Na Lu, Ahmed Arabi Hassen, Krishan Chawla, Mohamed Selim, and Selvum Pillay. A review of long fibre-reinforced thermoplastic or long fibre thermoplastic (lft) composites. *International Materials Reviews*, 2018.

[22] Tepex gf pp datasheet. `https://lanxess.com/-/media/Project/Lanxess/Corporate-Internet/Products-and-Solutions/Brands/Tepex/Data-sheets/MDS104RG600x47-1.pdf`. [Online; accessed 02-07-2023].

[23] Tepex gf pa6 datasheet - campus plastics. `https://www.campusplastics.com/campus/en/datasheet/Tepex%C2%AE+dynalite+102-RG600%28x%2947/LANXESS/99/fdfaae65/SI?pos=1`. [Online; accessed 02-07-2023].

[24] What parts are considered structural. `https://www.pnlestimology.com/wp-content/uploads/2012/02/What-Parts-are-Actually-Considered-Structural-Oct10.pdf`. [Online; accessed 12-07-2023].

[25] Regulation (eu) 2019/631 of the european parliament and of the council of 17 april 2019 setting co2 emission performance standards for new passenger cars and for new light commercial vehicles, and repealing regulations (ec) no 443/2009 and (eu) no 510/2011 (recast) (text with eea relevance. `https://eur-lex.europa.eu/legal-content/EN/TXT/?uri=CELEX%3A32019R0631`. [Online; accessed 19-05-2023].

[26] Robert A. Witik, Jérôme Payet, Véronique Michaud, Christian Ludwig, and Jan Anders E. Månson. Assessing the life cycle costs and environmental performance of lightweight materials in automobile applications. *Composites Part A: Applied Science and Manufacturing*, 42:1694–1709, 11 2011.

[27] Bloomberg battery cost compared to total vehicle cost. `https://www.bloomberg.com/opinion/newsletters/2019-04-12/electric-vehicle-battery-shrinks-and-so-does-the-total-cost-juebizw9`. [Online; accessed 12-07-2023].

[28] Thomas Jollivet, Catherine Peyrac, and Fabien Lefebvre. Damage of composite materials. *Procedia Engineering*, 66:746–758, 2013. Fatigue Design 2013, International Conference Proceedings.

[29] Rebecca Bernatas, Sylvie Dagréou, Auriane Despax-Ferreres, Anaïs Barasinski, Anaïs Barasinski Recycling, and Sylvie Dagreou. Recycling of fiber reinforced composites with a focus on thermoplastic composites-nc-nd license recycling of fiber reinforced composites with a focus on thermoplastic composites. *Cleaner Engineering and Technology*, 2021.

[30] Marcia Kurcz, Burak Baser, Harri Dittmar, Joachim Sengbusch, and Hans Pfister. A case for replacing steel with glass-mat thermoplastic composites in spare-wheel well applications background and requirements. In *SAE 2005 World Congress and Exhibition*, 2005.

[31] Guohua Zhu, Guangyong Sun, Hang Yu, Shunfeng Li, and Qing Li. Energy absorption of metal, composite and metal/composite hybrid structures under oblique crushing loading. *International Journal of Mechanical Sciences*, 135:458–483, 1 2018.

[32] Hamidreza Zarei, Matthias Kröger, and Henrik Albertsen. An experimental and numerical crashworthiness investigation of thermoplastic composite crash boxes. *Composite Structures*, 85:245–257, 10 2008.

[33] Richard Stewart. Thermoplastic composites - recyclable and fast to process. *Reinforced Plastics*, 55:22–28, 5 2011.

[34] John Z. Lin and Stephen M. Pitrof. Analytical design of cockpit modules for safety and comfort. In *SAE 2004 World Congress and Exhibition*. SAE International, mar 2004.

[35] Mingde Ding, Bo Liu, Chongqing Changan, Jinyan Wang, Fuqiang Zhai, Lu Li, Jin-Yan Wang, Ming-De Ding, • Zhen-Hua Fan, • Fu-Qiang Zhai, • Lu Li, and Wangjinyan@dlut Edu Cn. Damping property of carbon fiber reinforced plastic for noise/vibration/harsh of steering column support assembly title page damping property of carbon fiber reinforced plastic for noise/vibration/harsh of steering column support assembly damping property of carbon fiber reinforced plastic for noise/vibration/harsh of steering column support assembly. *Research Square*, 2021.

[36] ISO Central Secretary. Road vehicles-environmental conditions and testing for electrical and electronic equipment-part 4: Climatic loads véhicules routiers-spécifications d'environnement et essais de l'équipement électrique et électronique-partie 4: Contraintes climatiques. Technical report, International Organization for Standardization, 2010.

[37] Neil Reynolds and Arun Balan Ramamohan. *High-Volume Thermoplastic Composite Technology for Automotive Structures*, chapter 2, pages 29–50. John Wiley and Sons, Ltd, 2013.

[38] evvolumes. `https://www.ev-volumes.com/`. [Online; accessed 12-07-2023].

[39] Faurecia composite cross car beam molded. `https://www.youtube.com/watch?v=9qyj_l7dTPg&ab_channel=Faurecia`. [Online; accessed 12-09-2022].

[40] Faurecia composite cross car beam thermoformed. `https://slideplayer.com/slide/6104579/`. [Online; accessed 12-09-2022].

[41] Faurecia composite cross car beam thermoformed. `https://www.marklines.com/statics/topSuppliers/img/exhibit/naias2015/images/faurecia_IMG_4466.jpg`. [Online; accessed 12-09-2022].

[42] Curved pultruded auto parts. `https://www.compositesworld.com/articles/curve-in-the-road-first-curved-pultruded-auto-parts`. [Online; accessed 19-05-2023].

[43] Lightvehicle 2025 automotive. `https://www.lightvehicle2025.eu/wp-content/uploads/2020/08/Webinar-Automotive-NL-AVK-Final-16062020.pdf`. [Online; accessed 13-07-2023].

[44] Bing Du, Zhengxuan Li, Huimin Bai, Qian Li, Changqi Zheng, Jingwei Liu, Feng Qiu, Zhenhua Fan, Hanjie Hu, and Liming Chen. Mechanical property of long glass fiber reinforced polypropylene composite: From material to car seat frame and bumper beam. *Polymers*, 14, 5 2022.

[45] Composites used in bmw ix 2022. `https://www.compositesworld.com/articles/bmw-rolls-out-multi-material-carbon-cage-with-2022-ix-vehicle-line`. [Online; accessed 06-12-2022].

[46] Curved bumper beam corvette. `https://www.compositesworld.com/articles/curved-profiles-radius-pultrusion`. [Online; accessed 19-05-2023].

[47] Richard A. Brooks, Hongyan Wang, Zerong Ding, Jie Xu, Qinghua Song, Haibao Liu, John P. Dear, and Nan Li. A review on stamp forming of continuous fibre-reinforced thermoplastics. *International Journal of Lightweight Materials and Manufacture*, 5:411–430, 9 2022.

[48] Composites used in bmw ix - jec composites. `https://www.jeccomposites.com/news/the-first-ever-bmw-ix/`. [Online; accessed 12-07-2023].

[49] Vw use of pp injection molding and tepex. https://www.plasticstoday.com/automotive-and-mobility/continuous-fiber-reinforced-thermoplastic-composite-displays-potential-tool. [Online; accessed 12-07-2023].

[50] Ccb comparison tesla model 3 and s plaid. https://www.youtube.com/watch?v=rvpK-4RJtcY&ab_channel=MunroLive. [Online; accessed 07-12-2022].

[51] J.L. Thomason. The influence of fibre length and concentration on the properties of glass fibre reinforced polypropylene: 5. injection moulded long and short fibre pp. *Composites Part A: Applied Science and Manufacturing*, 33(12):1641–1652, 2002.

[52] Mihai Brebu. Environmental degradation of plastic composites with natural fillers—a review. *Polymers*, 12:166, 1 2020.

[53] P. K. Mallick. *Materials, design and manufacturing for lightweight vehicles*. CRC Press, 2010.

[54] Normasmira A. Rahman, Aziz Hassan, R. Yahya, and R. A. Lafia-Araga. Impact properties of glass-fiber/polypropylene composites: The influence of fiber loading, specimen geometry and test temperature. *Fibers and Polymers*, 14:1877–1885, 11 2013.

[55] P.K. Mallick. Thermoplastics and thermoplastic–matrix composites for lightweight automotive structures. *Materials, Design and Manufacturing for Lightweight Vehicles*, pages 187–228, 2021.

[56] Youngbum Kim and O. Ok Park. Effect of fiber length on mechanical properties of injection molded long-fiber-reinforced thermoplastics. *Macromolecular Research*, 28:433–444, 5 2020.

[57] Albert P. Philipse. The random contact equation and its implications for (colloidal) rods in packings, suspensions, and anisotropic powders. *Langmuir*, 12(5):1127–1133, 1996.

[58] Norman J. Mewis, Jan Wagner. *5.2 Landmark Observations*. Cambridge University Press, 2012.

[59] Thomas Höftberger, Florian Dietrich, Gernot Zitzenbacher, and Christoph Burgstaller. Influence of fiber content and dosing position on the the mechanical properties of short-carbon-fiber polypropylene compounds. *Polymers*, 14, 11 2022.

[60] Erik Emilsson, Lisbeth Dahllöf, and Maria Ljunggren. Plastics in passenger cars a comparison over types and time method on environmental organisation of material flows view project towards sustainable waste management view project. *IVL Swedish Environmental Research Institute*, 2019.

[61] Sabic pp dashboard carrier. https://docplayer.net/60762570-Long-glass-fiber-polypropylene-light-weight-instrument-panel-retainers-door-modules-matthew-marks-september.html. [Online; accessed 25-10-2022].

[62] Django Mathijsen. Thermoplastic composites keep gaining momentum in the automotive industry. *Reinforced Plastics*, 60:408–412, 11 2016.

[63] Formula 1, motorsport, and high performance automotive composite materials selector guide - toray. https://www.toraytac.com/products/thermoplastic. [Online; accessed 04-10-2022].

[64] Omnexus resin selector thermoplastic composites. https://omnexus.specialchem.com/selection-guide/resin-selection-for-thermoplastic-composites. [Online; accessed 04-10-2022].

[65] Pa6 composite insert a-pillar porsche 911. https://www.compositesworld.com/articles/composite-insert-as-a-structural-reinforcement-for-a-pillars. [Online; accessed 25-10-2022].

[66] C-shock pultruded bumper beam. https://www.cqfd-composites.com/ultimate-mechanics/. [Online; accessed 06-12-2022].

[67] Omnexus pa thermoplastics. https://omnexus.specialchem.com/selection-guide/polyamide-pa-nylon. [Online; accessed 26-10-2022].

[68] Leonid V. Pastukhov, Marc J.W. Kanters, Tom A.P. Engels, and Leon E. Govaert. Influence of fiber orientation, temperature and relative humidity on the long-term performance of short glass fiber reinforced polyamide 6. *Journal of Applied Polymer Science*, 138, 5 2021.

[69] Omnexus - glass transition temperature plastics. https://omnexus.specialchem.com/polymer-properties/properties/glass-transition-temperature. [Online; accessed 09-02-2023].

[70] E Parodi. *Structure properties relations for polyamide 6*. PhD thesis, Technische Universiteit Eindhoven, 2017.

[71] Polypropylene moisture sensitivity. https://www.akplastics.com/wp-content/uploads/2020/06/asahikasei_polypropyleneprocessingguide_2018_0.pdf. [Online; accessed 16-02-2023].

[72] Venkata S. Chevali, Derrick R. Dean, and Gregg M. Janowski. Flexural creep behavior of discontinuous thermoplastic composites: Non-linear viscoelastic modeling and time-temperature-stress superposition. *Composites Part A: Applied Science and Manufacturing*, 40:870–877, 7 2009.

[73] Haibin Ning, Na Lu, Ahmed Arabi Hassen, Krishan Chawla, Mohamed Selim, and Selvum Pillay. A review of long fibre-reinforced thermoplastic or long fibre thermoplastic (lft) composites. *International Materials Reviews*, 2019.

[74] Omnexus toughness thermoplastics. https://omnexus.specialchem.com/polymer-properties/properties/toughness. [Online; accessed 04-10-2022].

[75] Klaus Friedrich and Abdulhakim A. Almajid. Manufacturing aspects of advanced polymer composites for automotive applications. *Applied Composite Materials*, 20:107–128, 4 2013.

[76] Imen Ksouri, Olivier De Almeida, and Nader Haddar. Long term ageing of polyamide 6 and polyamide 6 reinforced with 30% of glass fibers: physicochemical, mechanical and morphological characterization. *Journal of Polymer Research*, page 24, 2017.

[77] Ivanna Pivdiablyk, Patrick Rozycki, Frédéric Jacquemin, Laurent Gornet, and Stéphane Auger. Experimental analysis of mechanical performance of glass fibre reinforced polyamide 6 under varying environmental conditions. *Composite Structures*, 245, 8 2020.

[78] *Zukunftstechnologien für den multifunktionalen Leichtbau Technologies for economic and functional lightweight design*, 2020.

[79] Bethany Middleton. 3 - composites: Manufacture and application. In Vannessa Goodship, Bethany Middleton, and Ruth Cherrington, editors, *Design and Manufacture of Plastic Components for Multifunctionality*, pages 53–101. William Andrew Publishing, Oxford, 2016.

[80] M. De Araújo. 1 - natural and man-made fibres: Physical and mechanical properties. In R. Fangueiro, editor, *Fibrous and Composite Materials for Civil Engineering Applications*, Woodhead Publishing Series in Textiles, pages 3–28. Woodhead Publishing, 2011.

[81] Fiberglass types. https://polser.com/en/frp/fiberglass-types. [Online; accessed 23-12-2022].

[82] Fiberglass. https://reader.elsevier.com/reader/sd/pii/B0080431526005581?token=3DCAE647BF8CEEC39842C257110F4EFD0C4C0E8A8467D2E231FFCFEE8DB2AB9FCDFD04E5C8CFF452FF71B1D4466674A8&originRegion=eu-west-1&originCreation=20221223151122. [Online; accessed 23-12-2022].

[83] Robert A. Witik, Fabrice Gaille, Rémy Teuscher, Heike Ringwald, Véronique Michaud, and Jan Anders E. Månson. Economic and environmental assessment of alternative production methods for composite aircraft components. *Journal of Cleaner Production*, 29-30:91–102, 7 2012.

[84] Jack Howarth, Sada S.R. Mareddy, and Paul T. Mativenga. Energy intensity and environmental analysis of mechanical recycling of carbon fibre composite. *Journal of Cleaner Production*, 81:46–50, 10 2014.

[85] Compositesworld - carbon boeing 787. https://www.compositesworld.com/articles/boeing-787-update. [Online; accessed 11-07-2023].

[86] Toray composite material. https://www.cf-composites.toray/resources/brochures/pdf/composite_material.pdf. [Online; accessed 11-07-2023].

[87] Tepex cf pa6 datasheet. https://lanxess.com/-/media/Project/Lanxess/Corporate-Internet/Products-and-Solutions/Brands/Tepex/Data-sheets/MDS202C200x50.pdf. [Online; accessed 30-06-2023].

[88] Toray cetex pa6 cf and gf tape. https://www.toraytac.com/media/694245aa-3765-43b4-a2cd-8cf76e4aeec5/lmhIVg/TAC/Documents/Data_sheets/Thermoplastic/UD%20tapes,%20prepregs%20and%20laminates/Toray-Cetex-TC910_PA6_PDS.pdf. [Online; accessed 13-07-2023].

[89] Michael F. Ashby. Chapter 5 - materials selection—the basics. In Michael F. Ashby, editor, *Materials Selection in Mechanical Design (Fourth Edition)*, pages 97–124. Butterworth-Heinemann, Oxford, fourth edition edition, 2011.

[90] Autar K. Kaw. *Mechanics of Composite Materials*. Taylor and Francis, 2005.

[91] Ansys performance indices. https://www.ansys.com/content/dam/amp/2021/august/webpage-requests/education-resources-dam-upload-batch-6/performance-indices-booklet-bokpeien22.pdf. [Online; accessed 08-06-2023].

[92] Kloecknermetals - aluminum in cars. https://www.kloecknermetals.com/blog/aluminum-in-cars/. [Online; accessed 11-07-2023].

[93] Plastic portal - prices pa6. https://www.plasticportal.eu/en/ceny-polymerov/lm/14/price/4158/. [Online; accessed 30-06-2023].

[94] Mass reduction roadmap study 2025-2035, 2020 report. https://www.cargroup.org/wp-content/uploads/2021/04/Mass-Reduction-roadmap-report-final-Nov10.pdf. [Online; accessed 30-06-2023].

[95] René Holschuh, David Becker, and Peter Mitschang. Techno-economic feasibility study of new concept for build-up of local load specific reinforced hybrid structures. *Polymers and Polymer Composites*, 24:347–364, 6 2016.

[96] Lightweight heavy impact, mckinsey, 2012. https://www.mckinsey.com/~/media/mckinsey/dotcom/client_service/automotive%20and%20assembly/pdfs/lightweight_heavy_impact.ashx. [Online; accessed 04-10-2022].

[97] M. K. Hagnell, S. Kumaraswamy, T. Nyman, and M. Åkermo. From aviation to automotive - a study on material selection and its implication on cost and weight efficient structural composite and sandwich designs. *Heliyon*, 6, 3 2020.

[98] Michael F. Ashby. Chapter 7 - multiple constraints and conflicting objectives. In Michael F. Ashby, editor, *Materials Selection in Mechanical Design (Fourth Edition)*, pages 197–216. Butterworth-Heinemann, Oxford, fourth edition edition, 2011.

[99] K. L. Edwards. Strategic substitution of new materials for old: Applications in automotive product development. *Materials and Design*, 25:529–533, 2004.

[100] Rouilloux G. and Znojek B. Plastics - the future for automakers and chemical companies. https://www.kearney.com/industry/chemicals/article/-/insights/plastics-the-future-for-automakers-and-chemical-companies, 2012. [Online; accessed 04-10-2022].

[101] Biggest hurdles for automotive composites. https://www.compositesworld.com/articles/biggest-hurdles-for-automotive-composites-. [Online; accessed 02-06-2023].

[102] J.P. Carey. *1 - Introduction to braided composites*. Woodhead Publishing, 2017.

[103] D Tatsuno, & T Yoneyama, & T Kinari, E Sakanishi, & T Ochiai, and Y Taniichi. Braid-press forming for manufacturing thermoplastic cfrp tube. *International Journal of Material Forming*, 2020.

[104] Maximilian Volk, Joanna Wong, Shelly Arreguin, and Paolo Ermanni. Pultrusion of large thermoplastic composite profiles up to Ø 40 mm from glass-fibre/pet commingled yarns. *Composites Part B: Engineering*, 227, 12 2021.

[105] Marco Valente, Ilaria Rossitti, Ilario Biblioteca, and Matteo Sambucci. Thermoplastic composite materials approach for more circular components: From monomer to in situ polymerization, a review. *Journal of Composites Science*, 6, 5 2022.

[106] Kirill Minchenkov, Alexander Vedernikov, Alexander A. Safonov, and Iskander Sh. Akhatov. Thermoplastic pultrusion: A review. *Polymers*, 13, 2021.

[107] A.K. van der Vegt and L.E. Govaert. *Polymeren: Van keten tot kunststof*. VSSD, Netherlands, 5 edition, 2005.

[108] Marco Valente, Ilaria Rossitti, and Matteo Sambucci. Different production processes for thermoplastic composite materials: Sustainability versus mechanical properties and processes parameter. *Polymers*, 15, 1 2023.

[109] Braiding thermoplastic prepreg tape. `https://www.reinforcedplastics.com/content/features/expanded-role-for-thermoplastic-composites-part-2`. [Online; accessed 07-12-2022].

[110] *CONTINIOUS PRODUCTION OF BRAIDED PARTS WITH THERMOPLASTIC MATRICES*, 2014.

[111] Overbraiding eurocarbon. `https://www.eurocarbon.com/composite-reinforcement/overbraiding-and-turn-key-solutions/`. [Online; accessed 22-05-2023].

[112] J. Schäfer and T. Gries. Braiding pultrusion of thermoplastic composites. *Advances in Braiding Technology*, pages 405–428, 2016.

[113] Fuh-Gwo Yuan. Woodhead publishing series in composites science and engineering. In *Structural Health Monitoring (SHM) in Aerospace Structures*, pages xiii–xvi. Woodhead Publishing, 2016.

[114] Louis Laberge-Lebel and Suong Van Hoa. Manufacturing of braided thermoplastic composites with carbon/nylon commingled fibers. *Journal of Composite Materials*, 41:1101–1121, 5 2007.

[115] Nh90 braided composite landing gear. `https://www.gknaerospace.com/en/our-technology/2017/the-future-has-landed-2/`. [Online; accessed 06-12-2022].

[116] Anubhav Singh, Neil Reynolds, Elspeth M. Keating, Alastair E. Barnett, Steve K. Barbour, and Darren J. Hughes. The effect of braid angle on the flexural performance of structural braided thermoplastic composite beams. *Composite Structures*, 261, 4 2021.

[117] J Schäfer, N Hawelka, and T Gries. Continuous production of braided parts with thermoplastic matrices. *Mitteilungen, Institut fur Textiltechnik*, pages 22–26, 2014.

[118] J. Schäfer and T. Gries. 17 - braiding pultrusion of thermoplastic composites. In Yordan Kyosev, editor, *Advances in Braiding Technology*, Woodhead Publishing Series in Textiles, pages 405–428. Woodhead Publishing, 2016.

[119] F.C. Campbell. Chapter 7 - polymer matrix composites. In F.C. Campbell, editor, *Manufacturing Technology for Aerospace Structural Materials*, pages 273–368. Elsevier Science, Oxford, 2006.

[120] Tjitse K. Slange, Wouter J.B. Grouve, Laurent L. Warnet, S. Wijskamp, and Remko Akkerman. Towards the combination of automated lay-up and stamp forming for consolidation of tailored composite components. *Composites Part A: Applied Science and Manufacturing*, 119:165–175, 4 2019.

[121] Pinettepei tailored blank. `https://pinetteemidecau.eu/en/`. [Photo taken at K-Fair 2022].

[122] T. K. Slange, L. Warnet, W. J.B. Grouve, and R. Akkerman. Influence of preconsolidation on consolidation quality after stamp forming of c/peek composites. *AIP Conference Proceedings*, 1769, 10 2016.

[123] Tjitse Slange. *Rapid Manufacturing of Tailored Thermoplastic Composites by Automated Lay-up and Stamp Forming A Study on the Consolidation Mechanisms Tjitse K. Slange*. PhD thesis, University of Twente, 2018.

[124] Flexform. `https://www.flexformtech.com/News/pdfs/Composites-World-Thermoformable-Composite-Panels.pdf`. [Online; accessed 22-03-2023].

[125] Sebastiaan Haanappel, Ulrich Sachs, René H.W. ten Thije, Bert Rietman, and Remko Akkerman. Forming of thermoplastic composites. *Key engineering materials*, 504-506:237–242, 2012. Volume: Material Forming ESAFORM 2012, ed. by M. Merklein and H. Hagenah.

[126] Osman Atalay and Fahrettin Ozturk. Effects of gripper location and blank geometry on the thermoforming of a carbon-fiber woven-fabric/polyphenylene sulfide composite sheet. *Journal of Thermoplastic Composite Materials*, 2022.

[127] R. Akkerman and S.P. Haanappel. 6 - thermoplastic composites manufacturing by thermoforming. In Philippe Boisse, editor, *Advances in Composites Manufacturing and Process Design*, pages 111–129. Woodhead Publishing, 2015.

[128] Jui He Tai and Autar Kaw. Transverse shear modulus of unidirectional composites with voids estimated by the multiple-cells model. *Composites Part A: Applied Science and Manufacturing*, 105:310–320, 2 2018.

[129] Thermoplastic cfrp preforming and forming line qsp. `https://pinetteemidecau.eu/en/advanced-materials-and-technologies/preforming-and-forming/2015-11-28-03-56-65`. [Online; accessed 12-07-2023].

[130] Variotherm temperature control for organo sheets. `https://www.plastverarbeiter.de/roh-und-zusatzstoffe/variotherme-temperierung-fuer-organobleche.html`. [Online; accessed 13-07-2023].

[131] Remko Akkerman, Mark Bouwman, and Sebastiaan Wijskamp. Analysis of the thermoplastic composite overmolding process: Interface strength. *Frontiers in Materials*, 7, 2 2020.

[132] Thermopre engineering. `https://thermopre-engineering.de/en/`. [Photo taken at K-Fair 2022].

[133] Lanxess welding two tepex shells for mercedes. `https://www.youtube.com/watch?v=h_Yn_TY00vc&ab_channel=LANXESS`. [Online; accessed 19-05-2023].

[134] Norbert Zwicklhuber, Pauland Muller. Net shape stacking and consolidation of thermoplastic composite tapes. In Klaus Droder and Thomas Vietor, editors, *Technologies for economic and functional lightweight design*, pages 25–34, Berlin, Heidelberg, 2021. Springer Berlin Heidelberg.

[135] automated-preforming-quilted-stratum-process-qsp. `https://www.compositesworld.com/articles/automated-preforming-quilted-stratum-process-qsp`. [Online; accessed 12-07-2023].

[136] J. Verrey, M. D. Wakeman, V. Michaud, and J. A.E. Månson. Manufacturing cost comparison of thermoplastic and thermoset rtm for an automotive floor pan. *Composites Part A: Applied Science and Manufacturing*, 37:9–22, 1 2006.

[137] A Burkhart and D Cramer. Feasibility of continuous-fiber reinforced thermoplastic tailored blanks for automotive applications. In -, 2005.

[138] C Brecher, A Kermer-Meyer, and M Emonts. Flexible and automated production of composite parts. In *European Conference on Composite Materials (ECCM) 2014*, pages 22–26, 2014.

[139] Christian Brecher, Tido Peters, and Henning Janssen. Selective high-speed tape placement using cut-on-the-fly for local reinforcement of gmt substrates towards a waste-reducing production of multi-material components. *Int. J. Automotive Composites*, 2:113–138, 2016.

[140] Vincenzo Lunetto, Manuela Galati, Luca Settineri, and Luca Iuliano. Sustainability in the manufacturing of composite materials: A literature review and directions for future research. *Journal of Manufacturing Processes*, 85:858–874, 1 2023.

[141] Ivw automated tape placement. `https://www.ivw.uni-kl.de/en/news/details/start-of-operation-of-the-worlds-fastest-tape-laying-machine-1`. [Online; accessed 21-06-2023].

[142] Michael Kropka, Mathias Muehlbacher, Thomas Neumeyer, and Volker Altstaedt. From ud-tape to final part – a comprehensive approach towards thermoplastic composites. *Procedia CIRP*, 66:96–100, 2017.

[143] Airborne pick and weld. `https://www.airborne.com/airborne-introduces-automated-preforming-by-pick-and-weld/`. [Online; accessed 31-05-2023].

[144] Andreas Björnsson, Marie Jonsson, and Kerstin Johansen. Automated material handling in composite manufacturing using pick-and-place systems – a review. *Robotics and Computer-Integrated Manufacturing*, 51:222–229, 2018.

[145] Kentaro Sato, Toru Inazumi, Akihide Yoshitake, and Sheng Dong Liu. Effect of material properties of advanced high strength steels on bending crash performance of hat-shaped structure. *International Journal of Impact Engineering*, 54:1–10, 2013.

[146] Shiqiang Deng, Luke Djukic, Rowan Paton, and Lin Ye. Thermoplastic-epoxy interactions and their potential applications in joining composite structures - a review. *Composites Part A: Applied Science and Manufacturing*, 68:121–132, 2015.

[147] P. J. Bates, S. Tan, G. Zak, and M. McLeod. Shear strength and meltdown behavior of reinforced polypropylene assemblies made by resistance welding. *Composites Part A: Applied Science and Manufacturing*, 40:28–35, 1 2009.

[148] Yohei Abe, Wataru Ijichi, Ken Ichiro Mori, and Kazuma Nakagawa. Hemming with pre-bent inner sheet for joining ultra-high strength steel sheets of automobile parts. *Journal of Manufacturing and Materials Processing*, 4, 9 2020.

[149] The outlook for thermoplastic composites cw trending episode 7 - composites world. `https://www.compositesworld.com/articles/the-outlook-for-thermoplastic-composites-cw-trending-episode-7-`. [Online; accessed 06-12-2022].

[150] Tobias Mattner, Julian Popp, Tobias Kleffel, Christian Gröschel, and Dietmar Drummer. High-speed forming of continuous fiber reinforced thermoplastics. *Applied Composite Materials*, 27:37–54, 4 2020.

[151] Sebastiaan Wijskamp Richard de Vries, Edwin Lamers, Blasimir Villa Rodriguez, and Remko Akkerman. Theoretical background in woven fabric composite properties. `https://www.utwente.nl/en/et/ms3/research-chairs/pt/Tools/#u20mm`.

[152] Warren C Young, Richard G Budynas, and Ali M Sadegh. *Roark's formulas for stress and strain; 8th ed.* McGraw Hill, New York, NY, 2012.

[153] Cae of organo-sheet material. `http://techcenter.lanxess.com`. [Online; accessed 07-12-2022].

[154] Aniform. `https://aniform.com/`. [Online; accessed 24-03-2023].

[155] Lucid air frontend by elringklinger. `https://www.elringklinger.de/en/press/pressreleases/11-10-2021`. [Online; accessed 17-05-2023].

[156] Anna Galińska. Mechanical joining of fibre reinforced polymer composites to metals—a review. part i: Bolted joining. *Polymers*, 12:1–48, 10 2020.

[157] Ron R. Schmitt. Viscoelastic relaxation in bolted thermoplastic composite joints, 1984.

[158] Srinivasa D. Thoppul, Ronald F. Gibson, and Raouf A. Ibrahim. Phenomenological modeling and numerical simulation of relaxation in bolted composite joints. *Journal of Composite Materials*, 42:1709–1729, 9 2008.

[159] Jiaxin Lv, Yi Xiao, and Yuande Xue. Time–temperature-dependent response and analysis of preload relaxation in bolted composite joints. *Journal of Reinforced Plastics and Composites*, 37:460–474, 4 2018.

[160] Daniel Tobalina-Baldeon, Felix Sanz-Adán, Marian Martinez-Calvo, Carmelo Gómez, Inigo Sanz-Pena, and Francisco Cavas. Feasibility analysis of bolted joints with composite fibre-reinforced thermoplastics. *Polymers*, 13, 6 2021.

[161] Robert W. Messler. Joining composite materials and structures: Some thought-provoking possibilities. *Journal of Thermoplastic Composite Materials*, 17:51–75, 1 2004.

[162] Xiaochang Duan, Hongwei Yuan, Wei Tang, Jingjing He, and Xuefei Guan. An engineering prediction model for stress relaxation of polymer composites at multiple temperatures. *Polymers*, 14, 2 2022.

[163] Numaira Obaid, Mark T. Kortschot, and Mohini Sain. Predicting the stress relaxation behavior of glass-fiber reinforced polypropylene composites. *Composites Science and Technology*, 161:85–91, 6 2018.

[164] Material dsm: Pa6 - gf k20hg60. https://plasticsfinder.com/en/datasheet/UDea%E2%84%A2%20Akulon%C2%AE%20K20HG60/5OQJm. [Online; accessed 05-04-2023].

[165] Thermoplastics composites research center. https://tprc.nl/. [Online; accessed 05-04-2023].

[166] Iso 1110 plastics — polyamides — accelerated conditioning of test specimens. https://www.iso.org/standard/76395.html. [Online; accessed 05-04-2023].

[167] Astm d7028-07 - standard test method for glass transition temperature (dma tg) of polymer matrix composites by dynamic mechanical analysis (dma). https://www.astm.org/d7028-07r15.html. [Online; accessed 12-05-2023].

[168] C.M. Stokes-Griffin, A. Kollmannsberger, P. Compston, and K. Drechsler. The effect of processing temperature on wedge peel strength of cf/pa6 laminates manufactured in a laser tape placement process. *Composites Part A: Applied Science and Manufacturing*, 121:84–91, 2019.

[169] Elnura Artykbaeva, Bedriye Ucpinar Durmaz, Pelin (Parisa) Aksoy (Golshaei), and Ayse Aytac. Investigation of the properties of pa6/pa610 blends and glass fiber reinforced pa6/pa610 composites. *Polymer Composites*, 43(10):7514–7525, 2022.

[170] Lin Sang, Yingying Wang, Chuo Wang, Xingshuang Peng, Wenbin Hou, and Liyong Tong. Moisture diffusion and damage characteristics of carbon fabric reinforced polyamide 6 laminates under hydrothermal aging. *Composites Part A: Applied Science and Manufacturing*, 123:242–252, 2019.

[171] Dynamic mechanical analysis (dma) guide. https://resources.perkinelmer.com/corporate/cmsresources/images/44-74546gde_introductiontodma.pdf. [Online; accessed 22-06-2023].

[172] Christopher W. Macosko. *Rheology: Principles, Measurements, and Applications*. Wiley, 1994.

[173] Iso 6721 plastics — determination of dynamic mechanical properties — part 11: Glass transition temperature. https://www.iso.org/standard/74988.html. [Online; accessed 12-05-2023].

[174] Anne Bergeret, Laurent Ferry, Patrick Ienny, A Bergeret, L Ferry, and P Ienny. Influence of the fibre/matrix interface on ageing mechanisms of glass fibre reinforced thermoplastic composites (pa-6,6, pet, pbt) in a hygrothermal environment. *Polymer Degradation and Stability*, 94:1315–1324, 2009.

[175] George H. Staab. *2.5 Strain-Stress Relationships*. Elsevier, 1999.

[176] Jaebong Jung, Sungwook Jun, Hyun Seok Lee, Byung Min Kim, Myoung Gyu Lee, and Ji Hoon Kim. Anisotropic hardening behaviour and springback of advanced high-strength steels. *Metals*, 7, 11 2017.

[177] Composites world material parameters. https://www.compositesworld.com/articles/how-do-i-know-if-my-measured-composite-properties-are-correct-or-even-reasonable. [Online; accessed 15-06-2023].

[178] Shell 281 element. https://www.mm.bme.hu/~gyebro/files/ans_help_v182/ans_elem/Hlp_E_SHELL181.html. [Online; accessed 30-03-2023].

[179] Shell 281 element. https://www.mm.bme.hu/~gyebro/files/ans_help_v182/ans_elem/Hlp_E_SHELL281.html#:~:text=SHELL281%20is%20suitable%20for%20analyzing,translational%20degrees%20of%20freedom%20only.). [Online; accessed 30-03-2023].

[180] Viktor Kulisek. Finite element analysis of composite structure, 2016.

[181] Ever J. Barbero. *Finite element analysis of composite materials using Abaqus*. CRC Press Taylor and Francis Group, 2013.

[182] Daryl L. Logan. *A first course in the finite element method*. Thomson, 2007.

[183] Advances in element technology: Solid-shell element. https://www.nafems.org/downloads/North_America/NAFEMS_2020/presentations_post/xie_-_ansys_-_advances_in_element_technology_solid-shell_element_presentation.pdf. [Online; accessed 28-06-2023].

[184] Rodrigo P. Tavares, Vincent Bouwman, and W. Van Paepegem. Finite element analysis of wind turbine blades subjected to torsional loads: Shell vs solid elements. *Composite Structures*, 280, 1 2022.

[185] Solidshell 190 element. https://www.mm.bme.hu/~gyebro/files/ans_help_v182/ans_thry/thy_el190.html. [Online; accessed 03-04-2023].

[186] Solid 186 element. https://www.mm.bme.hu/~gyebro/files/ans_help_v182/ans_elem/Hlp_E_SOLID186.html#SOLID186L.description. [Online; accessed 30-03-2023].

[187] Fea tips solid vs shell vs solid shell elements. https://featips.com/2021/02/21/solid-vs-shell-vs-solid-shell-elements/. [Online; accessed 05-04-2023].

[188] Biswajit Banerjee, Zhenrong Jeremy Chen, Anjukan Kathirgamanathan, Jeremy Chen, and Raj Das. Comparison of ansys elements shell181 and solsh190 aircraft sustainment and repair view project measurement of composite materiales using the deep-hole-drilling method view project comparison of ansys elements shell181 and solsh190. Technical report, Industrial Research Limited, NZ, 2011.

[189] Abacus documentation classes. https://classes.engineering.wustl.edu/2009/spring/mase5513/abaqus/docs/v6.5/books/gss/default.htm?startat=ch03s01.html. [Online; accessed 03-04-2023].

[190] Fea tips mesh metrics. https://featips.com/2022/11/21/ansys-mesh-metrics-explained/. [Online; accessed 11-04-2023].

[191] Solid 185 element. https://www.mm.bme.hu/~gyebro/files/ans_help_v182/ans_elem/Hlp_E_SOLID185.html. [Online; accessed 30-03-2023].

[192] Eric Qiuli Sun. Shear locking and hourglassing in msc nastran , abaqus , and ansys. In -, 2006.

[193] Engineering toolbox torsion of shafts. https://www.engineeringtoolbox.com/torsion-shafts-d_947.html. [Online; accessed 05-04-2023].

[194] J. C. Benedyk. Aluminum alloys for lightweight automotive structures. *Materials, Design and Manufacturing for Lightweight Vehicles*, pages 79–113, 2010.

[195] Aluminum alloys. https://uacj-automobile.com/types_and_applications.html. [Online; accessed 20-03-2023].

[196] Report munro and associates. https://leandesign.com/reports/. [Tesla Model 3].

[197] Michael F. Ashby. Chapter 9 - selection of material and shape. In Michael F. Ashby, editor, *Materials Selection in Mechanical Design (Fourth Edition)*, pages 243–276. Butterworth-Heinemann, Oxford, fourth edition edition, 2011.

[198] Mingde Ding, Jiancai Liu, Jianbo Su, Zhong Su, Bo Liu, and Ligang Wang. On the development of lightweight ip carrier. *SAE Technical Papers*, 2017-March, 3 2017.

[199] D. Tobalina-Baldeon, F. Sanz-Adan, M. A. Martinez-Calvo, and J. Santamaría-Pena. Dynamic tensile stress-compressive stress behavior of thermoplastic matrix composite materials reinforced with continuous fiber for automotive damping and anti-vibration structural elements. *Materials*, 13:1–16, 1 2020.

[200] Tania P. Berber-Solano, Joseph Giacomin, and Marco Ajovalasit. Effect of steering wheel acceleration frequency distribution on detection of road type. *INGENIERÍA MECÁNICA TECNOLOGÍA Y DESARROLLO*, 4:145–151, 01 2013.

[201] Ansys mode superposition method. https://courses.ansys.com/index.php/courses/intro-to-modal-based-methods/lessons/understanding-the-mode-superposition-method-lesson-1/. [Online; accessed 25-06-2023].

[202] Thomas Bru, Chalmers tekniska hogskola. Department of Industrial, and Materials Science. *Material characterisation for crash modelling of composites*. PhD thesis, Chalmers University of Technology, 2018.

[203] Philippe Bussetta and Nuno Correia. Numerical forming of continuous fibre reinforced composite material: A review. *Composites Part A: Applied Science and Manufacturing*, 113:12–31, 10 2018.

[204] Anna Hedlund-Åström and Conrad Luttropp. Metal inserts and hazardous content in light weight composite structures in the context of recycling. In *13th CIRP International Conference on Life Cycle Engineering*, 2006.

[205] Campus plastics pa6 modulus over temperature. https://www.campusplastics.com/campus/en/datasheet/Ultramid%C2%AE+B3K/BASF/20/3a22f000/SI?pos=27. [Online; accessed 10-05-2023].

[206] Nasa desert temperatures. https://earthobservatory.nasa.gov/biome/biodesert.php#:~:text=During%20the%20day%2C%20desert%20temperatures,(about%2025%20degrees%20fahrenheit). [Online; accessed 06-08-2023].